RANGING ERROR OVERBOUNDS

FOR NAVIGATION INTEGRITY OF LOCAL AREA AUGMENTED GPS

BY

IRFAN SAYIM

Submitted in partial fulfillment of the
requirements for the degree of
Doctor of Philosophy in Mechanical and Aerospace Engineering
in the Graduate College of the
Illinois Institute of Technology

Approved _____
Adviser

Chicago, Illinois
May 2003

ProQuest Information and Learning Company
300 North Zeeb Road
P.O. Box 1346
Ann Arbor, MI 48106-1346

ACKNOWLEDGEMENTS

First of all, I wish to express my sincere thanks to my advisor, Professor Boris Pervan, for his general supervision, continuous encouragement, and insightful instructions throughout this research here at IIT. Boris, you gave me not only the opportunity to pursue this research, but also the confidence and the discipline to complete it. Your door was always open for a brief talk or a difficult discussion. I feel very lucky to have had you as my advisor.

Next, I would also like to thank my defense committee members, Professor Nair, Professor Dix, Professor Kallend, and Professor Cesarone, for their careful review, constructive suggestions, and valuable discussions of this dissertation.

I would like to thank the current members of the Navigation and Guidance Laboratory, Moon-Beom Heo, Livio Gratton, Fang-Cheng Chan, Mathieu Joerger, Samer Khanafseh, and former member John Andreacchi for their friendship.

My gratitude also goes to Dr. Sam Pullen, LAAS Project Manager at Stanford University, for his constructive suggestions, and John Warburton from the FAA Technical Center for his support in obtaining the LAAS Test Prototype data.

I would also like to thank the FAA LAAS Program Office and Gebze Institute of Technology, Turkey, for their financial support during my graduate studies at IIT.

Lastly, I would like to express my hearty gratitude to my wife, Gunay, for her patience, understanding, love and support, without which this thesis could never have been possible.

TABLE OF CONTENTS

CHAPTER Page

LIST OF TABLES

LIST OF FIGURES

Figure Page

Figure Page

Figure Page

LIST OF SYMBOLS AND ABBREVIATIONS

Symbol	Definition
β	Total Positive Correlation Between Reference Receivers
δ	Multipath Delay
$\hat{\sigma}$	Standard deviation of True Error
$\hat{e}$	Normalized Multipath Error
γ	Inflation Factor of Temporal Variation
μ	Mean Value
ρ	Estimated Correlation Coefficient Between RRs
σ_{pr_gnd}	Sigma Pseudorange Ground (Broadcast Sigma)
σ_{pr_air}	Standard Deviation of Aircraft Pseudorange Error
σ_{pr_iono}	Standard Deviation of Error Associated with Ionospheric Uncertainty
σ_{pr_tropo}	Standard Deviation of Error Associated with Tropospheric Uncertainty
σ_{pr_res}	Standard Deviation of Residual Error (Tropospheric and Ionospheric)
Φ	Carrier Pseudorange Error Measurement
n_r	Number of Independent Samples for Receivers Correlation Inflation
n_s	Number of Independent Samples for Sigma Inflation
k	Sample Index
k_{fmd}	Gaussian Multiplier for Fault Detection
k_{md}	Gaussian Multiplier for Fault Free Missed Detection
k_{ff_md}	Gaussian Multiplier for Missed Detection

Symbol	Definition
r	Computed Correlation Coefficients Between RRs
A	Satellite Azimuth Angle
C/N_0	Carrier-to-Noise Ratio (dB-Hz)
E	Satellite Elevation Angle
G	Geometry Matrix
H_0	Hypothesis Assume All Reference Receivers Faulty Free
H_1	Hypothesis Assume One Reference Receiver Faulty
M	Number of Reference Receivers
PR	Code Pseudorange Error Measurement
$\overline{PR}$	Smoothed Pseudorange Error
S	Projection Matrix
W	Weighting Matrix

Abbreviation	Definition
A/C	Aircraft
AAD	Airborne Accuracy Designator
ACF	Autocorrelation Function
CDF	Cumulative Distribution Function
CMC	Code Minus Carrier
D/U	Amplitude of reflected signal relative to direct
DGPS	Differential GPS
DH	Decision Height
DLL	Delay Lock Loop
DMP	Diffuse Multipath
DOD	Department of Defense
EB	Expanding Bin
EUROCAE	European Organization for Civil Aviation Equipment
FAA	Federal Aviation Administration
GAD	Ground Accuracy Designator
GBAS	Ground Based Augmentation System
GPS	Global Positioning System
GRMP	Ground Reflection Multipath
HAT	Height Above Threshold
HMI	Hazardous Misleading Information
HZA	High Zenith Antenna
IID	Independent and Identically Distributed

Abbreviation	Definition
ILS	Instrumental Landing System
L1	Link-1 GPS signal transmitted at a frequency of 1575.42 MHz
L2	Link-2 GPS signal transmitted at a frequency of 1227.60 MHz
LAAS	Local Area Augmentation System
LAL	Lateral Alert Level
LGF	LAAS Ground Facility
LPL	Lateral Protection Level
LTP	LAAS Test Prototype
MASPS	Minimum Aviation System Performance Standards for the LAAS
MEB	Modified EB-method
MLA	Multipath Limiting Antenna
MOPS	Minimum Operational Performance Standards for GPS LAAS
NMP	Normalized Multipath Error
NSE	Navigation Sensor Error
PDF	Probability Density Function
PL	Protection Level
PRN	Pseudo Random Number
RF	Radio Frequency
RMS	Root Mean Square
RR	Reference Receiver
RSS	Root Sum Square

Abbreviation	Definition
RTCA	Radio Technical Committee for Aviation
RV	Random Variable
SBAS	Space Based Augmentation System
SCMC	Smoothed Code Minus Carrier
SIS	Signal In Space
SV	Space Vehicle
VAL	Vertical Alert Limit
VDB	VHF Data Broadcast
VHF	Very High Frequency
VPL	Vertical Protection Level
WAAS	Wide Area Augmentation System

ABSTRACT

The use of Differential GPS (DGPS) in aviation has been especially attractive in the past decade because of its potential to provide the means for satellite-based aircraft navigation spanning all aspects of flight, from takeoff to touchdown, with low cost and high availability. While this has been an inspiring goal, serious technical obstacles exist, the most difficult of which are related with navigation integrity for aircraft precision approach and landing. For example, for Category I precision approach, it is required that integrity risk (probability of hazardously misleading navigation information) never exceed 10^{-8}.

The Local Area Augmentation System (LAAS) is the DGPS architecture standard under development by the Federal Aviation Administration (FAA) to provide precision approach and landing navigation for civil aircraft. Navigation integrity risk for LAAS will be managed at the aircraft via the computation of Protection Levels, which are position error bounds within which navigation integrity is to be ensured. Existing standardized algorithms for the generation of the protection levels implicitly assume zero-mean, normally distributed ranging error distributions. Unfortunately, while the assumed error model is likely consistent with the effects of certain error sources (receiver thermal noise and diffuse multipath), it is widely understood that significant remaining errors, such as ground reflection multipath and systematic receiver/antenna errors, cannot be directly modeled by zero-mean normal distributions.

In this dissertation, the critical issues concerning establishment and sufficiency of overbounding ranging error distributions are addressed in detail. These include: quantification of the sensitivity of integrity risk due to statistical uncertainty; derivation of theoretical bounding models for non-zero-mean error sources; derivation of new bounding distribution models for non-gaussian ground-reflection multipath error; quantification and compensation for the effects of seasonal variation of multipath error; development, implementation, and testing of a new, adaptive binning algorithm to conservatively accommodate non-stationary and time-correlated empirical satellite ranging error data.

CHAPTER I

INTRODUCTION

1.1 Introduction

The use of *differential GPS* (DGPS), [Teasley80, Beser82]*, in aviation has been especially attractive in the past decade as seamless satellite-based aircraft navigation, spanning all aspects of flight, from takeoff to touchdown, may now be possible with low cost, and high availability. While this has been an inspiring goal, serious technical challenges exist in the development of GPS-based navigation systems for aviation. The most difficult challenge arises from the severe requirement of navigation integrity for aircraft precision landing. In response, the central focus of this research is on the integrity of satellite-based navigation for the precision landing of aircraft.

1.1.1 The Global Positioning System. The Global Positioning System (GPS) is a satellite-based, all-weather radionavigation system developed and maintained by the Department of Defense (DOD) to provide precise positioning to unlimited users on the globe (see Figure 1.1). It consists of a nominal constellation of 24 satellites in 12-hour orbits (approximately 20,000 kilometers altitude) distributed over six orbital planes inclined at 55 degrees. The constellation provides at all times at least four satellites visible from anywhere on Earth's surface. Each satellite broadcasts a highly accurate

* Corresponding to references in the Bibliography

ranging signal and its own orbital parameters (ephemerides) that will enable the user to calculate the position of each satellite at the time of transmission of the signal.

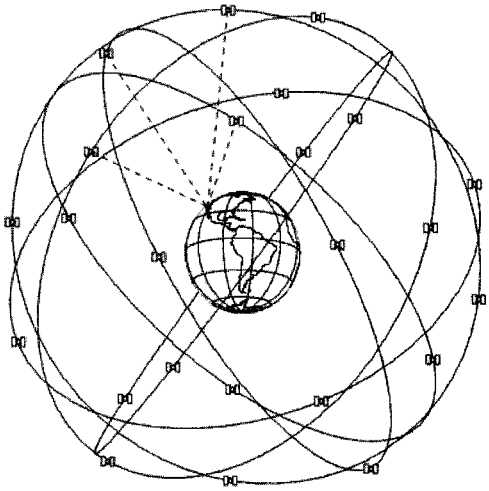

Figure 1.1 The Global Positioning System (GPS)

The signal consists of an L-band carrier, modulated with a pseudorandom noise (PRN) code and a data stream, which provides civilian users with easy access to the GPS signal. It also includes an additional ranging code, known as P-code, which provides military users precise positioning. A user who receives ranging signals from four or more satellites can solve for the three components of its position as well as deviation of its receiver clock from GPS system time.

1.1.2 Differential Positioning. While standalone GPS positioning (for both civil and military users) suffers from many error sources such as satellite clock, atmospheric, orbital, multipath, and receiver-related errors, the elimination of most of these errors is possible using differential positioning (DGPS). With DGPS, a reference receiver is placed at a precisely known location in the near-vicinity of the user. Then the

measurements collected by the reference receiver are subtracted from the computed distance of the satellite, which is calculated based on satellite ephemeris data, to form differential corrections. These corrections are then broadcast to local users to provide a more accurate differential position solution. Common errors between user and reference (usually associated with the satellite or space segment) are generally eliminated because those errors are highly spatially correlated between the two receivers (reference and user). Uncommon errors between reference and user (usually associated with receiver and local signal disturbances) will remain.

1.1.3 GPS For Civil Aviation. In the early 1990s, the Federal Aviation Administration (FAA) developed a plan to make satellite-based navigation technology available for use in the National Aerospace System (NAS). This plan defines a transition to GPS-based services. The transition is consistent with European Organization for Civil Aviation Equipment (EUROCAE) and International Civil Aviation Organization (ICAO) commitments to preserving the Instrumented Landing System (ILS) and transitioning to satellite-based navigation [MASPS98, Braff98, and Raymond98].

The stringent level of GPS-based navigation performance required for civil aviation is to be realized via two DGPS augmentation architectures currently under development. These are the Wide Area Augmentation System (WAAS) and the Local Area Augmentation System (LAAS). WAAS is a nationwide implementation, which collects satellite signals received by distributed ground stations throughout the NAS and transmits information from these signals to a master station. The WAAS master station monitors GPS satellites in view to ensure that each satellite is transmitting a reliable signal and

also estimates satellite clock, orbit, and other errors. The LAAS, internationally known as the Ground Based Augmentation System (GBAS), is a local area differential satellite navigation architecture. Because it is specifically designed to support civil aircraft precision approach and landing, it is more accurate than WAAS for users (aircraft) within the airport terminal area. The LAAS broadcasts a single correction for each satellite that accounts for all correlated (common) errors between a GPS reference receiver located on the airport property and local airborne users. A comprehensive review of the LAAS is given in Chapter 2.

1.1.4 LAAS Navigation Integrity. While the LAAS promises great practical benefit (all-weather precision approach and landing to all runways, simpler siting than ILS, services for terminal taxi and departure, etc.), a number of significant technical challenges have been encountered in the development of the architecture. In general, the most difficult of these challenges are associated with the stringent requirements for navigation integrity. For Category I precision approach, the probability of an undetected, hazardous navigation anomaly, known as an "integrity risk," is required to be lower than 10^{-8}. This research is focused on critical problems concerning the quantification and mitigation of integrity risk within the LAAS system.

The LAAS integrity risk is nominally quantified at the aircraft via the computation of Vertical and Lateral Protection Levels (termed VPL and LPL, respectively). These equations define aircraft position error upper bounds within which navigation integrity is to be ensured. The prescribed algorithms for the generation of these protection levels implicitly assume zero-mean, normally distributed fault-free error distributions for the

pseudorange corrections. The corrections are generated at LAAS Ground Facility (LGF) from the average of multiple reference receivers' pseudorange measurements and broadcast to the aircraft for a highly precise position solution. The standard deviation of broadcast correction error is assumed to be equal to σ_{pr_gnd} for each satellite. The value of σ_{pr_gnd} is also generated at LGF and broadcast to aircraft along with the corrections themselves. Regardless of true broadcast correction error distribution, σ_{pr_gnd} must represent a normal distribution standard deviation value for the correction error. While the assumed error model is likely consistent with the effects of thermal noise and diffuse multipath (see Section 2.2.3), it is widely understood that remaining errors such as ground reflection multipath and systematic reference receiver/antenna errors are not necessarily reliably modeled by zero-mean normal distributions. Therefore, to ensure that the computed values of VPL and LPL at the aircraft are meaningful and that integrity risk is properly managed, special care must be taken by the LGF in the establishment of the broadcast pseudorange correction error standard deviation (σ_{pr_gnd}).

The broadcast σ_{pr_gnd} must account for all true error sources associated with ground broadcast corrections for each satellite because σ_{pr_gnd} is used for the transformation of ranging error uncertainty to the position domain via Protection Levels for the user's satellite geometry. Furthermore, it is assumed that a normal distribution with the standard deviation of σ_{pr_gnd} overbounds the true (unknown) error distribution in the tails. This means *the proper quantification of integrity at the aircraft can only be ensured by the proper establishment of* σ_{pr_gnd}.

In this research, major unresolved issues concerning the establishment of σ_{pr_gnd} are addressed. These include the definition of a sufficient algorithm by which empirical error data may be processed to ensure spatial stationarity of error, quantification and compensation for the effects of seasonal variation of error, and a methodology to account for potential non-gaussian and non-zero mean gaussian error sources. For normally distributed errors such as receiver thermal noise and diffuse multipath, standard deviations can be estimated using experimental data alone. In this case, however, it is still necessary to account for the additional integrity risk incurred by statistical uncertainty (due to finite sample size) in the knowledge of reference receiver error standard deviation and error correlation between multiple reference receivers. In this regard, a detailed methodology has been developed for the definition of minimum acceptable inflation parameters for the sample standard deviation. (The inflation parameters are functions of the number of samples available and the sample correlation coefficient.) However, in order for such an empirical process to be applied, it is first necessary to define a proper method to collect data into spatial bins prior to sigma estimation. While large bin sizes are desired to maximize sample size (to limit required inflation factors), bin size is ultimately constrained by the need for spatial stationarity of all data within the bin (i.e., all error data within a bin must have the same underlying distribution). The quantitative resolution of this critical tradeoff is one of the major contributions of this research.

The effects of seasonal variations in pseudorange correction error (in particular multipath) must also be accounted for in the broadcast σ_{pr_gnd}. However, it is clearly

impractical to collect a full-year span of data (prior to commissioning) for each LGF to account for such effects. Therefore, archived error data collected at the LAAS Test Prototype (LTP) facility at the W. J. Hughes FAA Technical Center is used to define a baseline LGF model for seasonal variation in σ_{pr_gnd}. The observed LTP temporal variation is used to define a common standard inflation factor for use in the establishment of σ_{pr_gnd} in future LGF installations until sufficient site-specific data is collected.

Because ground multipath error is not necessarily normally distributed, empirically computed (and inflated) values of σ_{pr_gnd} are not sufficient to guarantee overbounding of the total LGF ranging error. Furthermore, it is impossible to rely on empirically constructed distributions (e.g., error data histograms) alone to define the nature of the underlying error distribution because little or no empirical data will exist in the 'tails' (which are of greatest interest in LAAS). Therefore, theoretical approaches are also emphasized in this research to incorporate ground reflection multipath effects into σ_{pr_gnd}.

For theoretical solutions, in the case of non-gaussian error distributions, position domain bounding must be specifically addressed because a gaussian bounding that holds in the range domain does not guarantee similar bounding in the position domain. The position domain bounding can, however, be verified by convolution of ground range error distributions. The procedure is numerically intensive but is necessary to establish overbounding gaussian distributions. Non-symmetric (with non-zero mean) distributions are even more difficult to bound in the position domain. The existence of a mean

requires the broadcast (ground) sigma bound to be a function of both ground-based and aircraft ranging error statistical parameters. Because all these parameters are not known by the LGF, the mean bounding problem presents a serious practical challenge.

The ultimate goal of this work is to define a sufficient methodology for the establishment of the LAAS broadcast σ_{pr_gnd}. Neither theoretical approaches nor empirical error data alone are adequate in this regard. The final broadcast pseudorange sigma will be a result of both elements. In this thesis, we introduce a practical way to synthesize the empirical and theoretical elements to quantitatively establish σ_{pr_gnd} for LAAS.

1.2 Summary of Relevant Work

Despite the rather impressive accomplishments and efforts to date, the fundamental goal of ranging error overbound under severe integrity requirements has not been achieved in previous work. Most importantly, proper processing for quantification of broadcast sigma directly from data has not yet been addressed in the literature. However, important related work in the area of GPS-based navigation integrity, is selected and summarized here. This information is sorted in three groups as follows:

1) *Navigation Integrity for Aviation, LAAS Architecture, and Specifications:* In 1996, Pervan provided in-depth study of navigation integrity using GPS carrier phase measurements and ground-based pseudolites for aircraft precision landing. Prototype algorithms and performance was verified after 110 successful automatic landing of

Boeing 737 [Pervan96]. Liu, in 1997, provided a detailed overview of the LAAS SIS 'signal-in-space' integrity monitoring system, explained the theoretical issues concerning derivation of protection level computation algorithms, and verified the theoretical analysis by simulation [Liu97]. Enge, in 1999, described the overall LAAS architecture, addressed the fundamental issues regarding accuracy, integrity and continuity, and discussed the use of LAAS for all categories of precision approach and landing [Enge99]. In 2000, McGraw et al. detailed the background of the derivation of LAAS pseudorange error accuracy models for the purposes of predicting service availability. These models are used as a common basis for setting LAAS performance requirements/specifications and to develop the test criteria [McGraw00].

2) *Bounding Efforts for Ranging Error:* In 1996, Braasch provided a comprehensive study of the characteristics of multipath error in the precision approach and landing environment [Braasch96]. Enge, [Enge99], examined the effects of multipath on code phase measurements and then developed bounds for code phase error due to multipath. In 2000, DeCleene studied ranging error distribution unimodality, symmetry, and overbounding conditions for the LAAS position domain integrity requirement [DeCleene00]. Shively, also in 2000, proposed a ranging error overbound model with Gaussian core/Laplacian tail distribution [Shively00].

3) *Multipath Mitigation Effort:* Brenner et al., in 1998, used experimental data to calibrate a deterministic signal model of set of uniformly distributed point detractors for the examination of the properties of diffuse multipath [Brenner98]. Counselman showed

that multipath rejection with a three-element vertical array antenna could be better than a conventional ground plane antenna [Counsel99].

1.3 Contributions of This Research

The main objective of this dissertation is the development of a complete and rigorous methodology for LAAS broadcast sigma establishment to ensure the stringent navigation integrity required for aircraft precision approach and landing. This is the first in-depth effort available for calculating broadcast sigma in the literature to date. Specific contributions were made in the following areas:

1. The sensitivity of navigation integrity risk was investigated and quantified with respect to the statistical uncertainty in the knowledge of reference receiver error standard deviation and correlation between multiple reference receivers. A detailed methodology was presented to define the minimum acceptable inflation parameters for the value of σ_{pr_gnd} broadcast to the aircraft. This work implicitly addressed the gaussian error structures associated with receiver thermal noise and diffuse multipath (Chapter 3).

2. A method for mean bounding was developed to: 1) account for the existence of non-zero means in gaussian distributions and 2) bound non-symmetric distributions (non-gaussian) in the tails after multiple convolutions in the position domain (Chapter 4).

3. A linearized multipath error model was developed. Based on the receiver/antenna performance and signal-tracking algorithm, two candidate ground reflection multipath error distributions were developed to bound the true non-gaussian error distribution theoretically (Chapter 5).

4. An analysis of seasonal variation of error was performed based experimental data collected at the FAA Technical Center LAAS Test Prototype. This was accomplished by processing an archived one-year-span of error data. The result is used as a basis for inflation of the short-term sigma to account for uncertainties due to slow (seasonal) variation of the error due to environmental changes (Chapter 6).

5. An adaptive spatial method known as Expanding Bin (EB) was developed to estimate sigma from data by accounting for existing nonstationary and serial correlation properties of ranging error data. The method guarantees the maximum obtainable sigma at any given time/elevation. It is also applicable for potential use in nonstationary parameter estimation in other applications (Chapter 6).

6. All of the above methods were applied to actual LTP data, and a synthesized experimental representative result for broadcast sigma was obtained. The result was used to test navigation accuracy specifications as defined in [MASPS98] (Chapter 7).

CHAPTER II

THE LOCAL AREA AUGMENTATION SYSTEM REVIEW

2.1 Introduction

This chapter provides an overview of LAAS, the pseudorange error observable, carrier-smoothed code filter, and generation of ground-broadcast correction values. It then follows with the integrity related issues such as protection levels, and specifications regarding accuracy requirements of ground and airborne signals.

2.2 The Local Area Augmentation System (LAAS)

2.2.1 The LAAS. The LAAS is a C/A (Coarse/Acquisition) Code-based differential GPS architecture designed to provide navigation services for civil aviation users during precision approach and landing. As shown conceptually in Figure 2.1, it consists of three components. These are: 1) The Space Segment (GPS satellites), 2) The LAAS Airborne Subsystem (users), and 3) The LAAS Ground Facility (LGF). The LGF consists of a set of (two to four) high quality GPS reference receivers placed at precisely known (surveyed) locations on the airport property. Ranging measurements from all satellites in view are collected by the reference receivers and passed to a processing unit which smoothes the measurements and generates a differential correction for each satellite. The corrections from all the reference receivers are averaged to form a composite ranging correction (one for each satellite) that is then uplinked, over a VHF data broadcast signal

transmitted in the 108.0-117.975 MHz band, to the airborne receiver. The airborne receiver applies the ranging corrections to its own satellite ranging measurements, thus enabling a highly accurate position solution.

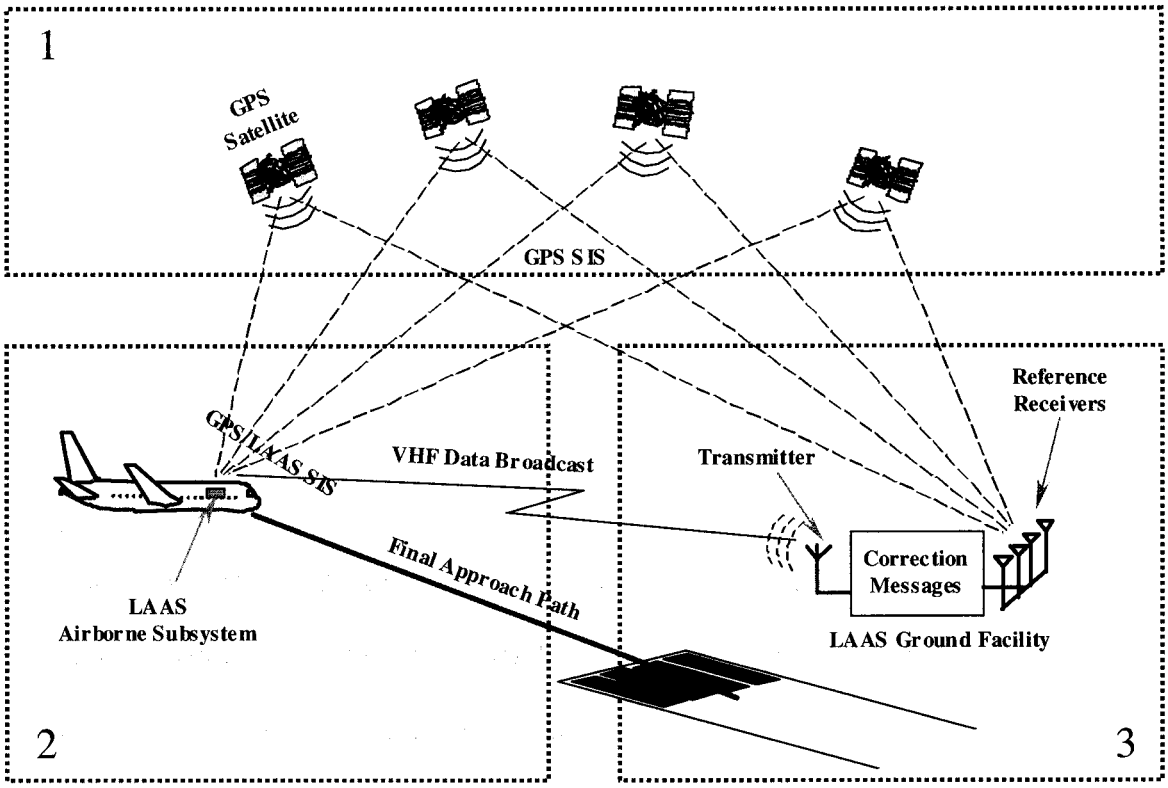

Figure 2.1 Local Area Augmentation System

The basic concept of LAAS is to eliminate the common errors between reference station and airborne measurements and to provide integrity-related information to aircraft during final approach. After elimination of common errors, the position accuracy improves greatly. For example, Code-based DGPS provides ~1 meter (95% probability) level positioning accuracy as shown in Figure 2.2 as compared to standalone GPS at ~20 meter level accuracy. The integrity improves as well in comparison to standalone

positioning since many types of space segment errors are successfully removed by DGPS.

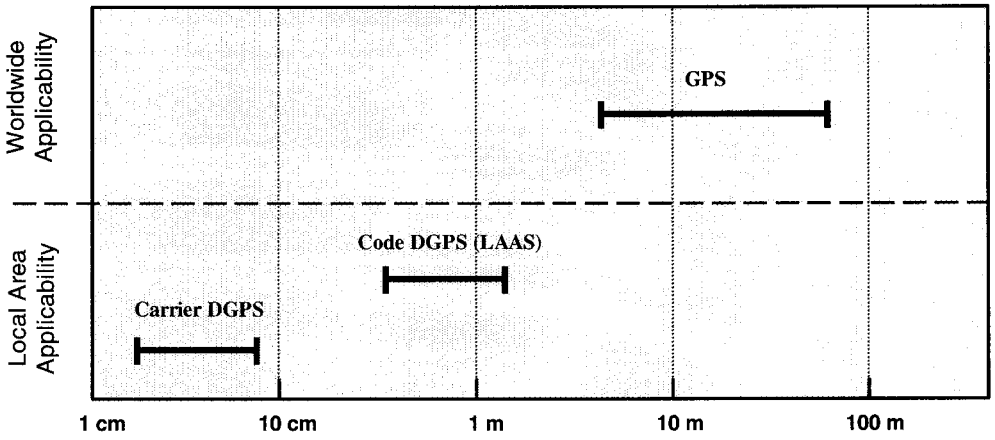

Figure 2.2 LAAS Capability in GPS

2.2.2 LAAS Positioning. In LAAS, code measurements are obtained from at least four satellites in view, passed trough a carrier-smoothing filter (to minimize noise), and then used in basic linearized DGPS code position solution as:

$$\mathbf{y} = G\mathbf{x} + \boldsymbol{\varepsilon} \tag{2.1}$$

where $\mathbf{y}_{(N\times 1)}$ is the measurement vector, N is the number of satellites in view at the time of position estimation ($N \geq 4$), $\boldsymbol{\varepsilon}_{(N\times 1)}$ is a vector of the measurement error, $\mathbf{x}_{(4\times 1)}$ is the state vector (three position components plus the time component), and $\mathbf{G}$ is the observation matrix defining the direction cosine line of sight vectors pointing from the

airborne receiver antenna to the satellites with an augmentation value of 1 for the clock. Thus,

$$\mathbf{G} = \begin{bmatrix} \cos E_1 \cos A_1 & \cos E_1 \sin A_1 & \sin E_1 & 1 \\ \vdots & \vdots & \vdots & \vdots \\ \cos E_N \cos A_N & \cos E_N \sin A_N & \sin E_N & 1 \end{bmatrix} \tag{2.2}$$

where, A and E are azimuth and elevation angle a satellite respectively. The weighted Least Square Estimate of states $\mathbf{x}$ is given as follows:

$$\hat{\mathbf{x}} = (\mathbf{G}^T\mathbf{W}\mathbf{G})^{-1}\mathbf{G}^T\mathbf{W}\mathbf{y} = \mathbf{S}\mathbf{y} \tag{2.3}$$

where,

$$\mathbf{S} \equiv (\mathbf{G}^T\mathbf{W}\mathbf{G})^{-1}\mathbf{G}^T\mathbf{W} \tag{2.4}$$

$\mathbf{S}_{(4\times N)}$ is also called the "projection matrix," as it projects the pseudorange domain error into the position domain. The weighting matrix, $\mathbf{W}_{(N\times N)}$, is a covariance of the total estimated pseudorange error (ground broadcast and aircraft together) seen by aircraft.

$$\mathbf{W}^{-1} = [\varepsilon\varepsilon^T] = \begin{bmatrix} \sigma^2_{pr,1} & 0 & \cdots & 0 \\ 0 & \sigma^2_{pr,2} & \cdots & 0 \\ \vdots & \vdots & \ddots & \vdots \\ 0 & 0 & \cdots & \sigma^2_{pr,N} \end{bmatrix} \tag{2.5}$$

The composite pseudorange measurement errors for the GPS/LAAS Signal-In-Space (satellite signals and broadcast reference data collectively) are formed at aircraft for an arbitrary satellite by:

$$\sigma^2_{pr,n} = \sigma^2_{pr\_gnd,n} + \sigma^2_{pr\_air,n} + \sigma^2_{pr\_res,n} \tag{2.6}$$

where, σ_{pr_gnd} is the standard deviation of broadcast correction error and associated with the LGF pseudorange measurements, σ_{pr_air} is the standard deviation of airborne pseudorange error, and σ_{pr_res} is the standard deviation of residual pseudorange errors not directly attributable to ground or airborne (such as ionospheric and tropospheric decorrelation). All these standard deviations are assumed to be parameters of normal distributions with zero means as follows:

$$\varepsilon_n \sim N(0, \sigma^2_{pr,n}) \tag{2.7}$$

Here, ε_n is the total measurement error associated with three independently distributed sources, *ground*, *airborne*, and *residuals*. Among these error sources (2.6), the ground error is of specific interest in this research, but the methodologies presented are generally applicable. In section 2.2.3, the observability of this error source is briefly explained.

2.2.3 LGF Error Observable. The pseudorange measurement for the n^{th} satellite of the m^{th} receiver at an LGF can be expressed as:

$$PR_m^n = R_m^n + ct^n + ct_m + I^n + T^n + MP_m^n + DMP_m^n + RN_m^n \quad (2.8)$$

where,

R_m^n is the geometric range between the satellite and receiver antenna on the ground,

T^n is the tropospheric delay error,

I^n is the ionospheric delay error,

ct^n is the satellite clock error,

ct_m is the clock error of ground receiver,

MP_m^n is the multipath error of ground,

DMP_m^n is the diffuse multipath error of ground, and

RN_m^n is the receiver thermal noise.

The error sources may be sorted into two groups in terms of commonality between ground and airborne measurements as follows. The first group includes correlated errors between reference receivers and users caused by the space segment:

$$e_1^{PR} = ct^n + I^n + T^n \quad (2.9)$$

The second group consists of errors which are uncorrelated between reference and user receivers, usually caused by local signal disturbances and receiver-related errors:

$$e_2^{PR} = MP_m^n + DMP_m^n + RN_m^n \quad (2.10)$$

The effects of e_1^{PR} are negligible because the errors cancel for ground and airborne receivers in local proximity. Any residual errors due to spatial decorrelation can be bounded theoretically and will not be covered in this research. However, the effect of e_2^{PR} error remains in the DGPS process of LAAS. These errors are of primary interest in this research and are briefly described as follows:

Multipath: The reflection and diffraction of a transmitted GPS signal from ground surfaces and discrete objects in the vicinity of the antenna can cause multiple signals to be received by a user. This phenomenon, termed multipath, is the largest error contributor source in LAAS. Multipath basically distorts the GPS signal modulation, resulting in measurement errors in pseudorandom code. Ground multipath is not correlated with multipath at aircraft, and is not easily attenuated through filtering; therefore it causes DGPS positioning errors in LAAS. When the objects surrounding an antenna contain reflecting surfaces, multipath will most likely be present. Reflections from smooth, relatively flat and conducting surfaces are termed 'specular,' meaning the waveform structure of the signal energy is preserved and only the amplitude is attenuated.

Diffuse Multipath: As the surface roughness increases, the reflections become diffuse. The signal energy is dispersed, greatly reducing the signal power directed toward the antenna. Moreover, as the signal moves across the rough surface, the diffuse scatter takes on a random appearance. Diffuse multipath, in contrast to specular, may be greatly reduced in a filtering process.

Receiver Noise: Noise associated with the measurement of pseudorange and phases attributed to the receiver itself is called receiver noise. This noise is uncorrelated between measurements (white noise) and tends to be small in magnitude.

Observation of the e_2^{PR} type error can be obtained easily by processing the Code Minus Carrier (CMC) error observable. This method is used to generate the majority of the experimental results in this thesis. Although it requires the use of dual frequency (L1 and L2 together) measurements, the following two related advantages are significant: 1) Error can be observed on individual reference receivers (RRs) so errors across RRs need not be Independent and Identically Distributed (IID), and 2) It is useful for estimation of correlation between reference receivers.

In order to obtain the CMC error observable, first, the carrier error observable is introduced. The carrier measurement for the n^{th} satellite of the m^{th} receiver at the LGF can be expressed as:

$$\Phi_m^n = R_m^n + ct^n + ct_m + \lambda \widehat{N}_m^n - I^n + T^n + mp_m^n + dmp_m^n + rn_m^n \qquad (2.11)$$

where,

λ is the carrier wavelength,

$\widehat{N}_m^n$ is the integer ambiguity in cycles,

mp_m^n is the carrier phase multipath error,

dmp_m^n is the carrier phase diffuse multipath error,

rn_m^n is the carrier phase receiver noise.

Then Code Minus Carrier (CMC) can be formed as:

$$PR_m^n - \Phi_m^n = 2I^n - \lambda\widehat{N}_m^n + MP_m^n + DMP_m^n + RN_m^n - mp_m^n - dmp_m^n - rn_m^n \qquad (2.12)$$

It is clear that most of the common errors between code (2.8) and carrier measurements (2.12) are eliminated via the CMC process. However, a significant number of error sources still remain. These types of errors are uncorrelated between code and carrier measurements and therefore cannot be eliminated by the direct process of CMC.

Error components in Equation (2.12) are: 1) presence of the ionospheric error term ($2I^n$) due to the dispersive nature of the ionosphere which causes code delay and phase advance [Misra01], 2) a cycle ambiguity term ($\lambda\widehat{N}_m^n$) representing the number of complete carrier waves between the satellite and receiver, and 3) all other uncorrelated error terms presented in CMC corresponds to code and carrier measurements.

In this research, CMC error is used widely in the generation of empirical results from data after the following corrections were made. First, the ionospheric error term is obtained by aid of dual frequency carrier measurements (differencing L2 and L1 carrier measurements) as given by Equation (2.13) and then eliminated from CMC.

$$2I^n = 2\left(\Phi_{L1,m}^n - \Phi_{L2,m}^n\right)/\left(f_{L1}^2/f_{L2}^2 - 1\right) \qquad (2.13)$$

where,

Φ_{L1} is the carrier phase measurement for the L1 frequency

Φ_{L2} is the carrier phase measurement for the L2 frequency

f_{L1} is the frequency for the L1 band (1575.42 MHz)

f_{L2} is the frequency for the L2 band (1227.60 MHz)

The second correction is to remove the cycle ambiguity term ($\lambda \widehat{N}_m^n$). As this term occurs as a bias, it is easily removed during the process. The final step is to neglect the uncorrelated error terms corresponding to the carrier measurements as they are very small ($e_2^{\Phi} << e_2^{PR}$) compared to the code measurements. Correcting all these terms in the CMC measurement yields the following error terms corresponding to only the code measurement error:

$$PR_m^n - \Phi_m^n = GMP_m^n + DMP_m^n + RN_m^n \tag{2.14}$$

Equation (2.14) presents the error sources of greatest interest in this research. The statistical descriptive value of broadcast corrections will be generated based on these error sources. In Figure 2.3, an example of CMC error data versus time is plotted before and after removal of Ionospheric error, the first of the three CMC corrections.

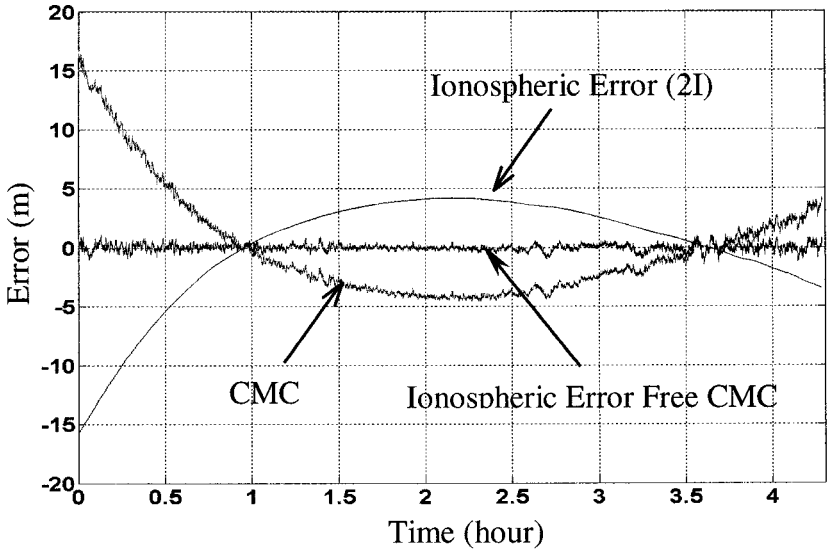

Figure 2.3 GPS Ranging Error Observable

2.2.4 Carrier Smoothed Code. As described in [MASPS98], a carrier aided smoothing filter is used in LAAS. Known as a 'Hatch Filter,' its purpose is to attenuate high frequency code measurement noise. The expression for filtered pseudorange (Carrier Smoothed Code) is given as:

$$\overline{PR}^{n}_{m,k} = \frac{1}{\tau} PR^{n}_{m,k} + \frac{(\tau - 1)}{\tau}\left(\overline{PR}^{n}_{m,k-1} + \Phi^{n}_{m,k} - \Phi^{n}_{m,k-1}\right) \tag{2.15}$$

where,

$\overline{PR}^{n}_{m,1} = PR^{n}_{m,1}$,

PR^{n}_{m} is the pseudorange measurement

τ is the carrier smoothing time constant (usually 100 seconds)

Φ_m^n is the carrier phase measurement

k is the sample index

An example result of smoothing filer output is plotted in Figure 2.4 for an arbitrary satellite pass. The dark solid line indicates the output of the smoothing filter (Smoothed Code Minus Carrier, SCMC) while dots represent original unsmoothed pseudorange noise (Code Minus Carrier, CMC).

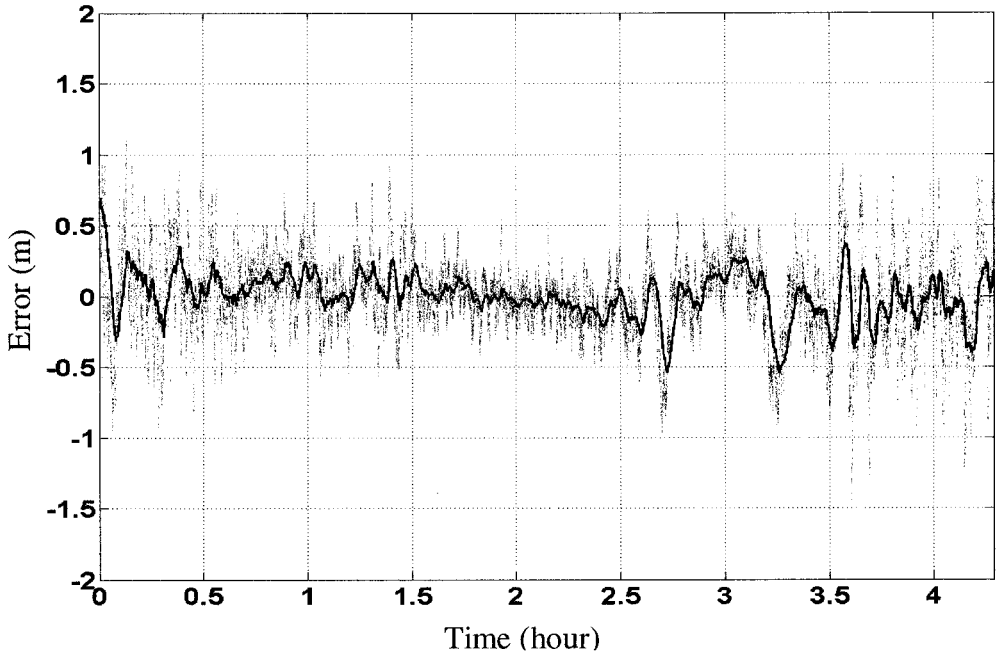

Figure 2.4 CMC and SCMC versus Time

2.2.5 LAAS Broadcast Correction Values. In LAAS, the following parameters are broadcast from the LGF to the airborne user for accurate positioning as well as integrity risk management: PRc (pseudorange correction), B-values (for integrity), and error

distribution parameters σ_{pr_gnd} (for integrity). This section briefly describes the generation of two of these corrections parameters, PRc and B -values.

PRc: The pseudorange corrections are computed by subtracting the known distance between satellite and reference antennae (phase centers) from pseudorange measurements made by receivers. For example, for an arbitrary satellite n and reference receiver m, the pseudorange correction can be expressed as PRc_m^n. The corrections of multiple (M) reference receivers are averaged for each satellite in order to form a single composite broadcast correction for each satellite (as follows for satellite n):

$$PRc^n = \frac{1}{M}\sum_{j=1}^{M} PRc_j^n \tag{2.16}$$

B-value: This value is formed by excluding one of the reference receiver's measurements form the correction and differencing the result from PRc^n. The process is repeated for all satellites. For an arbitrary satellite n and reference receiver m we have:

$$B_m^n = PRc^n - \frac{1}{M-1}\sum_{\substack{j=1,\\ j\neq m}}^{M} PRc_j^n \tag{2.17}$$

where,

j is index to reference receivers

n is an arbitrary satellite

m is an arbitrary reference receiver

M is the number of reference receivers

The B-value is used at aircraft in the computation of VPL/LPL under the reference receiver failure hypothesis [Liu97].

2.3 The LAAS Navigation Integrity Allocation

The basic function of the LAAS Ground Facility (LGF) integrity system is the detection and removal of anomalies present in the LAAS signal-in-space (SIS) that would otherwise result in an unacceptable integrity risk to an aircraft on final approach. The notion of SIS is introduced primarily to distribute accountability between the ground and airborne navigation subsystems. In general, the aircraft is responsible for the proper functionality of the airborne equipment (which would typically include the implementation of redundant sensor tracks to provide the means for detection and removal of airborne equipment failures), while the LGF is responsible for the detection of anomalies in both the received satellite signals and the LAAS reference data broadcast to the aircraft. A sketch of integrity risk allocation is given in Figure 2.5. The satellite signals and broadcast reference data collectively define the LAAS SIS.

As currently envisioned, LAAS SIS integrity monitoring is comprised of both ground and airborne elements. The need for an airborne processing component, even for SIS

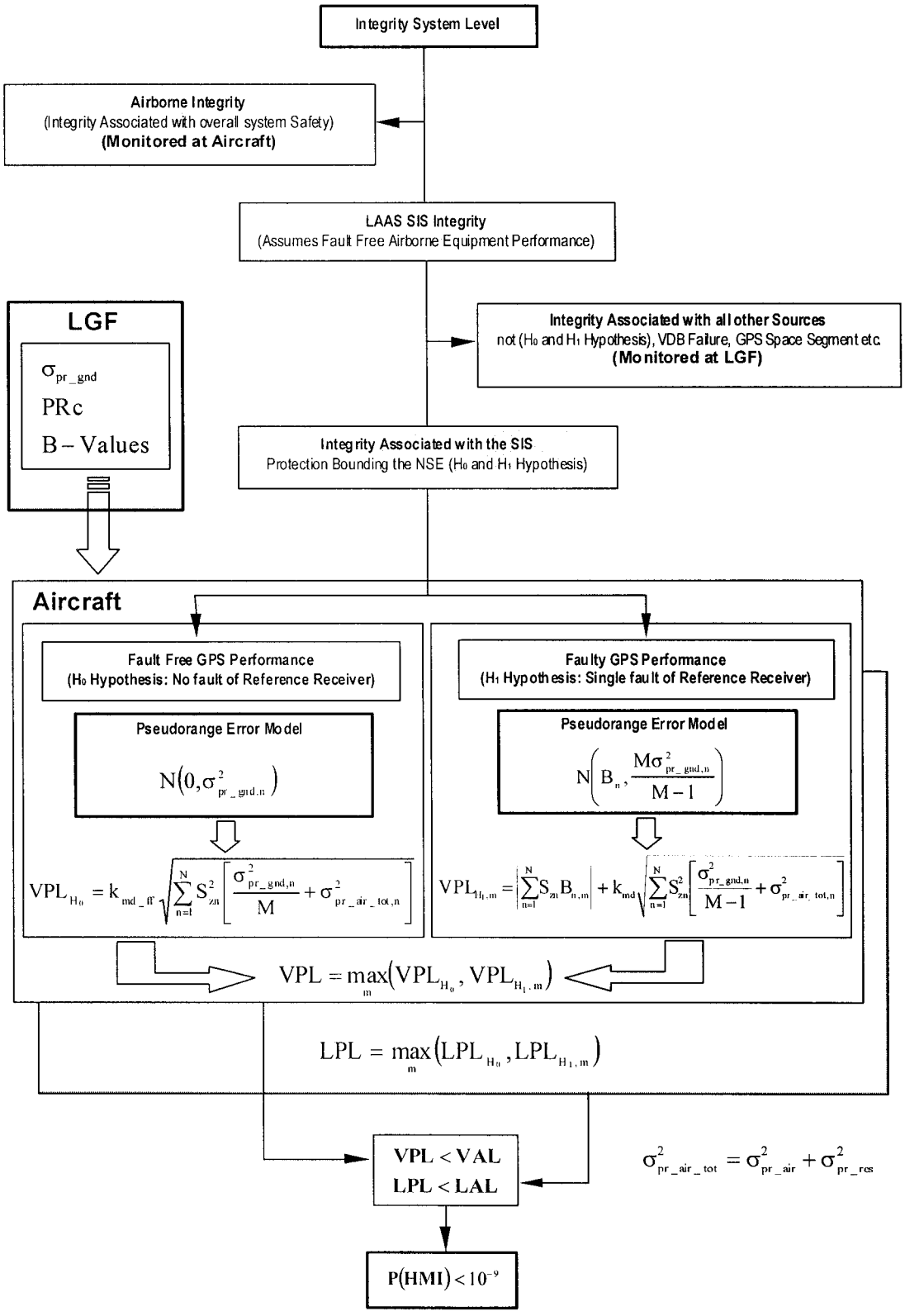

Figure 2.5 LAAS Integrity Allocation Diagram

monitoring, is motivated by the fact that the integrity specifications are expressed in the position (rather than range) domain. Because the LGF is generally unaware of the specific satellites being tracked by the airborne receiver at any given time, an airborne processing component is implemented specifically to convert ground-broadcast range domain statistics to position domain Protection Levels. Specific approaches for the airborne processing may be found in [MASPS98, Liu97, and LGF02].

2.3.1 Protection Level Equations. The Protection Level Equations (i.e., VPL/LPL) are frequently used in all chapters in the thesis. They are standardized and can be found in a number of references such as [MASPS98, MOPS00, and Liu97]. In the following a brief summary of them is provided. These Protection Levels define position error upper bounds of the aircraft to indicate whether or not the LAAS supports the availability of precision approach and landing under the following two fault hypothesis:

H_0 Ground measurements are fault free, $P(H_0) \approx 1$

H_1 A fault exists on one or more measurements made by one reference receiver. Based on historical performance, and the existence of monitors at the LGF, is assumed that *a priori* probability of one reference receiver faulting is 10^{-5}/approach. Since there are M reference receivers, the probability of H_1 is given by $P(H_1) \approx M \cdot 10^{-5}$

VPL_{H_0} bounds the fault-free vertical positioning error by the probability $1-P_{md\_ff}$ where P_{md_ff} is the probability of fault-free missed detection. VPL_{H_0} is defined as:

$$P(\text{vertical NSE} > VPL_{H_0} \mid \text{system fault-free}) = P_{md\_ff}$$

where NSE is Navigation Sensor Error. If VPL_{H_0} is greater than the Vertical Alert Limit (VAL), then the Hazardous Misleading Information (HMI) is said to exist.

VPL_{H_1} bounds the vertical positioning error by the probability $1-P_{md}$, where P_{md} is the probability of missed detection under H_1. VPL_{H_1} is defined as:

$$P(\text{vertical NSE} > VPL_{H_1} \mid \text{reference receiver failure}) = P_{md}$$

If VPL_{H_1} is greater than VAL, then HMI is said to exist. Since we do not know which hypothesis is true (H_0 or H_1), we must choose the larger of the VPL_{H_0} and VPL_{H_1}:

$$VPL = \max\{VPL_{H_0}, VPL_{H_1}\} \tag{2.18}$$

where,

$$VPL_{H_0} = k_{md\_ff}\sqrt{\sum_{n=1}^{N} S_{zn}^2\left[\frac{\sigma_{pr\_gnd,n}^2}{M_n} + \sigma_{pr\_air,n}^2 + \sigma_{pr\_res,n}^2\right]}, \tag{2.19}$$

$$VPL_{H_1} = \max_j\left[VPL_j\right], \tag{2.20}$$

and

$$VPL_j = \left|\sum_{n=1}^{N} S_{zn}^2 B_{n,j}\right| + k_{md}\sqrt{\sum_{n=1}^{N} S_{zn}^2\left[\frac{\sigma_{pr\_gnd,n}^2}{M_n - 1} + \sigma_{pr\_air,n}^2 + \sigma_{pr\_res,n}^2\right]} \tag{2.21}$$

In addition to generating the Protection Levels defined above, the airborne processor must also verify whether the satellite geometry supports system continuity requirements. This is done by assuring that the "predicted" VPL is less than VAL [Liu97]:

$$VPL_{predict} = \frac{k_{fmd/M}}{\sqrt{M(M-1)}}\sqrt{\sum_{n=1}^{N} S_{zn}^2 \sigma_{pr\_gnd,n}^2} + k_{md}\sqrt{\sum_{n=1}^{N} S_{zn}^2\left[\frac{\sigma_{pr\_gnd,n}^2}{M_n - 1} + \sigma_{pr\_air,n}^2 + \sigma_{pr\_res,n}^2\right]} \tag{2.22}$$

where,

n is the satellite index,

M is the number of reference receivers used to generate the broadcast correction,

N is the number of available satellites,

S_{zn} is the n^{th} element of the third row (representing the vertical component) of the weighted geometry projection matrix used to generate the position estimate,

B_n is the broadcast 'B-value' for satellite n associated with the given reference receiver,

M is the number of reference receivers used to generate the broadcast correction,

σ_{pr_gnd} is the LGF broadcast correction error standard deviation,

σ_{pr_air} is the airborne measurement error standard deviation,

σ_{pr_res} is the standard deviation of residual errors not directly attributable to ground or airborne error (such as tropospheric decorrelation),

k_{md} is a multiplier used to set the desired level of missed detection probability assuming gaussian errors,

k_{md_ff} is a multiplier used to set the desired level of fault-free missed detection probability assuming gaussian errors,

k_{fmd} is a multiplier used to set the desired level of fault-free detection probability given.

Detection multipliers are given in Table 2.1 (Fault-free missed detection and missed detection) and Table 2.2 (Fault-free detection). Each table contains detection multipliers as a function of performance type and number of reference receivers.

Table 2.1. Missed Detection Multipliers

Performance Type	k_{md_ff}			k_{md}		
	M = 2	M = 3	M = 4	M = 2	M = 3	M = 4
1	5.762	5.810	5.847	2.935	2.898	2.878
2	6.598	6.641	6.673	4.305	4.279	4.265
3	6.598	6.641	6.673	4.305	4.279	4.265

Table 2.2 Fault-Free Detection Multipliers

Performance Type	k_{ffd}		
	M = 2	M = 3	M = 4
1	5.026	5.104	5.158
2	N/A	5.233	5.286
3	N/A	5.451	5.502

2.4 LAAS Navigation Performance

LAAS Navigation Performance Requirements are specified in Table 2.1 to support implementation of advanced terminal navigation concepts as a function of Operational Categories [MASPS98]. These Navigation Performances are defined below:

2.4.1 Accuracy. Accuracy is the degree of deviation of navigation output from true position and/or velocity under fault-free conditions. It indicates how well the navigation system is performing.

2.4.2 Integrity. Integrity is the ability of a system to provide timely warnings to users when the system should not be used for navigation. *Integrity risk* is the probability of an undetected navigation system error or failure that results in hazardously misleading

information onboard the aircraft. It indicates how well the navigation system detects failure to meet the required operational accuracy.

2.4.3 Continuity. Continuity is the likelihood that the navigation SIS supports accuracy and integrity requirements for the duration of the intended operation. It indicates the ability of the navigation system to provide accurate positioning with integrity without interruption.

2.4.4 Availability. Availability is the fraction of time the navigation function meets the required performance of continuity, integrity, and accuracy for the initiation of the intended approach. It indicates how well the navigation system provides sufficient performance for continuity, integrity, and accuracy.

2.4.5 Operational Concept. The operational concept includes the requirements for a GPS/LAAS intended to support operations for Category I, II, IIIa and IIIb precision approaches and landings [MASPS98]. These requirements are summarized in Table 2.3.

- **Category I.** A Category I approach is defined as a precision instrument approach and landing with a decision height not lower than 60 m and with either a visibility not less than 800 m, or a runway visual range not less than 550 m. [MASPS98]

- **Category II.** A Category II approach is defined as a precision instrument approach and landing with a decision height lower than 60 m but not lower than 30 m and a runway visual range not less than 350 m. [MASPS98].

- **Category III.** A Category IIIa approach is defined as a precision instrument approach and landing with a decision height lower than 30 m or no decision height and a runway visual range not less than 200 m. A Category IIIb approach is defined as a precision instrument approach and landing with a decision height lower than 15 m or no decision height and a runway visual range less than 200 m but not less than 50 m. [MASPS98].

Table 2.3. LAAS Performance Requirements For Precision Approach [Enge99]

	Category I	Category II	Category III
Decision Height (DH)	60m	30m	0-30m
Vertical Accuracy (95%)	5m	2.5m	2.5m
Continuity	10^{-5}/approach	10^{-5}/ approach	10^{-7}/ approach
Integrity	**$4x10^{-8}$/approach**	$4x10^{-8}$/ approach	$4x10^{-9}$/ approach
Availability	0.999	0.999	0.999
Vertical Alert Limit (VAL)	10m	5m	5m
Time to Alarm	6sec	2sec	2sec

2.5 GPS/LAAS SIS Accuracy Requirement

In this section, a brief background of GPS/LAAS SIS accuracy requirements is given. These requirements are defined based on both availability concerns of LAAS and performance that can be achieved using currently available GPS receiver technology. They are not based on ranging error overbounds and do not reflect the work done in this thesis. However, the current requirements are extremely valuable in terms of providing a common basis for defining LAAS performance in terms of availability. The requirements are widely used in the simulation-based analysis in Chapter 3 and again in Chapter 5 to evaluate LAAS performance under availability concerns.

Recall from Equation (2.6) that the total differential pseudorange correction error standard deviation computed at the aircraft is $\sigma^2_{pr,n} = \sigma^2_{pr\_gnd,n} + \sigma^2_{pr\_air,n} + \sigma^2_{pr\_res,n}$. The related accuracy models will now be discussed. Details of these values can be found in [MASPS98 and McGraw00].

2.5.1 Ground Accuracy Designator (GAD) Model. The required accuracy allocation for ground error is formed by the combining the contributions of receiver noise, multipath, and the SIS residual error as follows:

$$\sigma_{pr\_gnd,GPS}(\theta_i) \le \sqrt{\frac{\left(a_0 + a_1 e^{-\theta_i/\theta_0}\right)^2}{M} + a_2^2 + \left(\frac{a_3}{\sin\theta_i}\right)^2} \tag{2.23}$$

where the values used in Equation (2.23) are given in Table 2.4.

Table 2.4 GPS/LAAS SIS Accuracy Requirement

Ground Accuracy Designator (GAD)	θ_i (degree)	a_0 (meter)	a_1 (meter)	θ_0 (degree)	a_2 (meter)	a_3 (meter)
A	>5	0.5	1.65	14.3	0.08	0.03
B	>5	0.16	1.07	15.5	0.08	0.03
C	>35	0.15	0.84	15.5	0.04	0.01
	≤ 35	0.24	0	---	0.04	0.01

The letter 'A' stands for the performance type of a standard correlator receiver and single-aperture antenna technology. The letter 'B' stands for the performance type of an advanced narrow correlator receiver technology with a conventional antenna. Finally the

letter 'C' stands for the performance type of an advanced narrow correlator with a multipath Limiting Antenna (MLA).

2.5.2 Airborne Accuracy Designator (AAD) Model. The Airborne Accuracy Model (AAD) is similar to GAD but is defined based on error due to wide band noise, interference and error due to airframe multipath as follows:

$$\sigma_{pr\_air,GPS}(\theta_i) \le a_0 + a_1 e^{-\theta_i/\theta_0} \tag{2.24}$$

where the values used in Equation (2.24) are given in Table 2.5.

Table 2.5 Airborne Accuracy Requirements

Airborne Accuracy Designator (AAD)	θ_0 (degree)	a_0 (meter)	a_1 (meter)
A	19.6	0.1600	0.23
B	27.7	0.0741	0.18

The letters 'A' and 'B' stand for the achievable performance of the receiver technology for aviation. Simply stated, the A indicates the worst performance and B the best. More detail maybe found in [McGraw00 and MASPS98].

2.5.3 Tropospheric/Ionospheric Uncertainties. Accuracy models developed in this section are for the residual effects due to ionospheric and tropospheric spatial

decorrelation: The two terms are defined separately and then combined into one residual uncertainty term.

Tropospheric Uncertainty (due to spatial decorrelation): The tropospheric error may be modeled as

$$\sigma_{pr\_trop} = \sigma_R h_0 \frac{10^{-6}}{\sqrt{0.002 + \sin^2(\theta_n)}} \left(1 - e^{-\Delta_0/h_0}\right) \tag{2.25}$$

where,

σ_R is refractivity uncertainty (unit-less),

h_0 is tropospheric scale height (meters),

Δh is aircraft distance above reference station (meters)

Ionospheric Uncertainty (due to spatial decorrelation): The ionosphere pseudorange error may be modeled as

$$\sigma_{iono} = F_{PP}\sigma_{vert\_iono\_grad}(x_{air} + 2\tau_{air}v_{air}) \tag{2.26}$$

where,

τ_{air} is the airborne carrier-smoothing time constant (100 sec),

v_{air} is the horizontal user velocity (~70 m/sec)

$\sigma_{vert\_iono\_grad}$ is the ionospheric delay change (as a function of ionospheric pierce-points separation between reference receiver and user, ~2mm/km),

x_{air} is the user-reference separation,

$F_{PP} = \left[1 - \left(\frac{R_e \cos(\theta_n)}{R_e + h_I}\right)^2\right]^{-\frac{1}{2}}$ is the obliquity factor,

R_e is the approximate radius of Earth's ellipsoid (6378.1363 km),

h_I is the height of the maximum electron density of the ionosphere (~350 km)

The residual uncertainty can now be formed as [McGraw00, MASPS98]:

$$\sigma^2_{pr\_res} = \sigma^2_{pr\_tropo} + \sigma^2_{pr\_iono} \tag{2.27}$$

2.6 Conclusion

A summary overview of fundamental LAAS-related issues is provided in this chapter. This includes a description of LAAS, integrity and accuracy-related issues, and the error observables. The concepts covered here form the basis for the subjects discussed in the remaining chapters of this thesis.

CHAPTER III

GAUSSIAN RANGING ERROR

3.1 Introduction

For normally distributed error sources such as receiver-related noise and diffuse multipath, standard deviations can be estimated using experimental data alone. In this case, however, it is still necessary to account for the additional integrity risk incurred by statistical uncertainty (due to finite sample size) in the knowledge of reference receiver error standard deviation as well as error correlation between multiple reference receivers. In this regard, a detailed methodology has been developed for the definition of minimum acceptable inflation parameters for the sample standard deviation to ensure navigation integrity.

3.2 Sigma Sensitivity Analysis

In the LAAS architecture, and in this analysis, integrity risk under the hypotheses of fault-free conditions (H_0) and integrity risk in the event of a single reference receiver failure (H_1) are considered separately. Nominally, the vertical protection limits, VPL_{H_0} and VPL_{H_1}, are computed at the aircraft based on values of broadcast correction error standard deviation (σ_{pr_gnd}) for each satellite sent by the reference station. In addition, the prescribed computation of VPL_{H_1} requires that the ground receiver broadcast

differences between the pseudorange corrections derived from various subsets of the multiple (typically 3 or 4) LGF reference receivers. The precise mathematical structure of these differences, termed 'B-values,' is defined in Equation (2.17). (In contrast, the nominal correction broadcast for each satellite, which is used for positioning but not in the computation of protection limits, is based on an average across all reference receivers.) The prescribed missed detection (MD) probabilities for H_0 and H_1 are specified, respectively, in terms of gaussian multipliers k_{md_ff} and k_{md}, which are defined in Table 2.1.

The general approach taken in this analysis is to first quantify *true* missed detection probability given that the actual value of reference receiver error standard deviation (σ) deviates from the broadcast value σ_{pr_gnd}. Since it is recognized that any realizable estimate of standard deviation will be based on a finite number of error samples, it is then also necessary to ensure that the broadcast value of σ_{pr_gnd} accounts for any statistical uncertainty that may lead to increased integrity risk.

3.2.1 H_1 Case. The vertical protection limit under the hypothesis of a failure (VPL_{H_1}) on any given reference receiver is given by (2.21). In this analysis, a Category 1 system with a class 'B3' ground facility ($M = 3$) and 'B' class airborne equipment is assumed as defined in Table 2.2. Although we will explicitly consider only variations in σ_{pr_gnd}, it should be noted that the method of analysis described below is in principle applicable to airborne and residual errors as well.

When the actual ground standard deviation (σ) differs from the nominal value ($\sigma_{pr\_gnd_1}$) used to generate VPL_{H_1}, the effective missed detection multiplier for the computed value of VPL_{H_1} is given by

$$k_{md_e} \equiv k_{md} \frac{\sqrt{\sum_{n=1}^{N} S_{zn}^2 \left[\frac{\sigma_{pr\_gnd_1,n}^2}{M_n - 1} + \sigma_{pr\_air,n}^2 + \sigma_{pr\_res,n}^2 \right]}}{\sqrt{\sum_{n=1}^{N} S_{zn}^2 \left[\frac{\sigma_n^2}{M_n - 1} + \sigma_{pr\_air,n}^2 + \sigma_{pr\_res,n}^2 \right]}} \tag{3.1}$$

where, $\sigma_{pr\_gnd_1} \equiv \sqrt{M}\sigma_{pr\_gnd}$, and k_{md} is a multiplier used to set the desired level of missed detection probability assuming gaussian errors. k_{md} holds a value of 2.898 for a Category I approach with three reference receivers (see Table 2.1).

Note that the B-value term in Equation (2.21) is not present here since it is invariant with respect to changes in σ. The associated MD probability is then

$$P_{H_1}(MD \mid \sigma_1, \ldots, \sigma_N) = Q(k_{md_e}) \tag{3.2}$$

where, the function $Q(x)$ is defined as the area to the right of x under a standard normal density function (i.e., the 'tail probability').

Clearly $P_{H_1}(MD)$ will in general be a strong function of satellite geometry through the projection matrix S. A GPS constellation simulation was therefore executed to establish this sensitivity. The details of the geometry simulation follow:

- *Constellation:* Nominal 24-satellite constellation as defined in RTCA DO-229A.
- *Elevation Mask:* 5 degree
- *Simulated Duration:* 24 hours
- *LGF Location:* Chicago O'Hare International Airport
- *SV Outage Conditions:* Both the complete 24-satellite constellation and worst-case (most sensitive) 22-satellite constellation subsets were simulated.

Geometries not meeting $VPL_{H_0} < VAL$ using the nominal value of σ_{pr_gnd} were excluded since aircraft approaches would not be conducted in these cases.

In the first set of simulations, all 24 Space Vehicles (SVs) were assumed to be usable, and the true standard deviation (σ) was varied from nominal ($\sigma_{pr\_gnd_1}$) on all visible SVs. The resulting integrity risk is shown in Figure 3.1 as a function of $\sigma/\sigma_{pr\_gnd_1}$. The discrete distribution of data points along the horizontal ($\sigma/\sigma_{pr\_gnd_1}$) direction in the figure corresponds to the discrete values of $\sigma/\sigma_{pr\_gnd_1}$ simulated. The vertical distribution of data points at each value of $\sigma/\sigma_{pr\_gnd_1}$ is due to the varying geometries accumulated over a 24-hour period. The upper bound integrity risk curve (solid) represents the highest level of integrity risk over the 24-hour duration. Note that when $\sigma/\sigma_{pr\_gnd_1} = 1$, the missed detection probability attains a nominal value of $Q(k_{md}) = 0.0019$.

Given that all 24 satellites are available, the results in Figure 3.1 are undoubtedly conservative since it is unlikely that broadcast σ_{pr_gnd} would underestimate the true error standard deviation for *all* visible satellites. In this regard, a second simulation was performed varying σ on only one (the most integrity-risk-sensitive) satellite for each geometry. The results are shown in Figure 3.2. When compared with the results of Figure 3.1, integrity risk is reduced for values of $\sigma/\sigma_{pr\_gnd_1} > 1$ (as expected) but increased for values of $\sigma/\sigma_{pr\_gnd_1} < 1$.

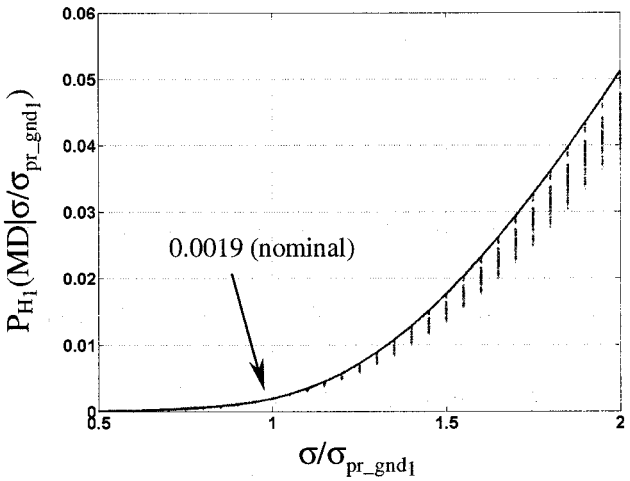

Figure 3.1 H_1 Integrity Risk Sensitivity to σ-Variations -- 24 SV Case
(σ Varied on All SVs In View)

The latter increase is due to the fact that σ is reduced on only one SV (in contrast with Figure 3.1 where σ was reduced on all SVs). Figure 3.3, which superposes the upper bound curves from Figures 3.1 and 3.2, clearly shows the difference in integrity risk sensitivity under the two sets of assumptions.

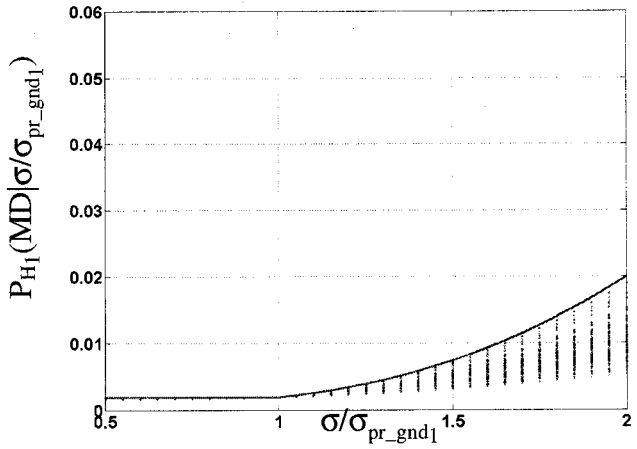

Figure 3.2 H_1 Integrity Risk Sensitivity to σ-Variations -- 24 SV Case
(σ Varied on Worst-Case SV Only)

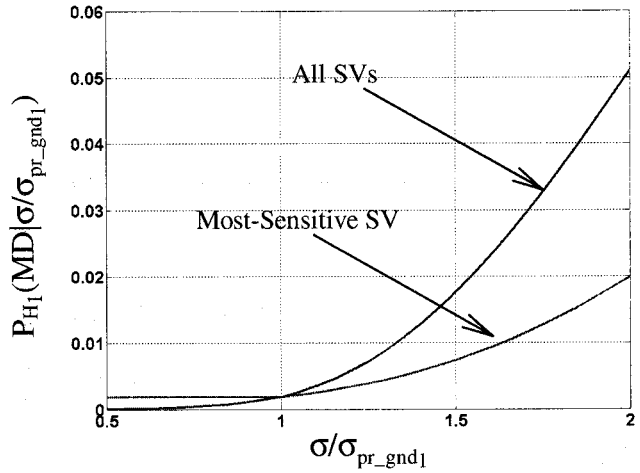

Figure 3.3 H_1 Integrity Risk Sensitivity to σ-Variations -- 24 SV Case
(Upper Bound Curves from Figures 3.1 and 3.2)

In general, however, it cannot be assumed that all 24 satellites will always be available for use. For example, existing simulation results of LAAS operational availability in the LAAS standard [MASPS98] are based on the worst-case (lowest resulting availability) 22 satellite subset geometries. In this context, the simulations

executed above were repeated for all 22-satellite subset geometries. The resulting upper bound sensitivity curves assuming σ variation on all satellites and σ variation only on a single (most sensitive) satellite are shown in Figure 3.4. The results clearly show that in the presence of a modestly depleted constellation, there is little difference in integrity risk sensitivity for the two approaches. This result is readily explained by the fact that when fewer satellites are available the effects in the position domain due to ranging error variations on individual geometry-critical satellites are more pronounced. For our analysis, we can conservatively define the actual integrity risk sensitivity curve for the H_1 case as a piecewise superposition of the two curves in Figure 3.4. Therefore, for any value of $\sigma/\sigma_{pr\_gnd_1}$, the upper of the two curves is used.

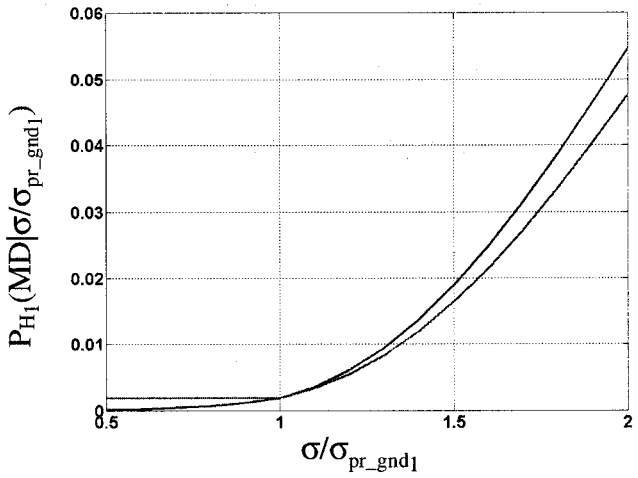

Figure 3.4 H_1 Integrity Risk Sensitivity to σ-Variations, 22 SV Case. (Upper Bound Curves)

Given that the conditional probability $P_{H_1}(MD \mid \sigma/\sigma_{pr\_gnd_1})$ has been established, it is still necessary to define a distribution for $\sigma/\sigma_{pr\_gnd_1}$ such that the overall risk probability can be quantified. In this regard, it is well known that the sample variance $\hat{\sigma}^2$ of n_s independent measurements derived from a gaussian distribution is Chi-Square distributed:

$$(n_s - 1)\frac{\hat{\sigma}^2}{\sigma^2} \sim \chi^2_{n_s-1} \tag{3.3}$$

Thus, for a given computed value of $\hat{\sigma}$, the probability that σ lies in any specified range is easily computed. For example, Figure 3.5 shows the resulting probability mass function $P(\sigma/\sigma_{pr\_grd_1} \mid \hat{\sigma}/\sigma_{pr\_gnd_1}, n_s)$ for the case where $\hat{\sigma}/\sigma_{pr\_gnd_1} = 0.9$ and $n_s = 20$.

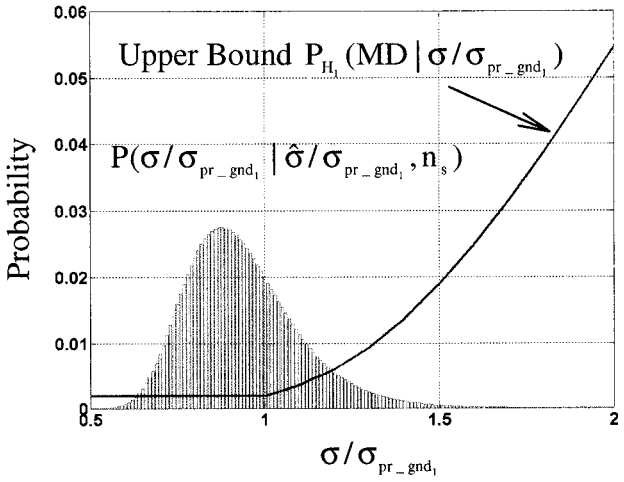

Figure 3.5 Probability Distribution for $\sigma/\sigma_{pr\_gnd_1} = 0.9$ $n_s = 20$

The result is plotted together with the conditional $P_{H_1}(MD|\sigma/\sigma_{pr\_gnd_1})$ curve already established.

Clearly, despite the fact that $\hat{\sigma}$ is lower than $\sigma_{pr\_gnd_1}$ for this case, the likelihood that the actual value of σ exceeds $\sigma_{pr\_gnd_1}$ is non-negligible. As the number of available samples, n_s, is increased, however, the likelihood that σ exceeds σ_{pr_gnd} decreases. Figure 3.6 illustrates the case where $n_s = 80$. Similarly, if the computed value of σ is lower, the likelihood that σ exceeds $\sigma_{pr\_gnd_1}$ is also lower. Figure 3.7 shows the case where $n_s = 20$ and $\hat{\sigma}/\sigma_{pr\_gnd_1} = 0.7$. A parametric analysis was performed in which n_s was varied with discrete values 20, 50, 100, 200 and 500, and $\hat{\sigma}/\sigma_{pr\_gnd_1}$ between 0.7 and 1.3 (in increments of 0.01).

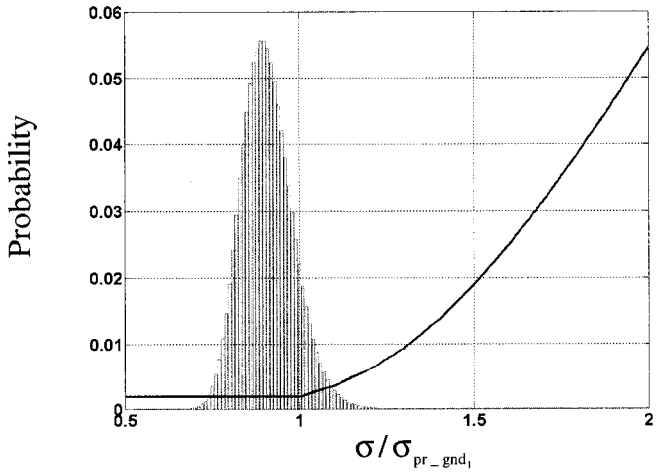

Figure 3.6 Probability Distribution for $\hat{\sigma}/\sigma_{pr\_gnd_1}$ for $\hat{\sigma}/\sigma_{pr\_gnd_1} = 0.9$, $n_s = 80$

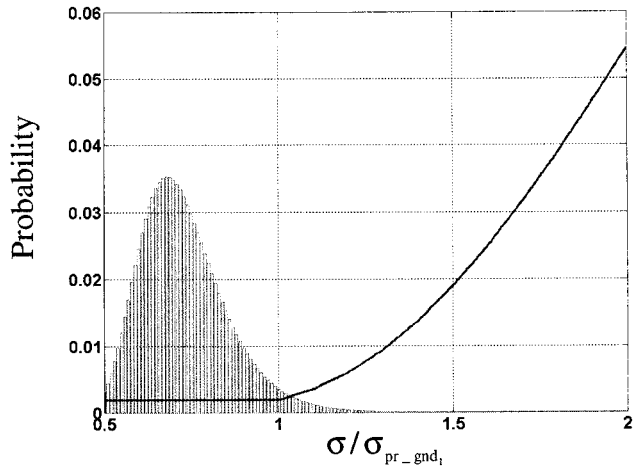

Figure 3.7 Probability Distribution for $\hat{\sigma}/\sigma_{pr\_gnd_1}$ for $\hat{\sigma}/\sigma_{pr\_gnd_1} = 0.7$, $n_s = 20$

The overall H_1 missed detection probability given $\hat{\sigma}/\sigma_{pr\_gnd_1}$ and n_s was then computed numerically via

$$P_{H_1}\left(MD|\hat{\sigma}/\sigma_{pr\_gnd_1}, n_s\right) = \sum_{\sigma} P_{H_1}\left(MD \mid \sigma/\sigma_{pr\_gnd_1}\right) \times P\left(\sigma/\sigma_{pr\_gnd_1} \mid \hat{\sigma}/\sigma_{pr\_gnd_1}, n_s\right) \quad (3.4)$$

The results are plotted in Figure 3.8, which shows quantitatively how the H_1 missed detection probability increases as $\hat{\sigma}/\sigma_{pr\_gnd_1}$ increases and as n_s decreases. The results are plotted in terms of percentage error (above the nominal value of 0.0019) in Figure 3.9.

To ensure integrity in an absolute sense $P_{H_1}\left(MD \mid s/\sigma_{pr\_gnd_1}, n_s\right)$ should not exceed the nominal specified value of 0.0019. However, the results in Figure 3.9 show that this criterion cannot be realistically attained because an infinitely large sample set is required.

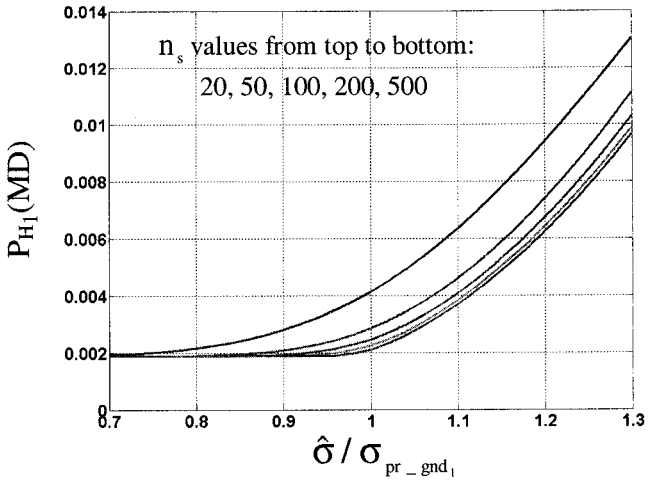

Figure 3.8 H_1 Integrity Risk Versus $\hat{\sigma}/\sigma_{pr\_gnd_1}$

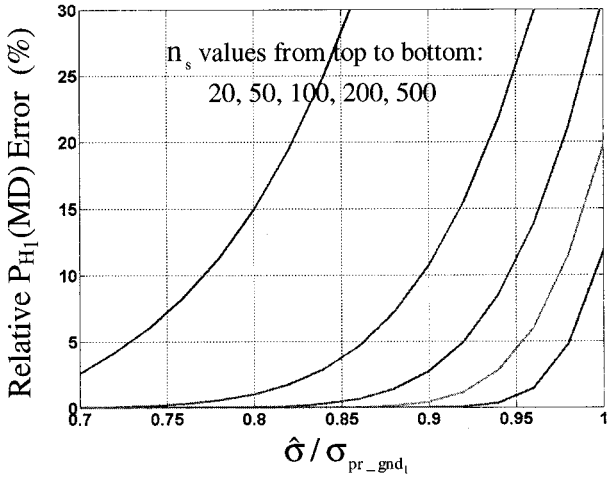

Figure 3.9 H_1 Integrity Risk Versus $\hat{\sigma}/\sigma_{pr\_gnd_1}$ (Relative Error)

Nevertheless, it can be ensured that the missed detection probability does not differ from the nominal value by a significant amount. For example, Table 3.1 summarizes the results obtained from Figure 3.9 assuming that a 5% tolerance is acceptable. Under this assumption, the table quantifies the minimum value of $\sigma_{pr\_gnd_1}$ that may be broadcast

given any value of $\hat{\sigma}$ obtained from n_s samples. Clearly, the broadcast $\sigma_{pr\_gnd_1}$ must in general be larger than $\hat{\sigma}$. As expected, however, the buffer factor (the amount by which $\hat{\sigma}$ must be scaled to define $\sigma_{pr\_gnd_1}$) approaches 1 as n_s grows large. (Note that the quantitative results in Table 3.1 apply for the H_1 case only.)

Table 3.1 Sigma Buffer Factor for H_1

n_s	Minimum Value of $\sigma_{pr\_gnd_1}$
20	$1.31\times\hat{\sigma}$
50	$1.16\times\hat{\sigma}$
100	$1.09\times\hat{\sigma}$
200	$1.05\times\hat{\sigma}$
500	$1.02\times\hat{\sigma}$

3.2.2 H_0 Case. For the fault–free hypothesis, the vertical protection limit is given by Equation (2.20). When the actual ground standard deviation (σ) differs from the nominal value ($\sigma_{pr\_gnd_1}$) used to generate VPL_{H_0}, the effective missed detection multiplier for the computed value of VPL_{H_0} is given by

$$k_{md\_ff_e} \equiv k_{md\_ff} \frac{\sqrt{\sum_{n=1}^{N} S_{zn}^2 \left[\frac{\sigma_{pr\_gnd_1,n}^2}{M_n} + \sigma_{pr\_air,n}^2 + \sigma_{pr\_res,n}^2 \right]}}{\sqrt{\sum_{n=1}^{N} S_{zn}^2 \left[\frac{\sigma_n^2}{M_n} + \sigma_{pr\_air,n}^2 + \sigma_{pr\_res,n}^2 \right]}} \tag{3.5}$$

where, k_{md_ff} is 5.810 for Category 1 approach with three reference receivers (see Table 2.1). The associated MD probability is

$$P_{H_1}(MD \mid \sigma_1,...,\sigma_N) = 2Q(k_{md\_ff_e}) \tag{3.6}$$

The factor of 2 in Equation (3.6) is present for H_0 case because the underlying fault-free distribution has a zero mean, and therefore both positive and negative errors are of interest. The sensitivity analysis executed for the H_1 case was repeated for H_0. The resulting sensitivity of missed detection probability for the H_0 case is quantified in Figure 3.10. As with the H_1 case, the integrity risk $P_{H_0}\left(MD \mid \hat{\sigma}/\sigma_{pr\_gnd_1}, n_s\right)$ increases as $\hat{\sigma}/\sigma_{pr\_gnd_1}$ increases and as n_s decreases. In Figure 3.11, the results of Figure 3.10 are plotted in terms of percentage error (relative to the nominal value of $2Q(k_{m\_dff}) = 6.2\times10^{-9}$).

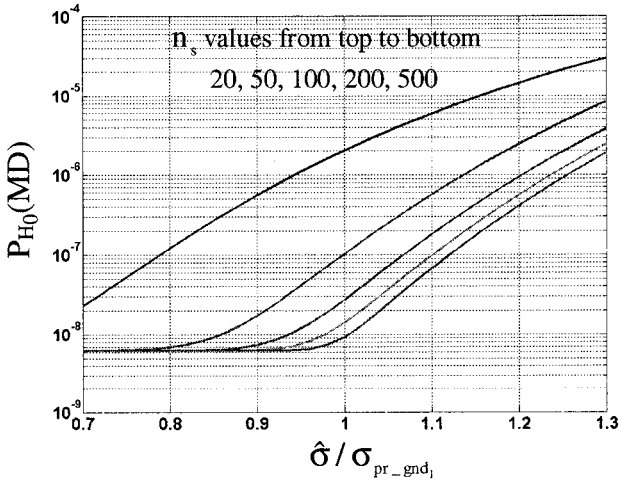

Figure 3.10 H_0 Integrity Risk Versus $\hat{\sigma}/\sigma_{pr\_gnd_1}$

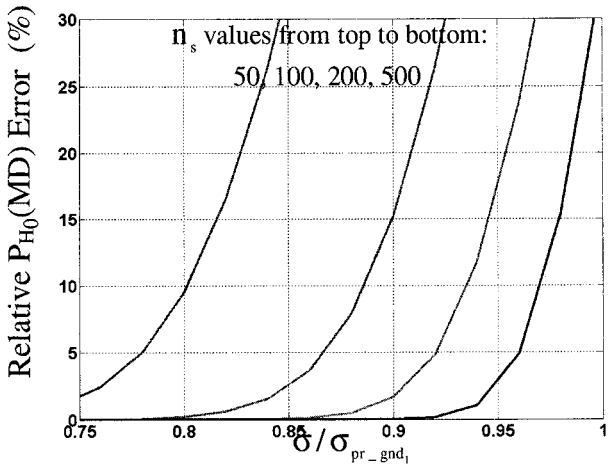

Figure 3.11 H_0 Integrity Risk Versus $\hat{\sigma}/\sigma_{pr\_gnd_1}$ (Relative Error)

The results of the H_0 σ-sensitivity analysis are summarized in Table 3.2, where a 5% missed detection tolerance (relative to nominal) has again been used. As with the H_1 case, the buffer factor approaches 1 as n_s becomes very large. Note that, in general, H_0 σ-sensitivity is greater than that found for the H_1 case. This is due to the fact that a small variation in σ for a gaussian random variable will cause a larger relative deviation in probability from the nominal value when the nominal probability is small.

Table 3.2 Sigma Buffer Factors for H_0

n_s	Minimum Value of $\sigma_{pr\_gnd_1}$
20	$1.46\times\hat{\sigma}$
50	$1.29\times\hat{\sigma}$
100	$1.16\times\hat{\sigma}$
200	$1.09\times\hat{\sigma}$
500	$1.04\times\hat{\sigma}$

Comparing the buffer factors in Table 3.2 with those in Table 3.1, it is clear that H_0 is the more restrictive case (i.e., the required buffer factors are larger). Table 3.2 therefore serves to define the minimum σ buffer factor.

3.3 Correlation Sensitivity Analysis

In the preceding analysis, it was implicitly assumed that ranging errors were uncorrelated across ground receivers. Note, in fact, that any such correlation is not consistent with the VPL equations since the $\sigma_{pr\_gnd_i}$ terms are always divided by the number of receivers (to account for the averaging of uncorrelated receiver measurements). In reality, however, it is possible that some measurable correlation exists. Furthermore, even if a negligibly small correlation coefficient is computed from a finite sample set, the statistical uncertainty in the estimate must also be accounted for. Such uncertainty is lessened, as one would naturally expect, as the sample size used to estimate correlation coefficient increases.

To examine sensitivity to correlation, we assume that the ground error standard deviation for any given reference receiver is $\sigma_{pr\_gnd_i}$. The effect of positive correlation between receivers when averaging M^* errors can be (with modest conservatism) modeled as an effective increase in σ as follows:

$$\sigma = \sigma_{pr\_gnd_i}\sqrt{1+(M^*-1)\rho} \tag{3.7}$$

where ρ is the maximum correlation coefficient between any pair of receivers, $M^* = M$ for H_0, and $M^* = M-1$ for H_1. The sigma sensitivity analysis results (in particular, the satellite geometry simulations) are directly applicable to correlation sensitivity as well through the following simple transformation:

$$\rho = \frac{(\sigma/\sigma_{pr\_gnd_1})^2 - 1}{M^* - 1} \tag{3.8}$$

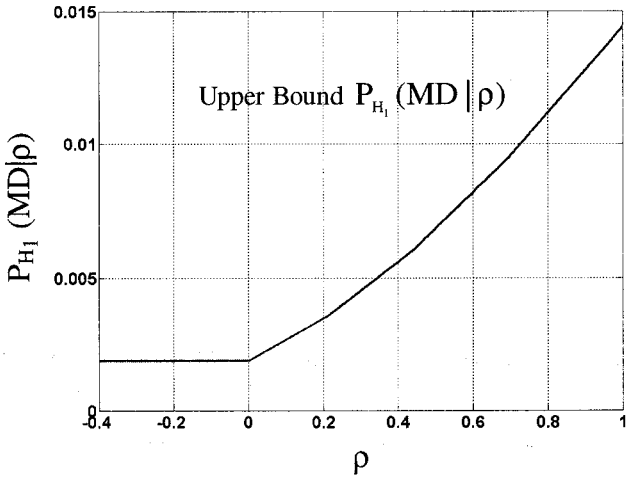

Figure 3.12 H_1 Integrity Risk Sensitivity to ρ - Variations, 22 SV Case. (Upper Bound Curves)

3.3.1 H_1 Case. Using the transformation above, the horizontal axis of Figure 3.3 may be rescaled in terms of ρ. The resulting upper bound curve for the conditional probability $P_{H_1}(MD|\rho)$ is shown in Figure 3.12. Now, given any pair of reference receivers, each with n_r samples of measurement error, we may compute a sample correlation coefficient r. To define a distribution for ρ given r, we use a similar approach to that in the sigma analysis except that the Chi-Square distribution no longer

applies. Instead, we make use of the Fisher Z statistic [Bendat86], which is approximately gaussian:

$$Z \equiv \tfrac{1}{2}\ln\left(\frac{1+r}{1-r}\right) \sim N_z\left[\tfrac{1}{2}\ln\left(\frac{1+\rho}{1-\rho}\right), (n_r - 3)^{-\frac{1}{2}}\right] \tag{3.9}$$

Figure 3.13 illustrates an example probability mass function $P(\rho \mid r, n_r)$ for $r = 0.3$, $n_r = 20$ and finely spaced intervals of ρ. (The $P_{H_1}(MD \mid \rho)$ curve from Figure 3.12 is overlayed.) A parametric analysis was then executed in which n_r varied with discrete values 20, 50, 100, 200, and 500 and r varied between -0.2 and 0.3. The overall H_1 missed detection probability given ρ and n_r was then computed numerically using a summation procedure equivalent to the sigma sensitivity case. The results are plotted in Figure 3.14, which shows quantitatively how the H_1 missed detection probability increases as r increases and as n_r decreases.

When compared to the nominal missed detection probability for H_1 (0.0019) substantial increases in relative integrity risk are clearly evident in the results. However, this is a not unexpected result because the VPL equations have no direct means to accommodate effect of positive correlation, and furthermore, integrity risk is magnified by uncertainty in correlation coefficient. Note, however, that in principle correlation can be accounted for by simply increasing the value of $\sigma_{pr\_gnd_i}$. For example for precisely

known values of error standard deviation (σ) and correlation coefficient (ρ) we may use any value of $\sigma_{pr\_gnd_1}$ such that

$$\sigma_{pr\_gnd_1} > \sigma\sqrt{1+(M^*-1)\rho} \tag{3.10}$$

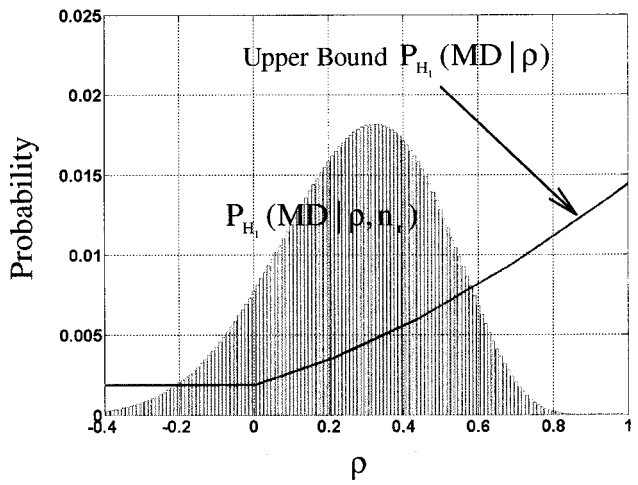

Figure 3.13 Probability Distribution for ρ given $r = 0.3$, $n_s = 20$

However, to account for the fact that σ is not known precisely (only the estimate $\hat{\sigma}$ based on n_r samples is available), σ in Equation (3.10) above must be replaced with $a(n_s)\hat{\sigma}$, where $a(n_s)$ is the scale factor defined in Table 3.2. Similarly, because ρ cannot be known precisely (only the correlation coefficient estimate r based on n_r samples is available), ρ must be replaced in Equation (3.10) with a buffered value ρ^*, where ρ^* is a function of r and n_r that is yet to be defined.

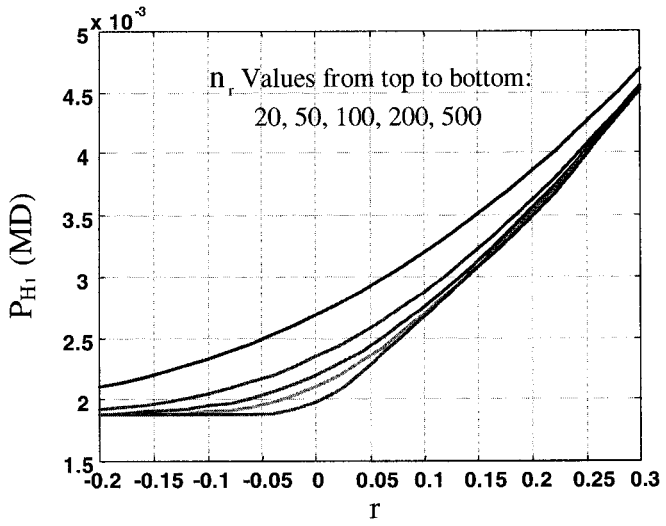

Figure 3.14 H_1 Integrity Risk Versus r

To determine the required value of ρ^* for a given number or samples n_r, the conditional probability $P(MD \mid \rho)$ was recomputed assuming that the value of $\sigma_{pr\_gnd_1}$ has already been buffered using the Equation (3.10) for selected values of ρ^* between 0 and 0.5. The resulting curves are given in Figure 3.15. Note that the curve corresponding to $\rho^* = 0$ (which represents the case where there is no buffering on $\sigma_{pr\_gnd_1}$) is identical to the $P(MD \mid \rho)$ curve in Figure 3.12. As expected, the influence of non-zero correlation coefficient on integrity risk is decreased as ρ^* is increased (i.e., as the buffer on $\sigma_{pr\_gnd_1}$ is increased).

For each of the ρ^* curves in Figure 3.15, it is possible to compute $P_{H_1}(MD \mid r, n_r)$ as was done for the $\rho^* = 0$ case in Figure 3.13. For example, the results for n_r = 20 are plotted in Figure 3.16. Note that the uppermost curve, which corresponds to the case

$\rho^* = 0$, is identical to the $n_r = 20$ curve on Figure 3.14. For a 5% acceptable tolerance on integrity risk relative to the nominal value of 0.0019, it is possible to obtain from Figure 3.16 the maximum value of r allowable for a given value of ρ^*.

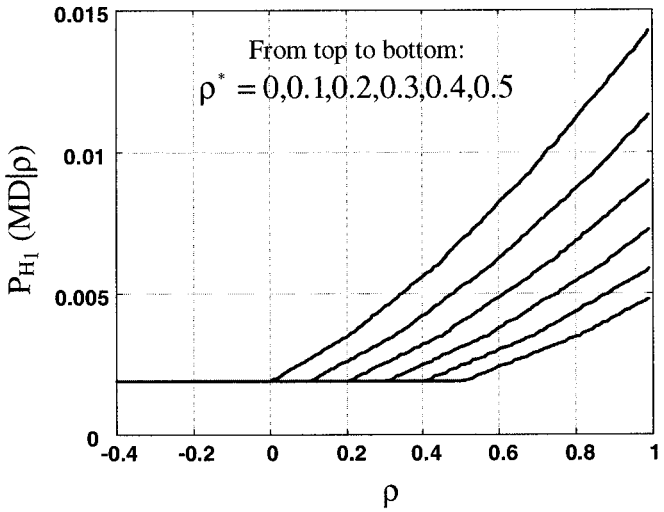

Figure 3.15 H_1 Integrity Risk Sensitivity to ρ - Variations, 22 SV Case. (With Correlation Buffering)

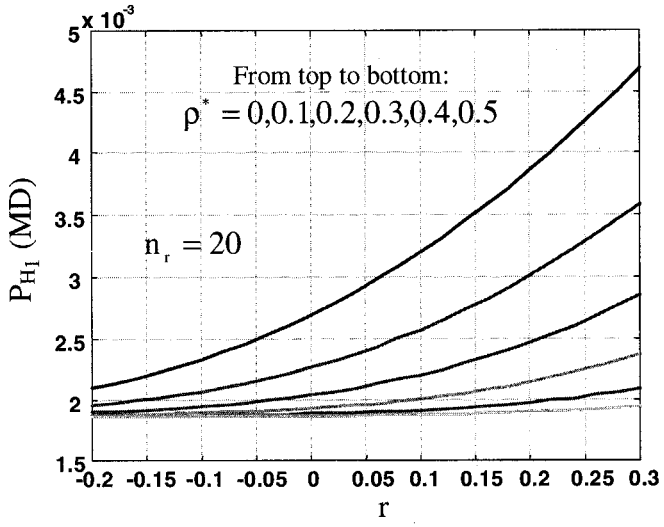

Figure 3.16 H_1 Integrity Risk Versus r (With Correlation Buffering)

This result can also be interpreted as the minimum value of ρ^* given a computed correlation coefficient estimate, r. Figure 3.17 shows the results for the $n_r = 20$ case under consideration and also for values of n_r equal to 50, 100, 200, and 500. It is clear from Figure 3.17 that a nearly linear relationship (with unity slope and positive y-intercept) exists between r and the minimum acceptable value of ρ^*. The (minimum) ρ^* can thus be approximately defined by the simple linear functions in Table 3.3.

Table 3.3 Correlation Buffer Parameters for H_1

n_r	Minimum Value of ρ^*
20	0.26 + r
50	0.14 + r
100	0.08 + r
200	0.05 + r
500	0.02 + r

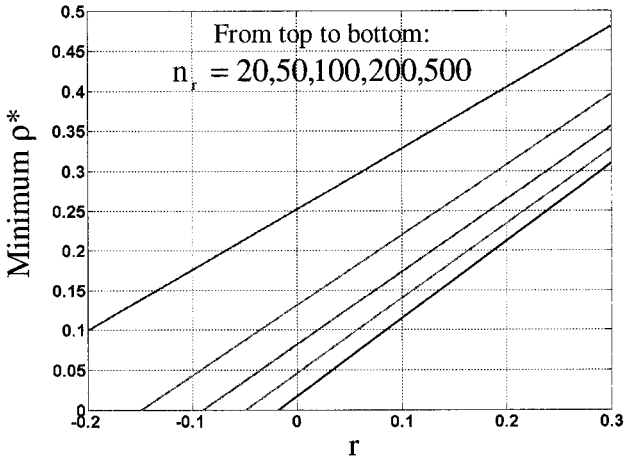

Figure 3.17 Minimum ρ^* for 5% H_1 Integrity Risk Tolerance

Note that ρ^* must always be larger than r in order to account for the statistical uncertainty due to a finite number of samples. As n_r becomes large, however, the minimum acceptable value of ρ^* asymptotically approaches r.

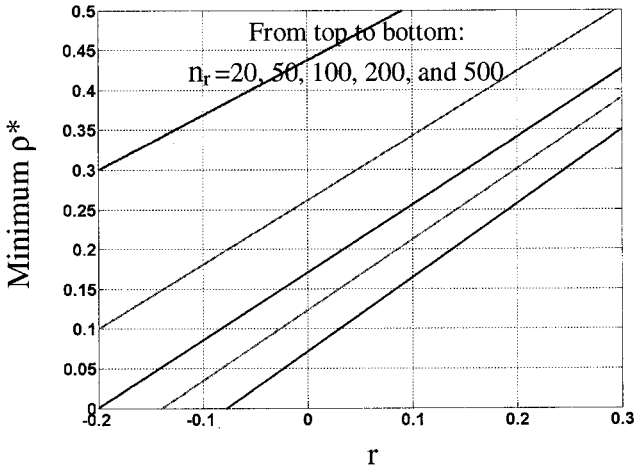

Figure 3.18 Minimum ρ^* for 5% H_0 Integrity Risk Tolerance

3.3.2 H_0 Case. The correlation sensitivity analysis executed for the H_1 case was repeated for H_0. Figure 3.18 shows the resulting minimum values of ρ^* given a computed correlation coefficient estimate r. Comparison of this figure with Figure 3.17 shows that, as with the sigma sensitivity analysis, the H_0 case is more restrictive because for a given computed value of r the value of ρ^* required to ensure a 5% integrity risk tolerance is larger for the H_0 case than the H_1 case. Hence the H_0 case must be the one used to define ρ^*. The approximate linear relations for H_0 derived from Figure 3.18 are given in Table 3.4.

Table 3.4 Correlation Buffer Parameters for H_0

n_r	Minimum Value of ρ^*
20	0.42 + r
50	0.27 + r
100	0.18 + r
200	0.12 + r
500	0.06 + r

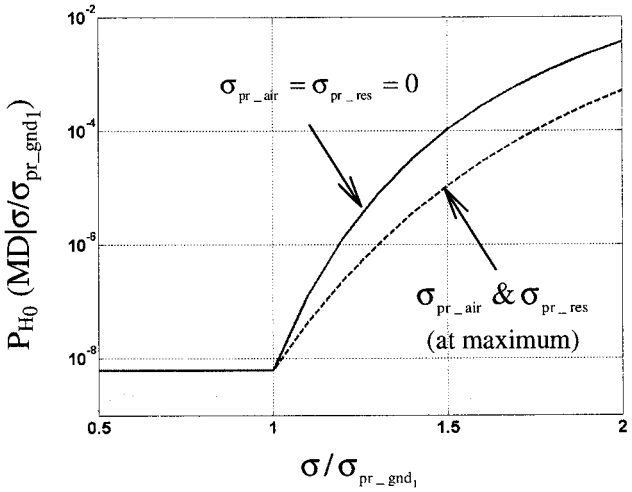

Figure 3.19 H_0 Integrity Risk Sensitivity to σ - Variations, 22 SV Case

3.4 Worst-Case Sensitivity

The results generated thus far have been based on the nominal functions for σ_{pr_air} and σ_{pr_res} defined in Chapter 2. Since these functions actually define the maximum permissible values for these parameters, in practical application it is likely that σ_{pr_air} and σ_{pr_res} will be smaller. In this case, it is expected that integrity risk will be more sensitive to variations in $\sigma_{pr\_gnd_1}$. It is therefore also instructive to examine the limiting scenario in

which σ_{pr_air} and σ_{pr_res} are zero. We consider here only the H_0 case (because it has already been shown to be more sensitive to variations in σ and ρ than H_1). In this regard, Figure 3.19 shows the upper bound curves for $P_{H_0}(MD \mid \sigma/\sigma_{pr\_gnd_1})$ for the 22 SV constellation case. The upper (solid) curve defines integrity risk sensitivity when σ_{pr_air} and σ_{pr_res} are zero. The lower (dashed) curve, which is included only for comparison, corresponds to the case already covered where σ_{pr_air} and σ_{pr_res} hold their maximum permissible values. It is clear that integrity risk sensitivity is increased for all values of $\sigma/\sigma_{pr\_gnd_1}$ greater than one. Note that in this region, where the curves are defined by the case where $\sigma/\sigma_{pr\_gnd_1}$ is varied on all satellites simultaneously, integrity risk sensitivity is invariant with respect to geometry for the case where σ_{pr_air} and σ_{pr_res} are zero. This is true since Equation (3.5) reduces to

$$k_{md\_ff_e} \equiv \frac{k_{md\_ff}}{\sigma/\sigma_{pr\_gnd_1}} \tag{3.11}$$

Using the same methodology described in the sections above, the minimum acceptable values for σ^* and ρ^* were computed assuming an acceptable integrity risk tolerance of 5%. These results are given in Table 3.5 for Category 1 approach and M = 3. Note, as expected, that the buffer parameters are slightly higher than those in Table 3.2 and Table 3.4 (which were derived using the maximum permissible values for σ_{pr_air} and σ_{pr_res}).

Table 3.5: Sigma/Correlation Buffer Parameters

(Results for Category 1 and M = 3)

n_s or n_r	Minimum σ^*	Minimum ρ^*
20	1.61×s	0.45 + r
50	1.34×s	0.30 + r
100	1.18×s	0.20 + r
200	1.10×s	0.13 + r
500	1.05×s	0.07 + r

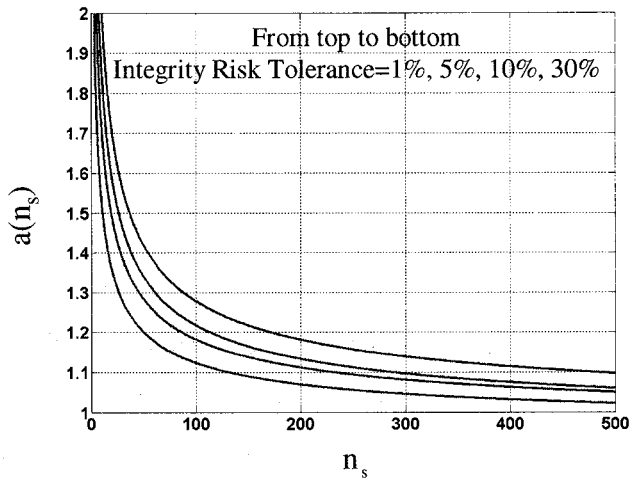

Figure 3.20 Sigma Buffer Factor Versus Number of Samples

3.5 Integrity Risk Tolerance

Taken together, the results of the sigma and correlation analyses above demonstrate that any value of σ_{pr_gnd} may be broadcast provided that the following inequality is satisfied:

$$\sigma_{pr\_gnd} > \sigma^* \sqrt{1+(M-1)\rho^*} \Big/ \sqrt{M} \tag{3.12}$$

where $\sigma^* = a(n_s)\hat{\sigma}$, $\rho^* = r + b(n_r)$, and $\hat{\sigma}$ and r are the maximum values of sample standard deviation and correlation coefficient for any receiver and reference receiver pair, respectively. For the Category 1 case with $M = 3$ and a 5% relative missed detection (integrity risk) tolerance, the values of a(.) and b(.) are given for a number of discrete values of n_s and n_r in Table 3.5.

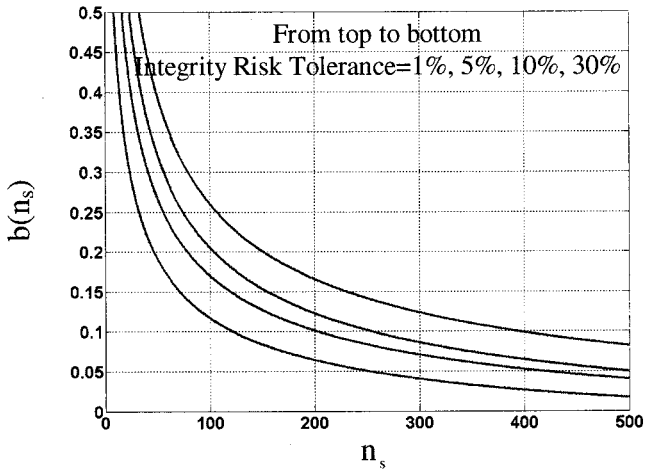

Figure 3.21 Correlation Buffer Factor Versus Number of Samples

Because the 5% integrity risk tolerance was arbitrarily selected, it is necessary to quantify how the buffer parameters vary with respect to integrity risk tolerance. In this regard, Figure 3.20 shows the required value of the σ buffer factor as a function of the number of samples for various values of integrity risk tolerance. As one would naturally

expect, the figure illustrates that for any given value of n_s, the buffer factor decreases as the integrity risk tolerance is relaxed.

Analogous behavior is exhibited for the required correlation buffer parameter in Figure 3.21. In both Figure 3.20 and Figure 3.21, it is also clear that only marginal reductions in buffer parameters will be realized for sample sets larger than 200 points. However, it is equally clear that sample sets smaller than 100 points will typically require rather large buffer parameters.

3.6 Conclusion

In this chapter, the sensitivity of LAAS integrity risk was investigated and quantified with respect to the statistical uncertainty in the knowledge of reference receiver error standard deviation and correlation between multiple reference receivers. A detailed methodology was presented to define the minimum acceptable buffer parameters for the value of σ_{pr_gnd} broadcast to the aircraft. This work implicitly addressed only the gaussian error structures associated with receiver-related noise and diffuse multipath. Additional effects of remaining errors, such as ground reflection multipath or systematic reference receiver/antenna errors are emphasized separately in Chapter 5.

CHAPTER IV

NON-ZERO MEAN GAUSSIAN RANGING ERROR

4.1 Introduction

LAAS navigation integrity risk is quantified at aircraft through the computation of Protection Levels. In the Protection Level algorithms, *zero-mean gaussian* distributions are assumed for each satellite's LGF broadcast correction error as well as aircraft ranging measurement error. In reality, however biases may exist in the ranging error of the LGF and/or the aircraft. Such biases may potentially be directly observed in data or may be purposely imposed as part of theoretical modeling. In either case, the existence of a mean value in the correction error can result unacceptable integrity risk; therefore, it must be accounted for in the sigma overbound. In LAAS, the sigma overbound implies a position error bound because the Protection Levels (VPL/LPL) are expressed in terms of aircraft position error. Thus, bounding a non-zero mean distribution in the ranging error domain (single error PDF) does not necessarily guarantee an overbound for the position error (multiple convolved PDFs). The satellite geometry (see Chapter 2 for *observation* and *projection* matrixes) adds further complexity to the bounding process.

4.2 Bounding Concept

An overbound for aircraft position error is needed when the true ranging error distributions are not zero-mean gaussian because, in LAAS, the aircraft assumes that the

broadcast sigma is a standard deviation of a zero-mean gaussian PDF. It is the responsibility of the LGF to provide a standard deviation of a zero-mean gaussian PDF that represents the true correction error distribution. In reality, however, situations may exist in which *non-gaussian* and/or *non zero-mean gaussian* distributions must be bounded.

Bounding for ranging error is defined as a method by which a sufficient zero-mean gaussian distribution is generated to overbound the tails of true aircraft position errors having non-gaussian or non-zero mean gaussian PDFs. To ensure the validity of bounding in the position domain, involves the convolutions of multiple non-gaussian PDFs (i.e., sum of non-gaussian RVs) and the convolution of the same number of gaussian PDFs. The resulting tail area Cumulative Distribution Functions (CDFs) are evaluated to determine whether the gaussian result overbounds the non-gaussian at the probability level of interest. The ratio of overbounding gaussian standard deviation to that of the non-gaussian PDF parameter is called the *Inflation Factor*. For example, the effect of ranging errors (e_n, $n = 1,2,3,...,N$) from N ($12 \geq N \geq 4$) satellites is projected into the vertical position error as:

$$e_v = \sum_{n=1}^{N} S_{zn} e_n \tag{4.1}$$

where S_{zn} is n^{th} element of the third row of the projection matrix detailed in Chapter 2. In terms of the *true* ranging error PDFs (f_n), the position error PDF is given by the convolution integral:

$$f_{e_t}(\varepsilon_v) = \frac{1}{\prod_n S_{3,n}} \int_{-\infty}^{\infty} \cdots \int_{-\infty}^{\infty} f_1\left(\frac{\varepsilon_v - \varepsilon_2}{S_{3,1}}\right) f_2\left(\frac{\varepsilon_2 - \varepsilon_3}{S_{3,2}}\right) \cdots f_N\left(\frac{\varepsilon_N}{S_{3,N}}\right) d\varepsilon_2 \cdots d\varepsilon_N \quad (4.2)$$

If all ranging errors are *assumed* gaussian (i.e., $e_n \sim N(0,\sigma_n)$), the vertical position error PDF will also be a gaussian, $f_{e_u}(\varepsilon_v) = \left(\sqrt{2\pi}\sigma_v\right)^{-1} \exp\left(-\varepsilon_v\left(2\sigma_v^2\right)^{-1}\right)$, with the following distribution:

$$e_v \sim N(0, \sigma_v) \quad (4.3)$$

where $\sigma_v = \sqrt{\sum_{n=1}^{N} S_{zn}^2 \sigma_n^2}$ is the vertical position error standard deviation. The bounding can be satisfied if the following inequality holds,

$$1 - \int_{\ell}^{\infty} f_{e_u}(\varepsilon_v) d\varepsilon_v \geq 1 - \int_{\ell}^{\infty} f_{e_t}(\varepsilon_v) d\varepsilon_v \quad (4.4)$$

where $\frac{1}{2}\left(1 - \int_{\ell}^{\infty} f_{e_u}(\varepsilon_v)\, d\varepsilon_v\right) = \frac{1}{4}\operatorname{erfc}\left(\ell/\sqrt{2}\right)$ is the area to right of ℓ under the standard normal density function (i.e., the tail probability; see Chapter 3 for $Q(\ell)$ function) and $\ell \equiv k\sigma_v$ is set for the desired probability level.

4.3 Mean Bounding for LAAS

As mentioned above, biases in ranging error are neither broadcast to the aircraft nor defined as a part of Protection Level Equations. Therefore, the existence such biases

must be accounted for by sigma overbounding. Overbounding non-zero mean gaussian distributions is easy in principle, but difficulties arise when the LGF and aircraft are unaware of distribution parameters corresponding to each other's error PDFs. For example, broadcast sigmas of correction error are *generated* at the LGF, *broadcast* to the aircraft, *combined* with sigmas of the aircraft, and then *used* in Protection Level equations at aircraft for the final *navigation integrity risk assessment* of precision landing. Both LGF and aircraft error statistics collectively must be considered in the mean bounding process. To precisely accommodate for the existence of a mean value in the correction error, the LGF must know aircraft ranging error distribution in order to generate an appropriate overbounding value of σ_{pr_gnd}. Unfortunately, the LGF obviously cannot know anything about the incoming aircraft errors. The critical problem, then, in the bounding process is to account for non zero LGF mean errors: 1) without prior knowledge of each other's error distribution parameters or 2) with predefined worst-case (maximum) mean values assumed at the LGF and/or aircraft.

A simple case of mean bounding is illustrated in Figure 4.1. Two non-zero mean gaussian PDFs and their convolution are plotted in first trace (upper trace). Then, a zero mean gaussian distribution, in second trace, is generated to overbound the convolved distributions. This is verified by CDF overbound at desired level of probability (see vertical dashed line) in third trace. Finally, two zero mean gaussian distributions are extracted from bounding distribution and are plotted in the lower trace. These are the overbound of individual non-zero mean gaussian distributions given in the first trace.

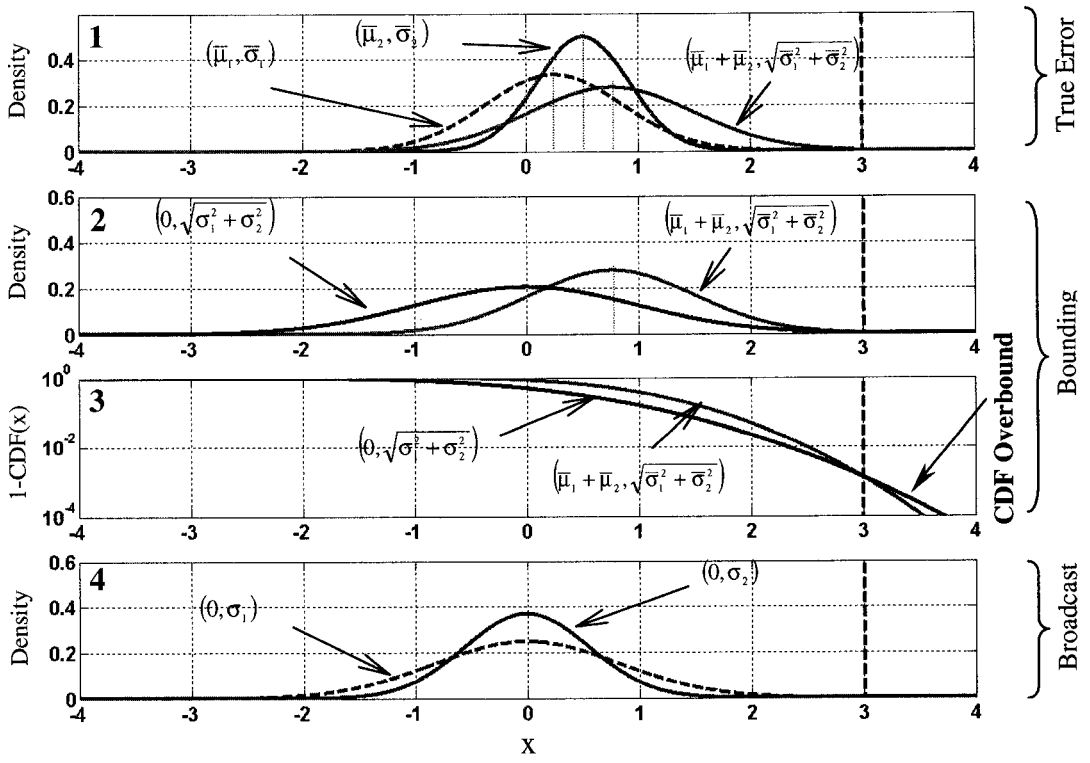

Figure 4.1 Gaussian Distribution Mean Bounding Concept

It is also noted that the mean values do not necessarily always have positive values. In reality, however, it is often only possible to define a bound on the absolute value of the mean ranging error (for example, from theoretical analysis ground multipath as described in Chapter 5). Therefore, for a conservative bound, the mean values can be assumed to be in the same direction (absolute values).

As described in Chapter 2, the computation of Protection Levels is based on a Weighted Least Square Estimation which is driven by the satellite geometry and ranging error covariance as described by Equation (2.19). In VPL, the sigmas are scaled with projection matrix elements. These elements change with satellite geometry. Therefore,

bounding is not a pure function of distribution parameters. Satellite geometries also add further complexity in bounding process. Let us recall the VPL equation and make a simple modification by grouping the error sources in terms of their association with LGF and aircraft,

$$VPL = k\sqrt{\sum_{n=1}^{N} S_{zn}^2 \left(\sigma_{gnd,n}^2 + \sigma_{air,n}^2\right)} \tag{4.7}$$

where, $k \equiv k_{md\_ff}$, $\sigma_{gnd,n}^2 \equiv \sigma_{pr\_gnd,n}^2 / M$, and $\sigma_{air,n}^2 \equiv \sigma_{pr\_air,n}^2 + \sigma_{pr\_res,n}^2$. Now, the *true* protection level equation (4.7) including biases can be expressed as VPL_{act} in the following form:

$$VPL_{act} = k\sqrt{\sum_{n=1}^{N} S_{zn}^2 \left(\overline{\sigma}_{gnd,n}^2 + \overline{\sigma}_{air,n}^2\right)} + \sum_{n=1}^{N} S_{zn} \left(\left|\overline{\mu}_{gnd,n}\right| + \left|\overline{\mu}_{air,n}\right|\right) \tag{4.8}$$

where, $\overline{\sigma}$ and $\overline{\mu}$ denote true values of sigmas and means describing the true error PDFs for the LGF and aircraft. The aircraft position error bound is desired and integrity is maintained if the following inequality holds,

$$VPL \geq VPL_{act} \tag{4.9}$$

In its expanded form, Equation (4.9) can be factored as follows,

$$\sum_{n=1}^{N} S_{zn}^2 \left(\sigma_{gnd,n}^2 + \sigma_{air,n}^2\right) \geq \left(1 + \frac{\sum_{n=1}^{N} S_{zn}\left(\left|\bar{\mu}_{gnd,n}\right| + \left|\bar{\mu}_{air,n}\right|\right)}{k\sqrt{\sum_{n=1}^{N} S_{zn}^2 \left(\bar{\sigma}_{gnd,n}^2 + \bar{\sigma}_{air,n}^2\right)}}\right)^2 \sum_{n=1}^{N} S_{zn}^2 \left(\bar{\sigma}_{gnd,n}^2 + \bar{\sigma}_{air,n}^2\right) \qquad (4.10)$$

We desire to define $\sigma_{gnd,n}$, $\sigma_{air,n}$ to ensure aircraft position error is bounded at desired level of probability of interest (defined by value of k). Such a bounding is ensured if for each satellite we require that,

$$\sigma_{gnd,n} \geq \xi \bar{\sigma}_{gnd,n} \qquad \sigma_{air,n} \geq \xi \bar{\sigma}_{air,n} \qquad (4.11)$$

where the *Inflation Factor* (ξ), a common multiplier for both LGF and aircraft sigmas, is

$$\xi = \left(1 + \frac{\sum_{n=1}^{N} S_{zn}\left(\left|\bar{\mu}_{gnd,n}\right| + \left|\bar{\mu}_{air,n}\right|\right)}{k\sqrt{\sum_{n=1}^{N} S_{zn}^2 \left(\bar{\sigma}_{gnd,n}^2 + \bar{\sigma}_{air,n}^2\right)}}\right) \qquad (4.12)$$

It is easily observed that the Inflation Factor (ξ) is a function of the true sigma and mean values for each satellite. Since ξ includes both LGF and aircraft statistical parameters, the bounding of mean values becomes a difficult task because the LGF is unaware of aircraft statistics prior sigma broadcast. Therefore solutions are sought that do not depend on knowledge of aircraft error distribution parameters. Three such solution approaches are examined here for accommodation of the possible existence of mean values: 1) a bounding is sought without any specific information regarding LGF

and/or aircraft error PDFs, 2) a conditional bounding is sought with predefined maximum values of mean at LGF and/or aircraft, and 3) a direct accommodation of mean values is sought by Alert Limit (i.e., VAL) buffering.

4.4 Unconditional Mean Bounding

An unconditional bounding method for ground error is introduced here to account for lack of aircraft information in bounding process. For example, let us recall the expanded form of Equation (4.9) and rewrite in the vector form as follows,

$$\left\|\sigma\right\|_2 \geq \left(\left\|\overline{\sigma}\right\|_2 + \frac{\left\|\overline{\mu}\right\|_1}{k} \right) \tag{4.13}$$

where, $\sigma = \left[S_{z1}\sigma_{gnd,1} \quad S_{z1}\sigma_{air,1} \quad S_{z2}\sigma_{gnd,2} \quad \cdots \quad S_{zN}\sigma_{air,N} \right]_{(1\times 2N)}$, $\overline{\sigma} = \left[S_{z1}\overline{\sigma}_{gnd,1} \quad S_{z1}\overline{\sigma}_{air,1} \quad S_{z2}\overline{\sigma}_{gnd,2} \quad \cdots \quad S_{zN}\overline{\sigma}_{air,N} \right]_{(1\times 2N)}$, $\overline{\mu} = \left[S_{Z1}\overline{\mu}_{gnd,1} \quad S_{Z1}\overline{\mu}_{air,1} \quad S_{Z2}\overline{\mu}_{gnd,2} \quad \cdots \quad S_{Zn}\overline{\mu}_{air,N} \right]_{(1\times 2N)}$, and N is the maximum number of satellites in view (by the LGF) at the time of sigma broadcast. The bias term can be bounded as (with its second norm) [Golub93],

$$\sqrt{2N}\left\|\overline{\mu}\right\|_2 \geq \left\|\overline{\mu}\right\|_1 \tag{4.14}$$

Applying this relation to inequality (4.13) results in the following expression, we can impose a more conservative requirement on $\left\|\sigma\right\|_2$ as follows.

$$\|\sigma\|_2 \geq \left(\|\overline{\sigma}\|_2 + \frac{\sqrt{2N}\|\overline{\mu}\|_2}{k} \right) \geq \left(\|\overline{\sigma}\|_2 + \frac{\|\overline{\mu}\|_1}{k} \right) \tag{4.15}$$

An even more conservative, but simpler bound can be defined.

$$\|\sigma\|_2 \geq \sqrt{2}\left(\left(\|\overline{\sigma}\|_2\right)^2 + \left(\frac{\sqrt{2N}\|\overline{\mu}\|_2}{k} \right)^2 \right)^{\frac{1}{2}} \geq \left(\|\overline{\sigma}\|_2 + \frac{\sqrt{2N}\|\overline{\mu}\|_2}{k} \right) \geq \left(\|\overline{\sigma}\|_2 + \frac{\|\overline{\mu}\|_1}{k} \right) \tag{4.16}$$

Now, let us expand this equation in the following form,

$$\sqrt{\sum_{n=1}^{N} S_{zn}^2 \left(\sigma_{gnd,n}^2 + \sigma_{air,n}^2 \right)} \geq \sqrt{2}\sqrt{\sum_{n=1}^{N} S_{zn}^2 \left(\overline{\sigma}_{gnd,n}^2 + \overline{\sigma}_{air,n}^2 \right) + \frac{2N}{k^2} \sum_{n=1}^{N} S_{zn}^2 \left(\overline{\mu}_{gnd,n}^2 + \overline{\mu}_{air,n}^2 \right)} \tag{4.17}$$

and then establish detailed mean bounding models from (4.17) as discussed next.

Model 1. Equation (4.17) is the most general form of bounding because it assumes that the mean values exist not only at LGF but also at aircraft. To date, the sigma generation and error processing for aircraft ranging error is not finalized and it is yet unclear whether biases will exist in the aircraft errors. In this analysis we consider all possible scenarios, including aircraft biases.

Case-1A: Mean values exist at the both LGF and aircraft. (i.e., $\overline{\mu}_{gnd,n} \neq 0$ *and* $\overline{\mu}_{air,n} \neq 0$*).* In this case, the following expressions can be written for the LGF broadcast and aircraft sigmas respectively,

$$\sigma_{gnd,n} \geq \sqrt{2}\sqrt{\overline{\sigma}^2_{gnd,n} + \frac{2N}{k^2}\overline{\mu}^2_{gnd,n}} \quad \sigma_{air,n} \geq \sqrt{2}\sqrt{\overline{\sigma}^2_{air,n} + \frac{2N}{k^2}\overline{\mu}^2_{air,n}} \tag{4.18}$$

It is clear that inequality (4.17) is preserved by (4.18) applied to each satellite individually.

Case-1B: Mean values exist only at the LGF (i.e., $\overline{\mu}_{gnd,n} \neq 0$ *and* $\overline{\mu}_{air,n} = 0$*).* In this case, the LGF and aircraft sigmas can be expressed as,

$$\sigma_{pr\_gnd,n} \geq \sqrt{2}\sqrt{\overline{\sigma}^2_{gnd,n} + \frac{N}{k^2}\overline{\mu}^2_{gnd,n}} \quad , \quad \sigma_{pr\_air,n} \geq \sqrt{2}\overline{\sigma}_{air,n} \tag{4.19}$$

In addition to the above two sub-cases, the biases may exist only at the aircraft (i.e., $\overline{\mu}_{gnd,n} = 0$ and $\overline{\mu}_{air,n} \neq 0$). Sigmas are inflated by $\sqrt{2}$ in Equation (4.19).

The results in the above two sub-cases are range domain bounds for the LGF and aircraft, respectively. As shown, these range domain bounds are sufficient to ensure a position error overbound. We can accommodate range error biases on individual satellites simply by assuming a zero mean and inflating sigma appropriately. The cost of such practicality and simplicity is an additional inflation on sigmas of aircraft even in

the absence of aircraft mean values. In other words, even if biases do not exist at the aircraft we still need to inflate aircraft sigmas by $\sqrt{2}$ in order to ensure a position domain error bound. However a lower inflation may be possible in some special cases. For example, in both sub-cases, N is assumed as maximum number of satellites in view; however, N need only be associated with the number of satellites whose distributions contain mean value. Such an assumption reduces the unnecessary inflation of LGF sigmas if some satellites in view do not have biases. In this case, the aircraft still needs to inflate its own sigmas by a factor of $\sqrt{2}$.

4.5 Conditional Mean Bounding

The solution in Model 1 does not require any knowledge of aircraft distribution parameters at the LGF. However, if some such knowledge is available, an alternative (less conservative) bounding model is possible. We specifically consider the case where it is known to the ground and aircraft that there exist a pre-defined maximum value for any bias.

Case-2A: Mean values exist at the LGF and aircraft (i.e., $\overline{\mu}_{gnd,n} \neq 0$ *and* $\overline{\mu}_{air,n} \neq 0$*).* To achieve a conservative bound, the following assumptions can be made at the LGF: $\overline{\sigma}_{air,n} = 0$ and $\overline{\mu}_{air,n} = \overline{\mu}_{air\_max,n}$. At the aircraft, the following assumptions can be made: $\overline{\sigma}_{gnd,n} = 0$ and $\overline{\mu}_{gnd,n} = \overline{\mu}_{gnd\_max,n}$. The resulting conservative inflation factors for the LGF and aircraft are, respectively,

$$\xi_{gnd} = \left(1 + \frac{\sum_{n=1}^{N} S_{zn} \left(\left| \overline{\mu}_{gnd,n} \right| + \left| \overline{\mu}_{air\_max,n} \right| \right)}{k \sqrt{\sum_{n=1}^{N} S_{zn}^2 \overline{\sigma}_{gnd,n}^2}} \right) \geq \xi \qquad \xi_{air} = \left(1 + \frac{\sum_{n=1}^{N} S_{zn} \left(\left| \overline{\mu}_{gnd\_max,n} \right| + \left| \overline{\mu}_{air,n} \right| \right)}{k \sqrt{\sum_{n=1}^{N} S_{zn}^2 \overline{\sigma}_{air,n}^2}} \right) \geq \xi \tag{4.21}$$

Case-2B: Mean values exist only at the LGF (i.e., $\overline{\mu}_{gnd,n} \neq 0$ *and* $\overline{\mu}_{air,n} = 0$*).* In this case, the following conservative assumptions can be made at the LGF: $\overline{\sigma}_{air,n} = 0$, and $\overline{\mu}_{air,n} = 0$. At the aircraft, the following assumptions can be made: $\overline{\sigma}_{gnd,n} = 0$ and $\overline{\mu}_{gnd,n} = \overline{\mu}_{gnd,max\_n}$. The new Inflation Factors for the LGF and aircraft are respectively,

$$\xi_{gnd} = \left(1 + \frac{\sum_{n=1}^{N} S_{zn} \left(\left| \overline{\mu}_{gnd,n} \right| \right)}{k \sqrt{\sum_{n=1}^{N} S_{zn}^2 \overline{\sigma}_{gnd,n}^2}} \right) \geq \xi \qquad \xi_{air} = \left(1 + \frac{\sum_{n=1}^{N} S_{zn} \left(\left| \overline{\mu}_{gnd\_max,n} \right| \right)}{k \sqrt{\sum_{n=1}^{N} S_{zn}^2 \overline{\sigma}_{air,n}^2}} \right) \geq \xi \tag{4.22}$$

In this model we assume ranging errors contain worst-case maximum mean values for each satellite. Therefore the use of this model requires the maximum mean values to be set prior broadcast and to also be known by aircraft. Additional work is needed for of such a model. In spite additional tasks in the implementation, this model may considerably reduce sigma inflation in some cases when compared to Model 1. In either of the above sub-cases (*Case-2a* and *Case-2b*), the overbounding sigmas can be formed as:

$$\sigma_{gnd,n} \geq \xi_{gnd} \overline{\sigma}_{gnd,n} \qquad \sigma_{air,n} \geq \xi_{air} \overline{\sigma}_{air,n} \tag{4.23}$$

Model 2. Since the use of either Model 1 or the conditional two sub-cases alone may result in highly inflated sigmas, an alternative is proposed here based on a synthesis of both Model 1 and the conditional sub-cases. As a loose bound, assuming there is no available information of the aircraft statistics at the LGF and aircraft, Model 1 can be used under any circumstances (whether or not biases actually exist). However at the aircraft, Model 1 and conditional bounds produce different results under different circumstances (mean values at aircraft or/and at LGF). Since both results accommodate mean values and we have no prior knowledge as to which bound is tighter is, an appropriate approach is to select the minimum value among the alternative results:

$$\sigma_{gnd,n} \geq \min\left\{\sqrt{2}\sqrt{\bar{\sigma}^2_{gnd,n} + \frac{2N}{k^2}\bar{\mu}^2_{gnd,n}}, \xi_{gnd}\bar{\sigma}_{gnd,n}\right\} \qquad \sigma_{air,n} \geq \min\left\{\sqrt{2}\sqrt{\bar{\sigma}^2_{air,n} + \frac{2N}{k^2}\bar{\mu}^2_{air,n}}, \xi_{air}\bar{\sigma}_{air,n}\right\} \quad (4.24)$$

where the first components of the terms in parenthesis are obtained from Equation (4.18), and the second terms are obtained from Equation (4.22). The additional sub-case for Model 2 is similarly established based on existence of mean values only at LGF. Results regarding these sub-cases are shown in Table 4.1.

4.6 Summary of Mean Bounding Models

Two mean bounding models are proposed. Each model consists of two sub-cases, corresponding to scenarios where the biases exist at the LGF and/or at the aircraft. It is shown that all of these models conservatively bound biases; therefore all are appropriate in the perspective of integrity. The significance of the Model 1 is that the bound does

not require any specific prior knowledge of aircraft error statistics. Model 2, however, requires some knowledge (maximum value) of predefined of error statistics corresponding to aircraft and LGF. The summary is shown in Table 4.1.

Table 4.1 Summaries of Mean Bounding Models for LAAS

	LGF	**Aircraft**
Model 1 Case 1A	$\sigma_{pr\_gnd,n} \geq \sqrt{2}\sqrt{\overline{\sigma}^2_{gnd,n} + \frac{2N}{k^2}\overline{\mu}^2_{gnd,n}}$	$\sigma_{pr\_air,n} \geq \sqrt{2}\sqrt{\overline{\sigma}^2_{air,n} + \frac{2N}{k^2}\overline{\mu}^2_{air,n}}$
Model 1 Case 1B	$\sigma_{pr\_gnd,n} \geq \sqrt{2}\sqrt{\overline{\sigma}^2_{gnd,n} + \frac{N}{k^2}\overline{\mu}^2_{gnd,n}}$	$\sigma_{pr\_air,n} \geq \sqrt{2}\overline{\sigma}_{air,n}$
Model 2 Case 2A	$\sigma_{gnd,n} \geq \min\left\{\sqrt{2}\sqrt{\overline{\sigma}^2_{gnd,n} + \frac{2N}{k^2}\overline{\mu}^2_{gnd,n}}, \xi_{gnd}\overline{\sigma}_{gnd,n}\right\}$ $\xi_{gnd} = \left(1 + \frac{\sum_{n=1}^{N} S_{zn}\left(\lvert\overline{\mu}_{gnd,n}\rvert + \lvert\overline{\mu}_{air\_max,n}\rvert\right)}{k\sqrt{\sum_{n=1}^{N} S^2_{zn}\overline{\sigma}^2_{gnd,n}}}\right)$	$\sigma_{air,n} \geq \min\left\{\sqrt{2}\sqrt{\overline{\sigma}^2_{air,n} + \frac{2N}{k^2}\overline{\mu}^2_{air,n}}, \xi_{air}\overline{\sigma}_{air,n}\right\}$ $\xi_{air} = \left(1 + \frac{\sum_{n=1}^{N} S_{zn}\left(\lvert\hat{\mu}_{gnd\_max,n}\rvert + \lvert\hat{\mu}_{air,n}\rvert\right)}{k\sqrt{\sum_{n=1}^{N} S^2_{zn}\hat{\sigma}^2_{air,n}}}\right)$
Model 2 Case 2B	$\sigma_{gnd,n} \geq \min\left\{\sqrt{2}\sqrt{\overline{\sigma}^2_{gnd,n} + \frac{N}{k^2}\overline{\mu}^2_{gnd,n}}, \xi_{gnd}\overline{\sigma}_{gnd,n}\right\}$ $\xi_{gnd} = \left(1 + \frac{\sum_{n=1}^{N} S_{zn}\left(\lvert\hat{\mu}_{gnd,n}\rvert\right)}{k\sqrt{\sum_{n=1}^{N} S^2_{zn}\hat{\sigma}^2_{gnd,n}}}\right)$	$\sigma_{air,n} \geq \min\left\{\sqrt{2}\overline{\sigma}_{air,n}, \xi_{air}\overline{\sigma}_{air,n}\right\}$ $\xi_{air} = \left(1 + \frac{\sum_{n=1}^{N} S_{zn}\left(\lvert\overline{\mu}_{gnd\_max,n}\rvert\right)}{k\sqrt{\sum_{n=1}^{N} S^2_{zn}\overline{\sigma}^2_{air,n}}}\right)$

4.7 Relationship Between Biases and Alert Limits

The existence of a non-zero mean value in the correction error can result in unacceptable integrity risk. Therefore, either the mean value must be specifically accounted for (e.g., using one of the methods defined above) or it must be shown to have a negligible effect on integrity. The second alternative is pursued here as an alternative.

The computed VPL is defined in Equation (4.7). When a mean error (μ_{pr_gnd}) exists, then the required VPL bound may be given by Equation (4.8). To illustrate the sensitivity of VPL to non-zero means, simulation results are presented in Figure 4.2. To generate this figure, a depleted constellation (22 out of 24 SVs) was used and a mean of magnitude of 0.2 m was assumed for all satellites. An approximate linear relationship between the computed VPL (using the nominal equation) and the actual value is exhibited. The residual integrity risk incurred by the existence of the mean is evident in the slope of this linear characteristic, which is larger than unity. In the most stringent interpretation of LAAS requirements, a slope greater than unity is unacceptable. Unfortunately, without sigma inflation, this situation is unavoidable since the LAAS VPL equation does not explicitly account for non-zero means. In a more practical interpretation of requirements, however, it is likely that the 10 m VAL requirement is actually conservative for LAAS Category I operation. The implication is that while a conservative 'threshold' VAL of 10 m is used for LAAS, an 'operational' value of approximately 12 m may actually be sufficient to ensure integrity. In this regard, it is only necessary to ensure that the slope of the linear characteristic is $12/10 = 1.2$ or lower. A geometry-independent upper bound for the actual VPL may be defined:

$$VPL_{act} \le \left(1 + \frac{\sqrt{N}\eta}{k_{md}}\right) VPL_{comp} \tag{4.25}$$

where $\eta = \max_n \left|\mu_{pr\_gnd,n} / \sigma_{pr\_gnd,n}\right|$. This bounding result also applies for the H_1 case (failed reference receiver) if H_0 is replaced with H_1 and k_{md_ff} is replaced with k_{md} (which

holds a minimum value of 2.878 for Category I). To ensure a limit slope of less than 1.2, it is sufficient to limit the acceptable value of η (which is simply the maximum magnitude of the mean relative to sigma in the range domain). For the worst case where $N_{max} = 12$, the maximum acceptable values of η are 0.335 and 0.167 for the H_0 and H_1 cases, respectively. Clearly, for both conditions to be met: $\eta < 0.167$. Note that this is a *sufficient condition* to ensure that the mean is negligible. It may be achieved either by verifying that the range-domain mean is small enough in comparison to the standard deviation or by inflating the broadcast standard deviation as necessary to ensure that the sufficient condition is satisfied.

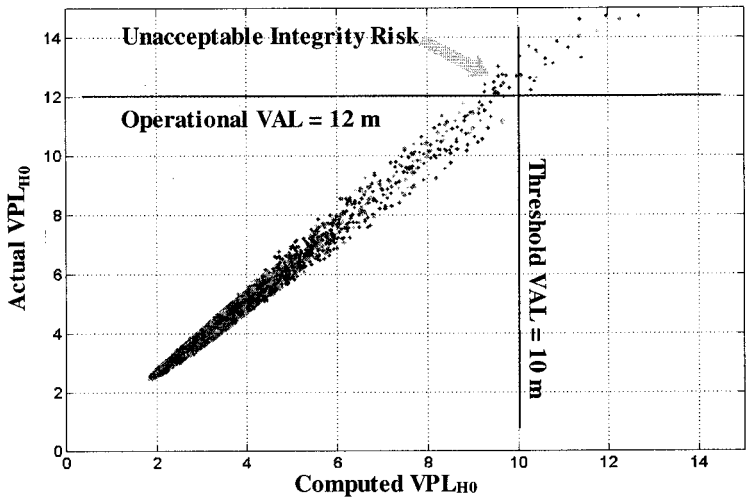

Figure 4.2. Actual VPL_{H_0} versus Computed VPL_{H_0} with Depleted Constellation (22 out of 24 Satellites)

Since the condition defined above is sufficient but not strictly necessary (in particular, it is conservative for good satellite geometries), alternatives are possible. For example, we may consider at the reference station (at any given time) all subset geometries that the

aircraft may use to compute VPL. First assume the largest specification-compliant values of standard deviation for *air* and *residual* (tropospheric and ionospheric uncertainty) errors, and for all candidate subset geometries compute both VPL_{H_0} and VPL_{H_1}. The LAAS ground station verifies that in all cases where these VPLs are less than 10 m the addition of the unaccounted for position domain mean term does not cause the actual bounding VPL to exceed 12 m. Note that by itself, this is not truly a sufficient condition because the *air* and *residual* standard deviation values used at the aircraft may be smaller than the maximum values assumed on the ground. If they are smaller at the aircraft, it is possible that geometries exist in which both VPLs computed on the ground exceed 10 m (and thus are not verified) but at the aircraft are slightly less than 10 m. To protect against such occurrences, the ground station would also have to consider a *range* of standard deviation values for *air* and *residual* below the largest values assumed above. Such an approach would probably be computationally intensive, but is possible in principle.

4.8 Conclusion

This chapter introduced a solution methodology to the bounding of biases in broadcast correction error. Candidate bounds are generated based on the presence of mean values not only at the LGF but also at the aircraft. These bounds are potentially useful in theoretical modeling of bias-like ground reflection multipath as well as experimentally observed hardware biases.

CHAPTER V

NON-GAUSSIAN RANGING ERROR

5.1 Introduction

The prescribed algorithms for the generation of the Protection Levels (VPL/LPL) assume a zero-mean normally distributed fault-free error model for the broadcast pseudorange corrections. The standard deviation of correction error is presumed by the aircraft to be equal to the broadcast value of σ_{pr_gnd} for each satellite. In reality, such a model is likely to be only consistent with receiver thermal noise error and diffuse multipath. However, additional errors such as ground reflection multipath and systematic reference receiver/antenna errors may not necessarily be gaussian or zero-mean. Any residual uncertainty unaccounted for in the true ranging error distribution will cause an impact on the integrity risk. Therefore, special care must be taken when generating a gaussian error distribution sigma for overbounding of such a non-gaussian distribution to guarantee the integrity risk at the desired level of probability at the aircraft. For example, the environmental factors affecting multipath may change with time; therefore the related uncertainty (i.e., the underlying error distribution) cannot be quantified by experimental means alone. This is particularly true for the 'tails' of the distribution where little or no empirical data will exist. Therefore, theoretical solutions are investigated in this chapter for establishment of broadcast σ_{pr_gnd} to accommodate such non-gaussian error sources. Furthermore, it is necessary to address *position domain*

bounding directly, since bounding in the range domain does not necessarily imply bounding in the position domain.

5.2 Ground Reflection Multipath

Multipath is a well-known cause of signal tracking error not only for GPS but also all types of Radio Frequency (RF) applications. It is caused by undesired reflected/diffracted signals from various surfaces in the near vicinity of the antenna. These surfaces can be the ground or other objects such as a building, a moving vehicle, or a tree. In general, due to the slowly varying nature of such environmental factors, it is unlikely that the effect of multipath error distributions can be quantified by experimental means alone. Collecting error data samples over many days (for example, for one year over all four seasons) may not reliably describe all variations of the error. There are two reasons for this: 1) sample sizes are limited and can be highly correlated over adjacent days; therefore, information about distribution tails cannot be easily extracted from a limited set of samples, and 2) for practical LGF initialization purposes it is impossible to rely on a long term error collection prior to system initialization.

Ground reflection multipath also can be resistant to filtering. For example, satellites at the same elevation but with different angular rates will have different multipath errors because for satellites with higher angular rates, carrier aided smoothing of pseudorange measurements (as discussed in Chapter 2) will for the most part mitigate multipath. This phenomenon can be explained by the noise attenuation performance of the smoothing filter, which is a function of filter bandwidth.

The persistency of ground reflection multipath error after the carrier-smoothing filter can be shown easily. For example, multipath error may be characterized by its doppler rate as:

$$\dot{\theta} = (4\pi h/\lambda)\dot{E}\cos E \tag{5.1}$$

where h is the antenna height as shown in Figure 5.1, λ is the GPS wavelength of 19 cm, and E and $\dot{E}$ are elevation and elevation rate, respectively.

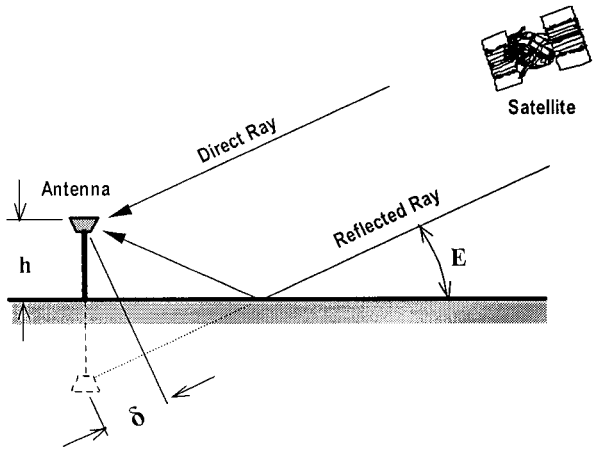

Figure 5.1 Ground Reflection Multipath

The bandwidth of the carrier smoothing filter loop is $1/2\tau$ Hz or $\pi/2\tau$ rad/s, where τ is the smoothing filter time constant. For example, if $\tau = 100$ second, so the bandwidth of the filter loop is 0.0314 rad/s. If the filter bandwidth is higher than the multipath doppler rate then the smoothing filter is unable to attenuate the multipath error. [Enge99].

In Figure 5.2, an example of noise attenuation versus antenna height is illustrated by simulating the GPS constellation of 24 satellites at O'Hare International Airport, Chicago. In the top trace of the figure, for an antenna height of 2 meters, the filter is unable to attenuate errors caused by the ground reflection multipath. However, in the bottom trace, for h=10 meters, the filter is more effective in attenuating noises because the height of the antenna is relatively tall leading to longer multipath delay and faster multipath Doppler. The LAAS Test Prototype antennas have a height of approximately 3 meters, so most ground reflection multipath will not attenuated by the smoothing filter.

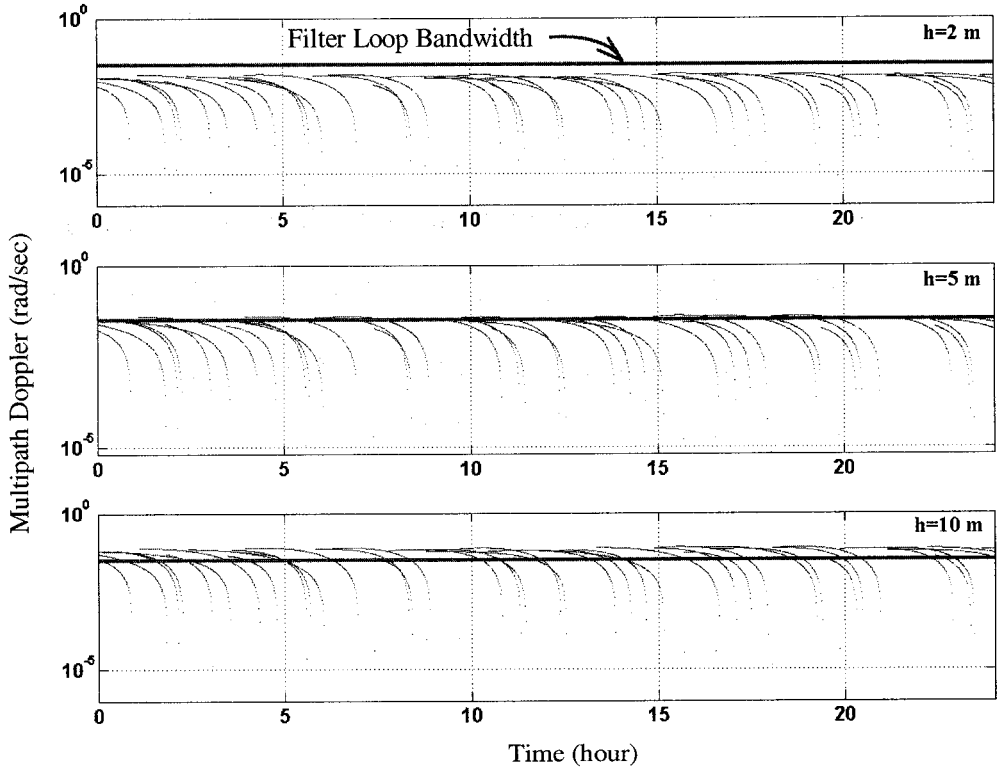

Figure 5.2 Ground Reflection Multipath Attenuation with Respect to Antenna Height (24 Satellites at Chicago, O'Hare Airport)

It is noted that a discrete object's reflection multipath error can be modeled in a similar manner but the delays are usually longer because of the larger reflection distances between antenna and reflection surfaces (relative to ground reflection). Therefore, the doppler rate for such multipath naturally is high. Secondly, an important characteristic of discrete object reflection multipath is the duration of reflected signals. The satellite position and reflection surface orientations may produce a specific geometry that contributes multipath for a longer duration of reflected signal but at a faster Doppler rate. In contrast, some geometries may contribute shorter durations of multipath and slower Doppler rates. In either case, the filter smoothing can successfully average out these types of error. The ground reflection multipath, unlike these cases, contains both disadvantages: longer duration of multipath and very slow doppler rate. In this chapter, therefore, theoretical approaches are emphasized only for ground reflection multipath error. Two candidate distribution models are proposed for the establishment and inflation of correction error standard deviation to account for the effect of ground reflection multipath.

5.2.1 Error Model. In this analysis, a Multipath Limiting Antenna (MLA) implementation is assumed at the LGF. Under this assumption, the amplitude of the ground-reflected signal relative to the direct signal is less than $-30\,\text{dB}$ (0.032). The intention of making such an assumption is not necessarily to restrict LAAS ground implementations to the use of the MLA, but instead to make the task of demonstrating at least one acceptable means for sigma establishment more easily tractable. In response, an error model for ground multipath was developed from [Braasch96] by neglecting second order and higher terms in α (since $\alpha^2 << 1$) as follows:

$$e = \min[\delta, d]\alpha\cos\theta \tag{5.2}$$

where, e is the ranging error due to ground reflection multipath, α is the amplitude of reflected signal relative to direct, θ is the phase of reflected signal relative to direct, d is the GPS receiver Delay Lock Loop (DLL) half correlator spacing (e.g., 0.05 chip or 15 m), and $\delta = 2h\sin E$ is the multipath delay (see Figure 5.1 for antenna-satellite-ground configuration). The envelope of ground reflection multipath error versus its delay is qualitatively sketched in Figure 5.3.

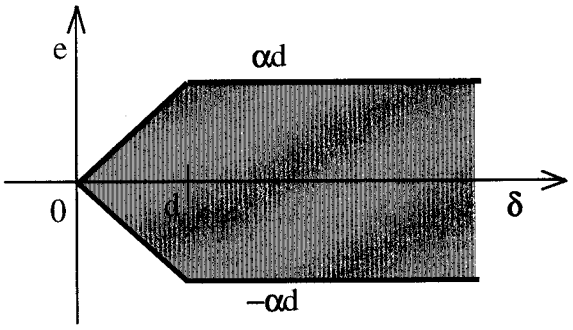

Figure 5.3 Multipath Error Envelope Versus Multipath Delay

An important observation from this sketch is that the maximum ground reflection multipath error depends on the magnitude of delay for short delays, whereas it is only a function of correlator spacing for long delays. This implies that the LAAS Test Prototype (LTP) ground reflection multipath is a function of delays rather than correlator spacing because the ground reflection multipath at high elevation and at antenna height of order of three meters do not exceed value 15 meters of correlator spacing,

5.2.2 Randomness in Ground Reflection Multipath. In the ground reflection multipath error model (5.2), the first term, $\min[\delta, d]$, is associated with antenna height, satellite position, and receiver correlator spacing. Since these values are known for any given site and satellite position, they may be defined as a constant value $c = \min[2h \sin E, d]$. Dividing ground reflection multipath by c results in the following normalized ground reflection multipath (NMP) error:

$$\hat{e} = e/c = \alpha \cos\theta \tag{5.3}$$

In principle, NMP is a deterministic error source. However, it is impossible to fully characterize the physical/spatial characteristics and temporal variation in the local RF environment. Therefore, it is treated as a random error in this analysis. In the NMP error model, there are two variables: 1) relative signal strength, α, and 2) relative phase, θ. These two quantities will be treated as random variables. Candidate models for their distributions are described below. The goal is to define a worst-case, realistic distribution for these quantities for use in the overbounding analysis.

Relative Phase Variation: A uniform phase distribution (θ varies randomly between 0 and 2π) is a widely used model distribution in RF applications. Such a model is also consistent with the assumption that the phase varies over widely spaced days between 0 and 2π due to small changes in reflection surface height and reflectivity for a given satellite elevation. Thus, θ is first treated as a uniformly distributed random variable: $\theta \sim U(0,2\pi)$. The corresponding PDF is:

$$f_\theta(\theta) = \begin{cases} 1/2\pi & 0 \le \theta \le 2\pi \\ 0 & \text{otherwise} \end{cases} \tag{5.4}$$

A second model for the phase, namely, a constant value of phase (worst-case scenario), is also considered. In making such an assumption, the effect of phase variation is directly eliminated since a constant value of phase is passed through the cosine function. In this case, for example, the relative phase distribution can be expressed by the following PDF.

$$f_\theta(\theta) = \delta_\theta(\theta - 2\pi) \tag{5.5}$$

where δ_θ is the Dirac delta function. It is noted that passing a zero value of phase variation in cosine function produces the same result as above PDF. However the PDF is described by Equation (5.5) is selected as representative case.

Since we have defined candidate PDFs for relative phase variation, now, a new random variable, $z = \cos\theta$, can now be introduced. With a uniform phase variation, $\theta \sim U(0,2\pi)$, corresponding PDF of z becomes,

$$f_z(z) = \begin{cases} \dfrac{1}{\pi\sqrt{1-z^2}} & -1 \le z \le 1 \\ 0 & \text{otherwise} \end{cases} \tag{5.6}$$

which is plotted in Figure 5.4. It can be easily observed that this PDF is *symmetric*, *bi-modal*, and has *singularity* at $z = \pm 1$. Bi-modality and singularity are important

characteristics and they lead to difficulties in bounding process since the position domain bounding condition requires multiple convolutions of such PDFs. Therefore, spatial care is taken when using this non-gaussian ranging error distribution for bounding.

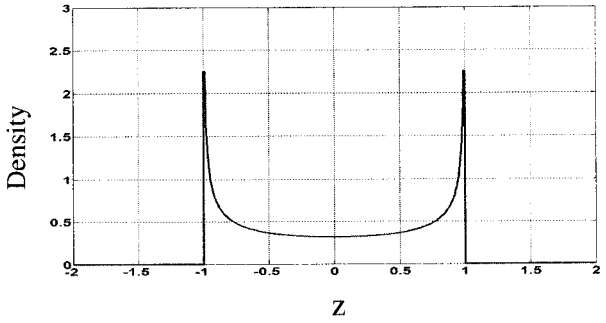

Figure 5.4. Probability Density for Random Variable z

With a constant phase, $f_z(z)$ becomes:

$$f_z(z) = \delta_z(z-1) \tag{5.7}$$

In this case, the relative signal strength (α) distribution will be the only effective random source in the final PDF (as the PDF of a product of two independent random variables, α and z).

Relative Signal Strength: A worst-case constant value, b, is assumed for reflection amplitude, α. The PDF is expressed as:

$$f_\alpha(\alpha) = \delta(\alpha - b) \tag{5.8}$$

An upper limit for this constant value can be defined from the performance of Multipath Limiting Antenna (MLA) used in LAAS Test Prototype (LTP) as plotted in the upper trace of Figure 5.10 as a function of satellite elevation.

5.3 Candidate Models

The NMP error is a product of α and z. Since two distributions are defined for random variable z and a single distribution is defined for α, it is possible to generate two model distributions for NMP error as products of α and z. These models refer to two special cases (limit cases): 1) *an obtainable worst-case symmetric zero-mean distribution* (a bi-modal distribution) of ground reflection multipath error, and 2) *a mean value* (a bias-offset) of ground reflection multipath error.

In Appendix A, additional less conservative two models for ground reflection multipath are explored, but the usefulness of these models is contingent on their experimental validation.

5.3.1 Model-1: Constant value of α and Uniformly distributed θ. With this model, the NMP error will be simply a product of a constant value of relative signal strength ($\alpha = b$, see Figure 5.10 for b values) and the random variable, z. The resulting PDF of NMP error is,

$$f_{\varepsilon}(x)=\begin{cases}\dfrac{1}{\pi b\sqrt{1-(x/b)^2}} & -b\le x\le b\\ 0 & \text{otherwise}\end{cases} \tag{5.9}$$

The associated CDF of NMP error is:

$$F_{\varepsilon}(x)=\begin{cases}0 & x<-b\\ \dfrac{1}{2}+\dfrac{1}{\pi}\sin^{-1}\dfrac{x}{b} & -b\le x\le b\\ 1 & x>b\end{cases} \tag{5.10}$$

One simple and conservative approach to defining an overbound, is to treat NMP error as a mean offset $\mu=b$. In this case we may apply the results for mean overbounding derived in Chapter 4: With 12 satellites, to protect an operation VAL of 12 m with a threshold VAL of 10 m, it must be that $b<0.167\sigma$. Thus NMP error will be overbounded with a gaussian with $\sigma \ge 6.02b$. In the general case where corrections for $N<12$ satellites are broadcast by the ground station $\sigma \ge (5\sqrt{N}/k_{md})b$ is sufficient.

It is important to clarify that this result is directly applicable for a constant phase model, but it is conservative for the uniform phase model under consideration. The reason is that the NMP error actually varies between $+b$ and $-b$, while the mean overbound assumes the worst-case magnitude and sign for each satellite. To accommodate the uniform phase model, we consider the direct convolution of the Model-1 PDFs. In the analysis that follows, we rely on the fact that it is only strictly necessary

to overbound above 2.878σ (set by the minimum k_{md} value for VPL_{H_1}) for linear combinations of up to 12 satellites.

Direct analytical convolution of Model 1 PDFs yields integrals that are not tractable in closed form. The characteristic function (Fourier Transform) of the Model 1 PDF can be readily shown to be a Bessel Function of the first kind. However, the inverse Fourier Transform of products (equivalent to convolution in the range domain) of Bessel Functions is not readily accessible in closed form. Furthermore, direct numerical convolution of Model 1 PDFs is also difficult since the PDF function has singularities at $\pm b$, requiring impractically fine discretization for accurate results. To circumvent these difficulties, we introduce a conservative approximation for the Model 1 PDF as follows:

$$f_{\hat{e}}(x) = \tfrac{1}{2}[\delta(x-b) + \delta(x+b)] \tag{5.11}$$

The associated CDF of NMP error is:

$$F_{\hat{e}}(x) = \begin{cases} 0 & -b < x \\ \dfrac{1}{2} & -b \le x < b \\ 1 & x \ge 1 \end{cases} \tag{5.12}$$

A graphical comparison of the actual Model 1 PDF and this conservative model is shown in Figure 5.5.

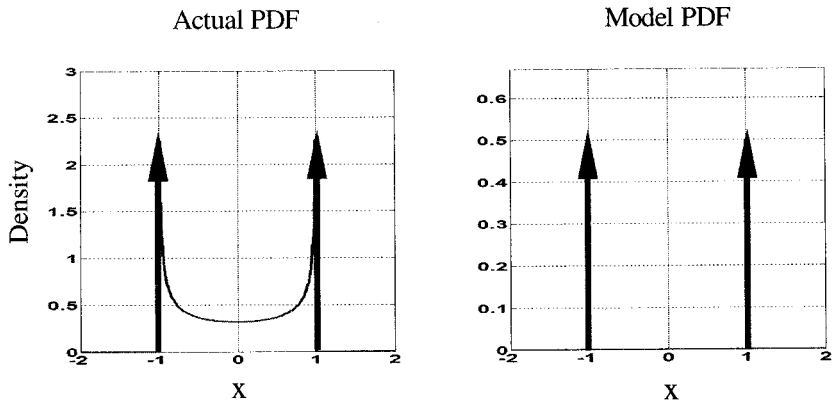

Figure 5.5 Actual PDF Approximation to a Conservative PDF

We first consider the hypothetical limiting case of a convolution of a large number of Independent, Identically Distributed (IID) sources. In this case, the Central Limit Theorem (CLT) defines the necessary bounding value of sigma for the actual PDF $\sigma \geq \sigma_{\hat{e}} = b/\sqrt{2}$ and for the conservative model $\sigma \geq \sigma_{\hat{e}} = b$. Unfortunately, while this result holds when N is very large, it is not sufficient for finite values of N. For the example case where $N = 9$, the CDF plots in Figure 5.6 show that using a gaussian PDF with $\sigma = \sigma_{\hat{e}} = b$ does not always overbound in the region of interest (above 2.878).

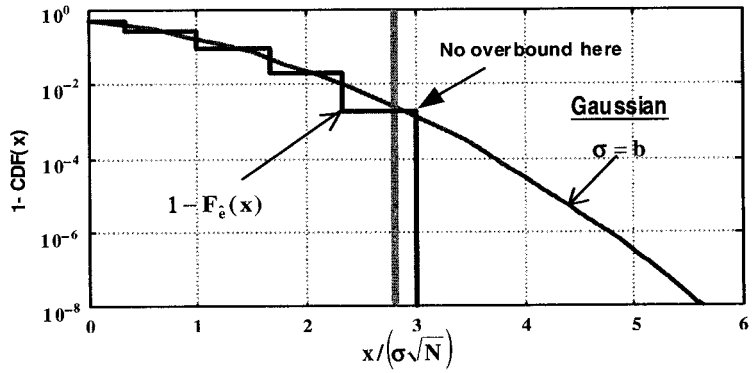

Figure 5.6 Convolution of Nine Model-1 Sources Compared with Convolution of Nine Gaussian Sources

From this example, it is clear that further inflation of the gaussian σ will be necessary to ensure CDF overbounding. For a given satellite n, we consider the NMP error, $\hat{e}_n$, is distributed according to the model:

$$\hat{e}_n \sim \tfrac{1}{2}[\delta(x-\beta_n)+\delta(x+\beta_n)] \tag{5.13}$$

Since $\sigma_n = \beta_n$, the maximum possible NMP error resulting from a linear combination of the N sources is:

$$\hat{e}_{max} \equiv \max \sum_{n=1}^{N} \hat{e}_n = \sum_{i=1}^{N} \beta_n = \sum_{n=1}^{N} \sigma_n \le \sqrt{N}\sqrt{\sigma_1^2+\sigma_2^2+\ldots+\sigma_N^2} \equiv \sqrt{N}\sigma_{tot} \tag{5.14}$$

Equality (largest e_{max}) in the bound above occurs when all β_n are the same (i.e., N IID sources). In this case, no inflation of σ_n is required when $\sqrt{N} \le 2.878$ ($N \le 8$) since the error will never exceed $2.878\sigma_{tot}$. In general, an inflation/deflation factor of $\sqrt{N}/2.878$ may be used in the range domain to ensure that the position domain NMP error never exceeds $2.878\sigma_{tot}$. For example, for $N = 12$, an inflation factor of 1.204 is implied. However, a zero probability of exceeding $2.878\sigma_{tot}$ is clearly not necessary. We only require that the gaussian bounds the actual NMP error in the CDF sense above $2.878\sigma_{tot}$. A sufficient inflation factor of 1.05 is obtained from direct convolution of N

(IID) sources. This result is sufficient for all N up to 12 (and conservative for $N < 9$). Figure 5.7 illustrates the CDF overbounding results for $N = 12$.

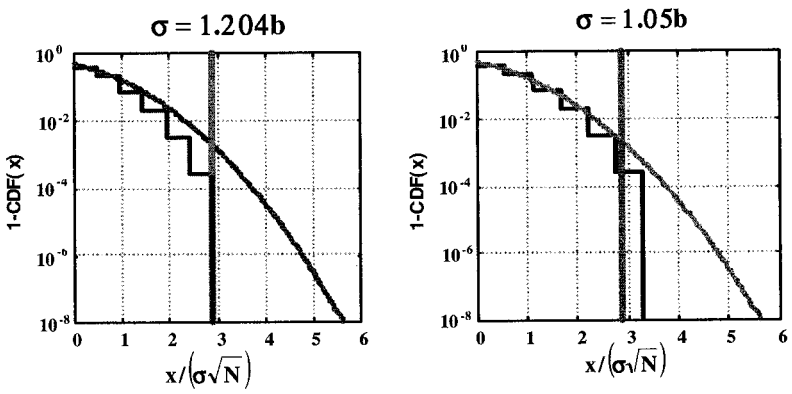

Figure 5.7 Overbound of Twelve Model 1 Sources with Gaussian Sources

We must also explicitly consider the effect of the addition of other contributing gaussian sources (due to diffuse MP and receiver noise). Clearly, the addition of such errors is not an issue in the following limiting cases:

- Gaussian sources are very small: Model 1 dominates, so an inflation factor of 1.05 is sufficient.
- Gaussian sources are very large: Model 1 errors are negligible by comparison (Model 1 inflation factor is irrelevant).

In cases where gaussian and Model 1 errors are of comparable size, the results are again evaluated by direct convolution. Figure 5.8 shows an example result of the convolution of $N = 12$ Model 1 sources and $N = 12$ gaussian sources.

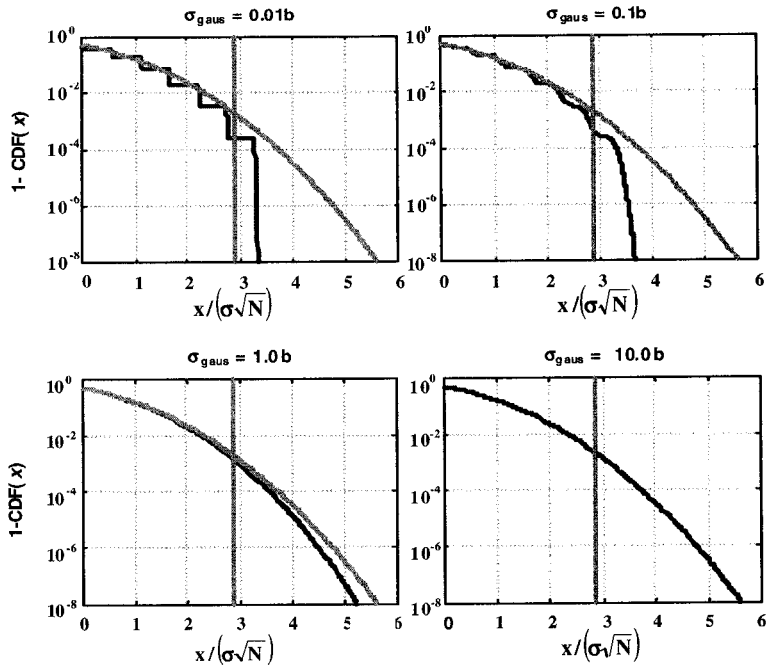

Figure 5.8 Convolution of Twelve Model-1 Sources with Twelve Gaussian Sources

An inflation factor of 1.05 was applied to overbound the Model 1 NMP error components. Each plot in Figure 5.8 corresponds to a different relative magnitude (0.01 to 10) of gaussian to ground multipath error. In all cases, the inflation factor of 1.05 is seen to be sufficient to ensure overbounding. Finally, the ground reflection multipath sigma can be written as

$$\sigma_e \geq 1.05bc \tag{5.15}$$

5.3.2 Model-2: Constant value of α and θ. With this model, the NMP error will be simply a product of a constant worst-case value of relative signal strength ($\alpha = b$, see upper trace of Figure 5.10) and a constant worst-case value of random variable, z. Here z

is unity because it is the largest output of cosine function (see Equation (5.7)). The normalized multipath error PDF for this case can be expressed as:

$$f_{\hat{e}}(x) = \delta(x - b) \tag{5.17}$$

and the associated CDF as,

$$F_{\hat{e}} = \begin{cases} 0 & x < b \\ 1 & x \geq b \end{cases} \tag{5.18}$$

With this PDF, the ground reflection multipath error is simply a bias value (i.e., normalized ground reflection multipath error $\mu_{\hat{e}} \geq b$):

$$\mu_e \geq bc \tag{5.19}$$

As previously discussed, the existence of a non-zero mean in the correction error can result in unacceptable integrity risk. Therefore, the mean value must either be specifically accommodated via sigma establishment or it must be shown to have a negligible effect on integrity. Both of these two alternatives are pursued in Chapter 4 under an assumption of non-zero mean gaussian ranging error distribution. The non-zero mean gaussian ranging error distribution is a combination of the above mean value (ground reflection multipath) and other gaussian error sources (receiver noise and diffuse multipath). The gaussian (or nearly gaussian) error sources in the broadcast correction,

such as receiver-related noise and diffuse multipath, are obtained by the direct use of experimental data. Proper processing for these error sources is discussed in Chapter 6 and Chapter 7 in detail.

5.3.3 Size of bc The lower trace of Figure 5.9 shows the size of product bc versus satellite elevation for three different antenna heights. The upper trace shows the relative signal strength, $b = \alpha$. The relative signal strength values are obtained from [Braff98] where they are specified as minimum requirements for MLA antennas for LAAS.

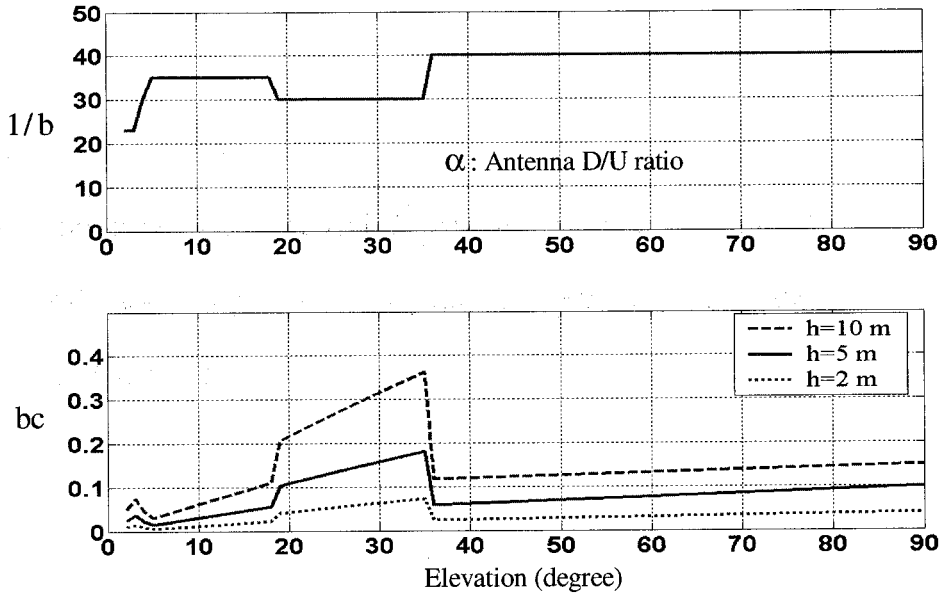

Figure 5.9 Size of Product bc Versus Satellite Elevation Angle for Three Different Antenna Heights

5.4 Summary of Error Models

Both models are summarized in Table 5.1 as follows:

Table 5.1 Summary of Non Gaussian Error Model

	Ground Reflection Multipath
Model 1 (Symmetric bi-modal)	$\sigma_e \geq 1.05bc$
Model 2 (Bias-type)	$\mu_e \geq bc$

Here, σ_e is a gaussian overbound of ground reflection multipath error where error distribution is modeled in the form of the *obtainable worst-case symmetric* PDF and μ_e is a gaussian overbound of ground reflection multipath error where error distribution is modeled in the form of *bias-type worst-case* PDF. Both quantities are functions of the product of relative signal strength and multipath delay, bc.

5.5 Conclusion

In this chapter, the effect of ground reflection multipath error has been investigated theoretically for the establishment of broadcast σ_{pr_gnd}. First, a new simple multipath error model, Equation (5.2), is developed from reference [Braasch96]. Then two non-gaussian distributions are generated to overbound ground reflection multipath error under limiting cases. Limiting cases are selected because of the difficulties in experimental validation of the physical underlying distribution. Finally, it is shown that knowing the antenna performance (b) is sufficient to describe a gaussian sigma or a mean value for ground reflection multipath.

CHAPTER VI

DATA QUANTIFICATION METHODOLOGY

6.1 Introduction

In Chapter 3, a detailed methodology was developed for the definition of minimum acceptable inflation parameters for the sample standard deviation to cover estimation uncertainties. In order for such an empirical process to be applied, it is necessary to define a proper method to collect data into bins prior to sigma estimation. While large bin sizes are desired to maximize sample size (to limit required inflation factors), bin size is ultimately constrained by the need for spatial stationary of all data within the bin (i.e., all error data within a bin must have the same underlying distribution). In this chapter, the quantitative resolution of this critical tradeoff, which is conceptually illustrated in Figure 6.1, has been addressed by an adaptive estimation method known as Expanding Bin method (EB-method). In addition, the effects of seasonal variations in pseudorange correction error (in particular multipath) are also accounted for in the broadcast σ_{pr_gnd}.

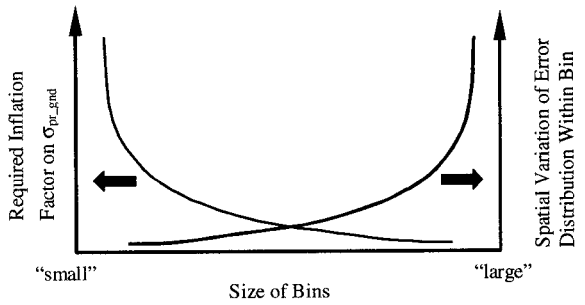

Figure 6.1 Sketch of Error Variation within Bins

6.2 Ranging Error Characteristics

In general, the pseudorange error has three important characteristics from the viewpoint of estimation. These are:

I. Repeatability

II. Serial Correlation

III. Nonstationarity

A simple illustration of data showing these characteristics is sketched in Figure 6.2. In the following analysis, we emphasize the quantification and accommodation of these characteristics in LAAS broadcast sigma establishment rather than their causes and mitigation.

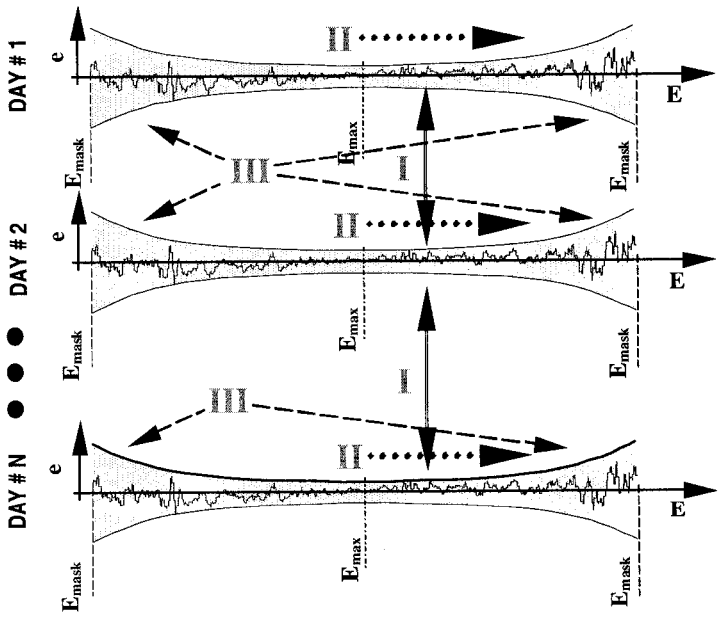

Figure 6.2 Sketch of Ranging Error Characteristics

I. Repeatability (Day-to-Day Correlation): It is well known that the ranging error, is generally repeatable (or correlated) day-to-day. The repeatability characteristic is mainly caused by multipath error and can be easily observed with a stationary (fixed) antenna when the environmental conditions are constant.

Because of the repeatability property, calibration of the error is possible in principle. For example, use of a prior day's error data to correct errors on the current day may reduce ranging error size. However, calibration is not always reliable since it assumes that environmental conditions do not change from day to day. Furthermore, the fundamental problem regarding statistical description of the residual error distribution and sigma bounding remains unsolved.

Another ramification of error repeatability is that sigma cannot be easily established by an ensemble of data over many days. There are two basic reasons for this: 1) data ensembled over many days will exhibit significant correlation effects between days (i.e., samples are not independent), and 2) the sigma establishment process must be reasonably short for practical LGF initialization.

Therefore, the approach taken in this work is to generate sigma from data collected over a single (commissioning) day and then inflate the result to account for long-term seasonal variation of the error observed at the LAAS Test Prototype (LTP) site (where several years worth of archived data are available).

II. Serial Correlation: One of the most significant characteristics of the observed ranging error is serial correlation between recorded samples of data. This correlation

effectively limits the number of independent samples that can be assumed in the calculation of inflation factors that account for statistical uncertainty in the estimated sigma. In general, the number of independent samples for computing the inflation factor will be a function of the size of the bin and the correlation time of the data within it.

III. Nonstationarity: A nonstationary process is defined as a process in which statistical parameters of the distribution do not stay constant in time. Elevation dependency of multipath delay and GPS antenna gain patterns are common sources of nonstationarity in observed ranging error. With the MLA antennas used for LAAS, these effects are reduced, but they are still present and significant near the cut-off angle between the MLA and the HZA (High Zenith Antenna). In addition, nonstationarity may also exist due to azimuthal variations (e.g., discrete reflectors or diffractors) in the antenna.

6.3 Expanding Bin Concept

The Expanding Bin (EB) method is a new approach for data-based sigma establishment that simultaneously manages the effects of nonstationarity and serial correlation of observed error data [Sayim02]. Traditional approaches toward data-based sigma establishment rely on fixed bin widths, which are selected *a priori* with intent to both minimize the effect of mixing of error data derived from different distributions and maximize the number of samples within each bin. In practice, the appropriateness of prior bin size selection is difficult to quantitatively validate and is therefore often judged via ad hoc inspection of the data. In contrast, the EB method is an *adaptive* scheme

which automatically selects the bin width at a given time (or elevation) for each satellite separately. In practice, the result is achieved by considering not only a single bin width but all possible bin widths at the given time/elevation. The inherent tradeoff in bin size selection resulting from the simultaneous presence of nonstationarity and serial correlation is gracefully controlled by *selecting the worst-case inflated sigma* as representative of a given time/elevation (E).

The EB method is implemented separately for each satellite by the following means. First, a core bin size, BI , is defined to provide a minimum allowable independent sample size for sigma estimation. This is performed by using the entire data set from the satellite pass to compute the error correlation time, which is in turn translated into the time between independent samples. With this result, the core bin size, BI , is set. Second, a maximum-size bin, BM , is defined in order to provide a wide range for estimating many candidate sigmas. In principle, BM , can be selected to include the entire data set. A simple sketch of inner (core) and outer bins, BI and BM , respectively, is shown in Figure 6.3 for an arbitrary time/elevation, E . The mathematical description of the process for a representative sigma at time/elevation E can be expressed as:

$$\sigma_E = \max_j \{\sigma_{E,j}\} \tag{6.1}$$

where j is the bin width index ranging from BI to BM . After sigma is selected for a given time/elevation using Equation (6.1), the entire process repeated at each subsequent data epoch until the end of the data set is reached.

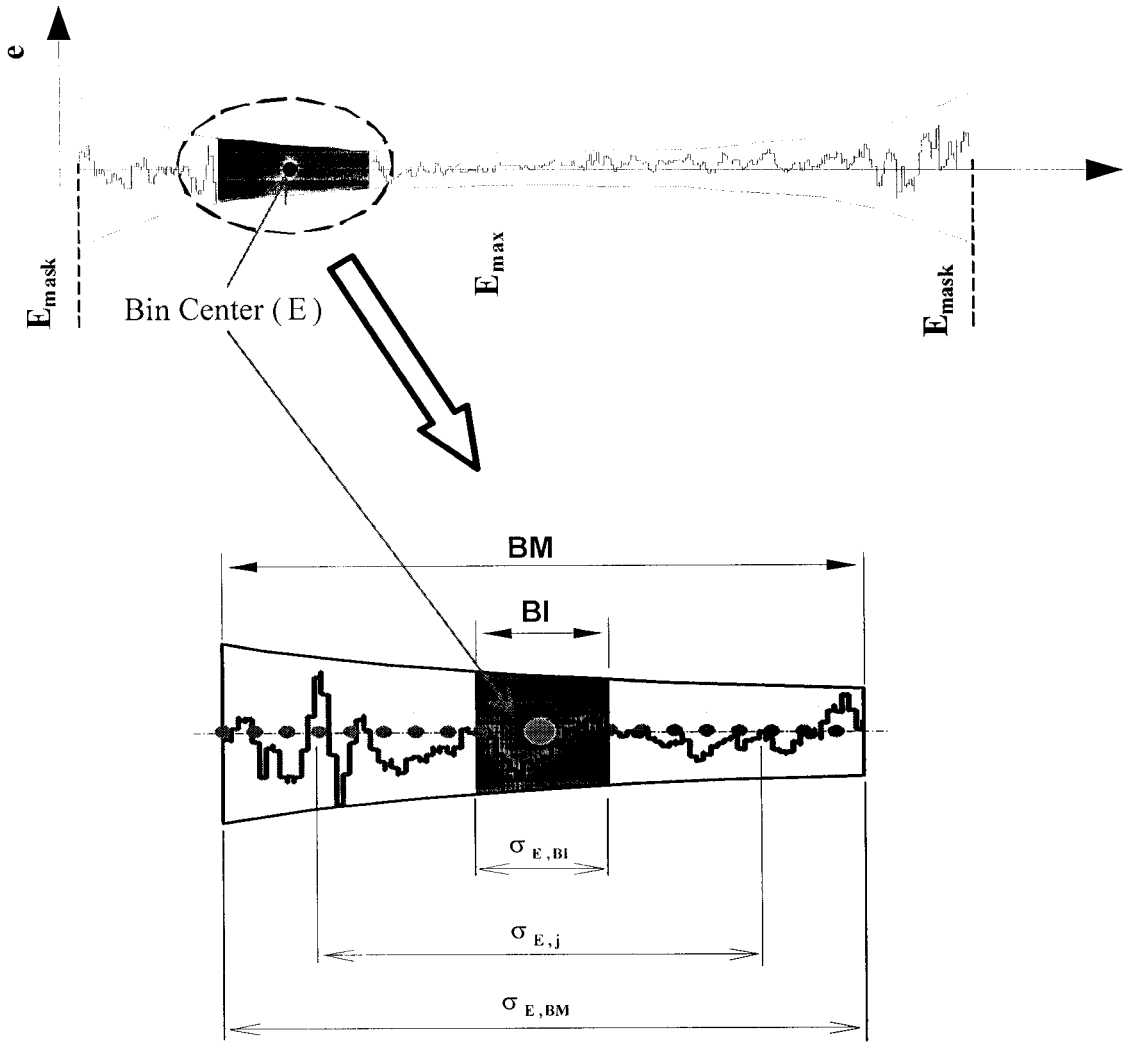

Figure 6.3 Sketch of EB Concept

6.4 Sigma Computation

Given the conceptual introduction of the EB method in the previous section, the mechanization of the process can now be described in greater detail. To aid in this description, a flow chart of the sigma computation process is shown in Figure 6.4.

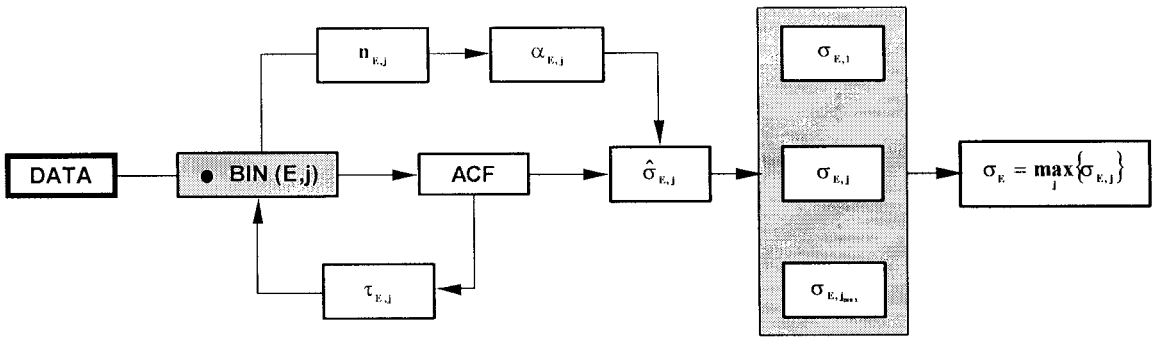

Figure 6.4 Flow Chart for Sigma Computation

As illustrated previously (Figure 6.3), the computation starts from a predefined range of data within BI and follows by continuously adding new measurements in both time directions of it. Each new increased data set is passed through the computation algorithm shown in the flow chart of Figure 6.4. First, the sample autocorrelation function (ACF) for the selected data set is computed, and a resulting correlation time estimate is extracted from the ACF by assuming a first order Gauss-Markov process [Gelb99]. Computed correlation times smaller than the known time constant used for smoothing filter are rejected and replaced by smoothing time constant. Simultaneously, the sample variances are computed from the selected data set. The number of independent samples in the binned data is computed by dividing the number of recorded samples in the selected data set by twice the estimated correlation time.

Based on the number of available independent samples, an inflation factor is applied to account for statistical uncertainty in the computed sample standard deviation. The details of the computation of these inflation factors from an integrity risk perspective are provided in Chapter 3. In Figure 3.20, the associated inflation factor is plotted as a

function of the number of independent samples. It is clear that a small number of independent samples require a high inflation factor on sigma to cover estimation uncertainty. For each bin size, the computed sample standard deviation is inflated and the result is stored. When all candidate bin sizes are processed, the upper bound inflated sigma is selected as follows:

$$\sigma^{s}_{m,E} = \max_{j}\{\sigma_{m,E,j}\} = \max_{j}\{\alpha_{m,E}(n_{m,E,j})\hat{\sigma}_{m,E,j}\} \tag{6.2}$$

where $\alpha_{m,E}(n_{m,E,j})$ is the inflation factor given that $n_{m,E,j}$ independent samples are available for reference receiver m, time epoch E, and bin width index j. $\hat{\sigma}_{E,j}$ is the computed standard deviation of data at epoch E and bin width index j.

6.5 Benchmark Test for EB Method

Two sigma results, obtained by two different methods, are shown in Figure 6.6. The black trace shows the sigma history generated by the EB method and the grey straight line shows the inflated sigma generated by use of the entire data set. It can be observed, by visual inspection of Figure 6.6, that the EB-generated sigma appears to be a faithful representation of the variation of the error data itself (which is also shown on the plot), because the sigma versus time profile is shaped not only by slow variation of error (serial correlation effect) but also by the size of the sample standard deviation (nonstationarity) of error data.

As mentioned, the grey straight line is the sigma obtained by use of the entire dataset. This sigma indicates that if we mix all the error distributions within a single bin (without regard to nonstationarity effects) the sigma will not represent error variation properly.

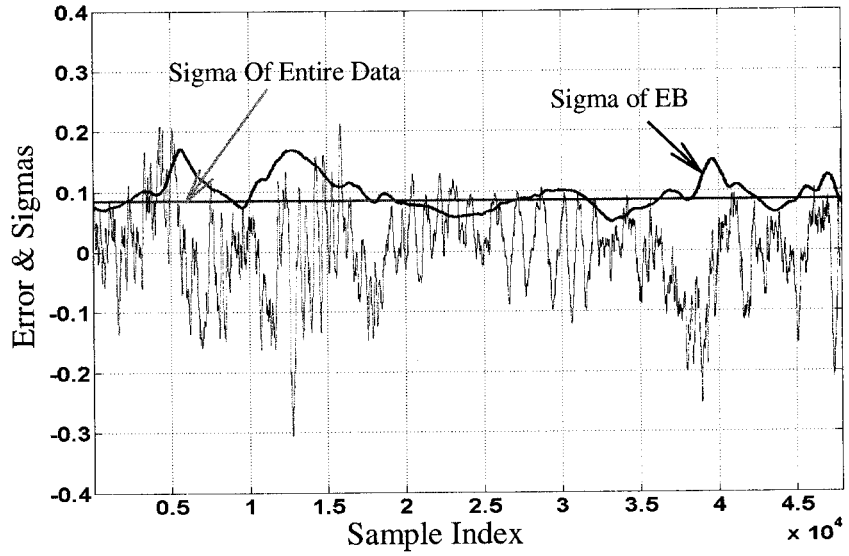

Figure 6.5 Sigma Generation for Nonstationary Process

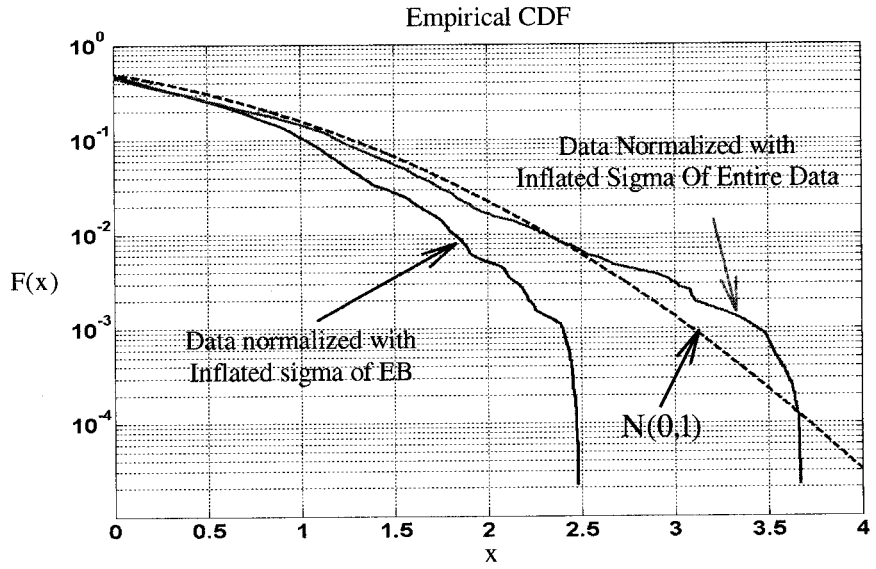

Figure 6.6 Performance Comparison of EB Method

A comparison of the two sigmas in the CDF (Cumulative Distribution Function) sense are shown in Figure 6.7. In this figure, the performance of both methods is compared against a standard normal distribution by normalizing the actual error data by each of the two-sigma curves and then plotting their corresponding CDFs.

It is clear from the figure that for the EB-normalized case, a significant margin exists with respect to an overbounding standard normal distribution. In contrast, the standard normal distribution is insufficient to overbound the error data normalized by the inflated sigma of the entire data set. The basic reason for this fact is that the latter approach does not account for nonstationarity (i.e., mixing of data from different error distributions during the satellite pass).

6.6 Correlation Between Receivers

In the LAAS Protection Levels computations, it is implicitly assumed that ranging errors are uncorrelated across ground receivers. In fact, the existence of any such correlation is not strictly consistent with the VPL equations since $\sigma^2_{pr\_gnd}$ for an individual reference receiver is always divided by the number of receivers to account for the averaging of uncorrelated receiver measurements (Equation (2.19)). In reality, however, it is possible that some measurable correlation exists. Furthermore, even if a negligibly small correlation coefficient is computed from a finite sample set, the statistical uncertainty in the estimate must also be accounted for. Such uncertainty is lessened, as one would naturally expect, as the sample size used to estimate correlation coefficient increases.

To accommodate the effects of correlation, a detailed methodology is presented in Chapter 3 based on the positive maximum correlation between reference receivers. For example, effective increase on the sigma due to maximum positive correlation is given by the factor of $\sqrt{1+M\rho^*}$ for H_0. However, since all the measured correlation between reference receivers is accessible from data, this inflation result can be refined as sigma increase based using all the estimated correlation values instead maximum value of any receiver pair. In this case, it is assumed that the ground error standard deviation for any given reference receiver is expressed by Equation (6.2) and then the effect of correlation between receivers (when averaging M reference receiver errors) can be modeled as an effective increase in $\sigma^s_{m,E}$ as follows:

$$\sigma^{sc}_{m,E} = \beta_m \sigma^s_{m,E} \tag{6.3}$$

where,

$$\beta_m = \begin{cases} \sqrt{1+\sum_{\substack{i=1 \\ i\neq m}}^{M} \rho_{mi}} & \rho^+_m \geq \rho^-_m \\ 1 & \rho^+_m < \rho^-_m \end{cases} \tag{6.4}$$

where, the total positive correlation between receivers is defined by, $\rho^+_m = \sum_{\substack{i=1 \\ i\neq m}}^{M} (\rho_{mi} \mid \rho_{mi} \geq 0)$, and the total negative correlation by $\rho^-_m = \left| \sum_{\substack{i=1 \\ i\neq m}}^{M} (\rho_{mi} \mid \rho_{mi} < 0) \right|$. Note that any inflation of

sigma due to negative correlation is irrelevant since the initial (implicit) assumption of uncorrelated receiver errors will already result in over-inflation in this case. The precise relation between measured correlation and accounted uncertainty in estimated correlation is given in Figure 3.21.

6.7 Temporal Variation of Ranging Error

In this section, the process of quantification and accommodation of temporal variation is detailed using a representative example. The procedure is based on the relative maximum variation between average sigmas across seasons. The goal is to establish sigma from a limited duration of LGF commissioning data (one day) and scale by a factor (γ_m), derived from long-term archived LTP data, to account for temporal variation:

$$\sigma_{m,E}^{sct} = \gamma_m \sigma_E^{sc} \tag{6.6}$$

The long-term temporal variation factor (γ_m) is obtained using a one-year span of LTP data, with four seasonal samplings of two weeks per season. Each day of archived LTP data consists of error measurements from three LAAS Integrated Multipath Limiting Antennas. A satellite (PRN#2, arbitrarily chosen in this example), for which we previously established sigma values using the EB method on the initial day's worth of data, is used to generate temporal variation effects. All of the ranging errors on the subsequent days of data for this satellite are first normalized by initial day's EB sigma values. (This is done so that the temporal variation relative to the initial day's EB result

can be directly observed.) Next, the standard deviations of each normalized error data set computed. The normalized error standard deviations are then grouped into four averaged seasonal samplings. The reason for seasonal grouping and averaging sigmas seasonally is that we are interested in characterizing long-term, slowly varying effects due to weather-related environmental changes. Finally, the average standard deviation of each season is sorted from minimum to maximum, and the ratio between maximum and minimum average sigma is selected as the temporal variation scale factor (γ_m) as shown:

$$\gamma_m = \max(\sigma_{m,seasons}) / \min(\sigma_{m,seasons}) \tag{6.7}$$

where $\sigma_{m,seasons} = \left[\overline{\sigma}_{m,winter} \quad \overline{\sigma}_{m,spring} \quad \overline{\sigma}_{m,fall} \quad \overline{\sigma}_{m,summer}\right]$, and $\overline{\sigma}_{m,winter}$, $\overline{\sigma}_{m,spring}$, $\overline{\sigma}_{m,fall}$, and $\overline{\sigma}_{m,summer}$ are averages of normalized error standard deviation for the winter, spring, fall, and summer seasons, respectively.

The seasonal variation inflation factor result for the particular satellite considered here (PRN#2) is $\gamma_1 = 1.1362$. It is important to note that in this work only a single satellite/single receiver case is considered so far. A more comprehensive, but otherwise identical, analysis is for multiple satellites and receivers must be conducted to define a generalized seasonal variation inflation factor suitable for use in the LGF sigma establishment process.

6.8 Conclusion

A new adaptive method of sigma estimation was developed to account for two major characteristics of empirically observed ranging error: nonstationarity and serial correlation. In addition, a method for quantification of temporal variation was proposed. Example applications of both methodologies using LTP data were also presented.

CHAPTER VII

SIGMA SYNTHESIS AND EXPERIMENTAL RESULTS

7.1 Introduction

In Chapters 3 through 6, methods and models are developed to account for independent component error sources individually. These methods address gaussian, non-gaussian, and non-zero mean gaussian error sources. In addition a process methodology has been developed to account for time correlated and non-stationary error processes. This chapter provides a synthesis of these independent elements to form a final broadcast sigma for LGF correction errors. In this regard, an experimental illustrative example is demonstrated with the use of actual LAAS Test Prototype (LTP) data. Finally, the performance of equipment used in the LTP is compared with the required accuracy specifications for LAAS.

7.2 Synthesis of Broadcast Sigma

To accommodate contributing independent error sources, the establishment of broadcast sigma σ_{pr_gnd} must include sigmas from the following sources:

I. *Sigma Estimated From Data* ($\sigma_{M,E}^{comp}$): To quantify the effects of gaussian (or nearly gaussian) error sources as well as the effects. The EB adaptive bin method

is used here to account for time correlation and nonstationarity (mixing) of error data within bins.

1. A limited (one day) data analysis must be done for every new installation and sigma must include:

    - Inflation due to sample standard deviation uncertainties (α)
    - Inflation due to correlation between receivers (β)

2. Seasonal Data Analysis:

    - Inflation due to long-term temporal variation (γ)

II. *Sigmas Generated From Theoretical Bounds and Analyses* ($\sigma_{MP,E}$)*:* To accommodate ground reflection multipath (non-gaussian) error sources, a theoretical sigma must be generated (using ground reflection multipath models from Chapter 5) and combined with independently estimated sigmas from other error sources.

III. *Sigmas Generated From Receiver Noise Model* ($\sigma_{RN,E}$)*:* To accommodate receiver-related error sources, thermal noise and interference, a sigma must be generated using the LAAS-defined ground receiver noise and interference model from [McGraw00 and Enge99], and combined with independently estimated sigmas from other error sources.

Because neither empirical error data (I) nor theoretical approaches (II or III) alone are adequate, the final broadcast pseudorange sigma will be a result of all these elements. The candidate final broadcast sigma establishment process can be defined as follows:

1. Use the EB method to generate the maximum obtainable sigma values from the data. (The EB approach implicitly incorporates nonstationarity effects and inflation for sample standard deviation estimation uncertainty.)

$$\sigma^{s}_{m,E} = \max_{j}\{\sigma_{m,E,j}\} = \max_{j}\{\alpha_{m,E}(n_{m,E,j})\hat{\sigma}_{m,E,j}\} \tag{7.1}$$

2. Account for correlation effects between reference receivers.

$$\sigma^{sc}_{m,E} = \beta_{m}\sigma^{s}_{m,E} \tag{7.2}$$

3. Account for long-term temporal (seasonal) error variation.

$$\sigma^{sct}_{m,E} = \gamma_{m}\sigma^{sc}_{E} \tag{7.3}$$

4. Generate the composite sigma from data.

$$\sigma^{I}_{pr\_gnd,E} = \sigma^{comp}_{M,E} = \sqrt{\sum_{m=1}^{M}\left(\sigma^{sct}_{m,E}\right)^{2}/M} \tag{7.4}$$

5. Combine composite sigma with the theoretical multipath sigma bound.

$$\sigma^{II}_{pr\_gnd,E} = \sqrt{\left(\sigma^{comp}_{M,E}\right)^2 + \sigma^2_{MP,E}} \tag{7.5}$$

6. Combine composite sigma, theoretical multipath sigma bound, and receiver noise to generate the final broadcast value of sigma

$$\sigma^{III}_{pr\_gnd,E} = \sqrt{\left(\sigma^{comp}_{M,E}\right)^2 + \sigma^2_{MP,E} + \sigma^2_{RN,E}} \tag{7.6}$$

Sigma obtained in Equation (7.4) is a purely empirical result and is the basic estimate of broadcast sigma. In the next step, the composite sigma obtained using Equation (7.5) is a conservative representation of broadcast correction error standard deviation since it explicitly accounts for ground reflection multipath error theoretically, even though some of effects of ground reflection multipath may already be captured empirically in (7.4). The last model, Equation (7.6), is an even more conservative sigma because two independent error sources (ground reflection multipath and receiver-related noise) are potentially captured by theoretical means and empirical means. It is noted that the last step Equation (7.6) will not be covered in this thesis because $\sigma_{RN,E}$ is typically very small ($\sigma_{RN,E} \leq 3$ cm. at 40 dB-Hz and correlator spacing of 0.1 chip of the MLA). For the interested reader, additional detail is provided in [McGraw00 and Enge99].

7.3 Example for LTP Broadcast Sigma

In the following example execution of the procedure, a broadcast sigma is formed by Equation (7.5) as outlined above. The following data specifications are used in this example analysis:

- *Site:* FAATC/LAAS Test Prototype, Atlantic City, NJ
- *BI:* 1000 Recorded Samples
- *BM:* 5000 Recorded Samples
- *Confidence Interval for Inflations:* 99.9%
- *Number of Reference Receivers:* 3
- *Satellite:* PRN#2
- *Elevation Mask:* 5 degrees
- *Cut-Off Angle of MLA:* 35 degrees
- *C/N_O Mask:* 40 dB-Hz
- *Smoothing Time Constant:* 100 sec
- *Raw Data Sample Rate:* 2 Hz
- *Time of Data Record:* February 2000

First, sigmas are estimated by direct use of data with the EB method. Each sigma trace is then plotted (solid curve) in Figure 7.1 for RR1 (Reference Receiver #1), RR2, and RR3, from top to bottom, respectively. For comparison, the actual error data is also plotted. It is observed that the sigma traces for RR1 and RR2 are generally larger than that for RR3. We should also note that the worst sigma values are obtained near the

transition elevation angles (vertical dashed lines) between the High Zenith Antenna (HZA tracks high elevation satellites > 35 degrees) and the MLA (a dipole antenna that tracks low elevation satellites, ≤ 35 degree).

The sigmas traces of Figure 7.1 are plotted in the upper plot of Figure 7.2 for more direct comparison of relative performance between reference receivers. The bottom plot within the figure shows the composite (average) sigma of the three RRs. The composite broadcast sigma of three reference receivers is about 10 cm except near the cut-off (transition) angle regions.

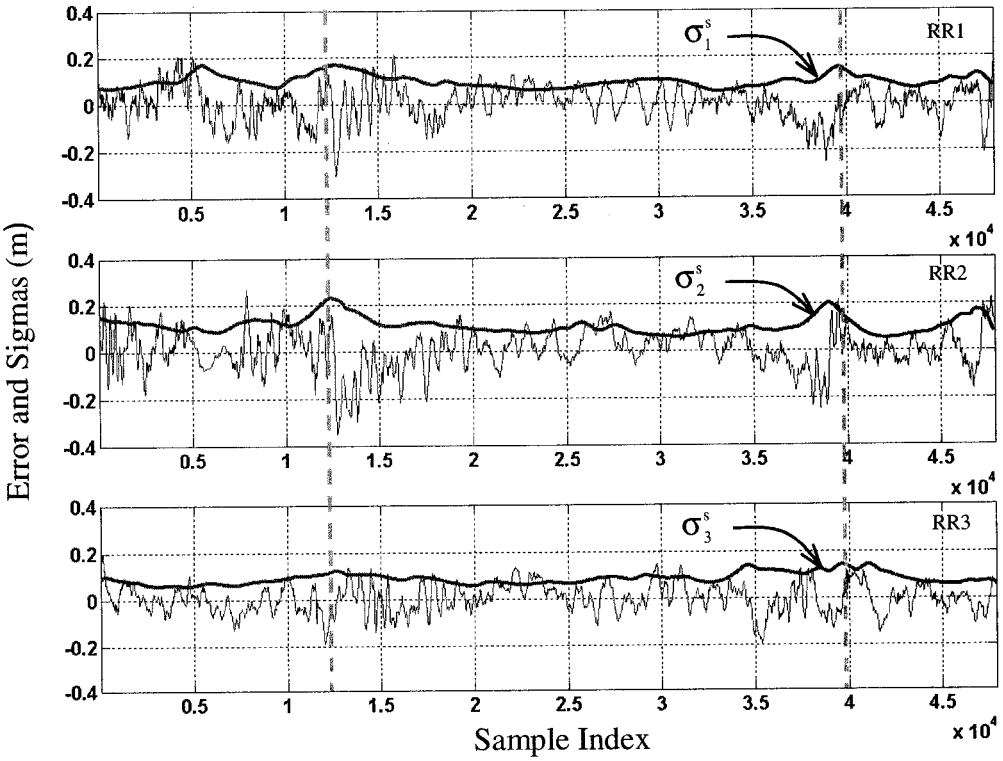

Figure 7.1 Sigma of EB Method for Each RR

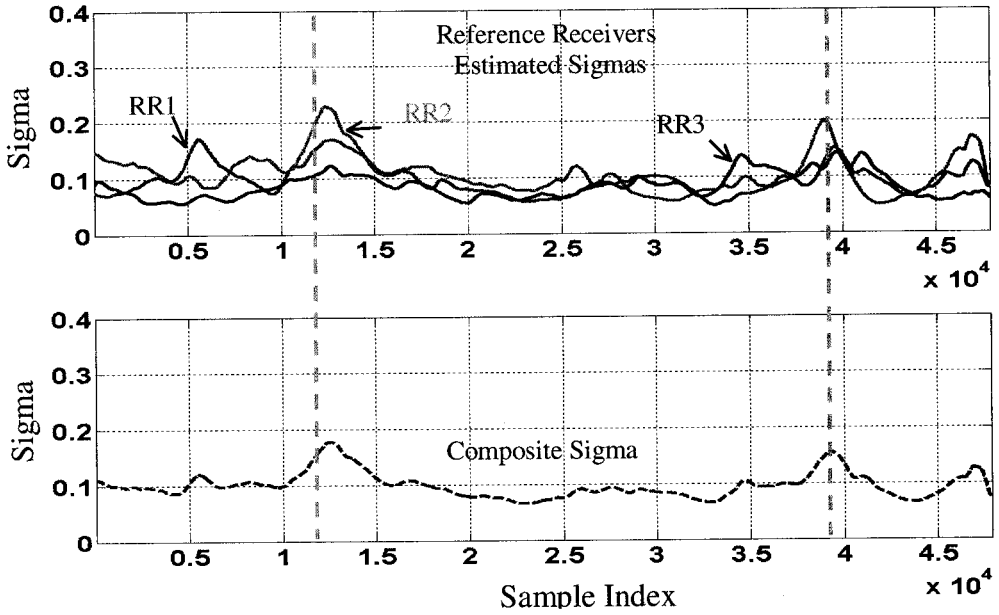

Figure 7.2 EB Sigmas (Individual and Composite)

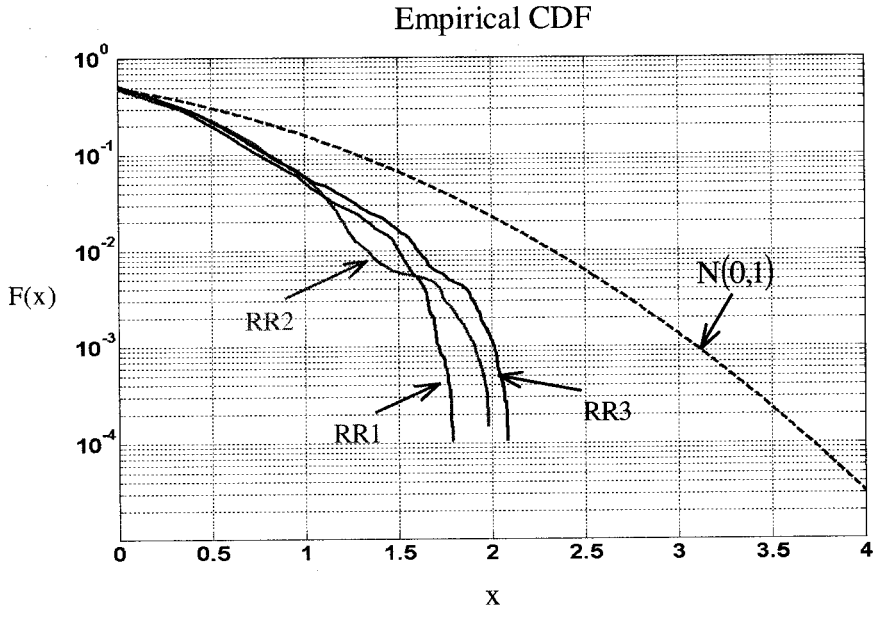

Figure 7.3 CDF Overbound of EB Sigmas

The EB-sigma-normalized error distributions (CDFs) for the three receivers are plotted in Figure 7.3. It is clear that each reference receiver's normalized error is conservatively overbounded by a standard normal CDF.

Correlation effects between receivers are applied to sigmas of EB and then plotted in Figure 7.4. For this example, the composite sigma of three reference receivers is inflated as a function of the number of independent samples within the data. The upper curve shows the composite sigma that is generated after each reference receiver's sigma is independently inflated for correlation using the values listed in Table 7.1.

Table 7.1 Correlation Values

r	m = 1	m = 2	m = 3
m = 1	1	0.21	0.19
m = 2	0.21	1	0.03
m = 3	0.19	0.03	1

ρ	m = 1	m = 2	m = 3	β
m = 1	1	0.38	0.37	1.33
m = 2	0.38	1	0.22	1.27
m = 3	0.37	0.22	1	1.26

In Table 7.1, the measured (r) and inflated (ρ) values of correlation between reference receivers are given. These values are converted to sigma inflation factors (β) listed in the last column.

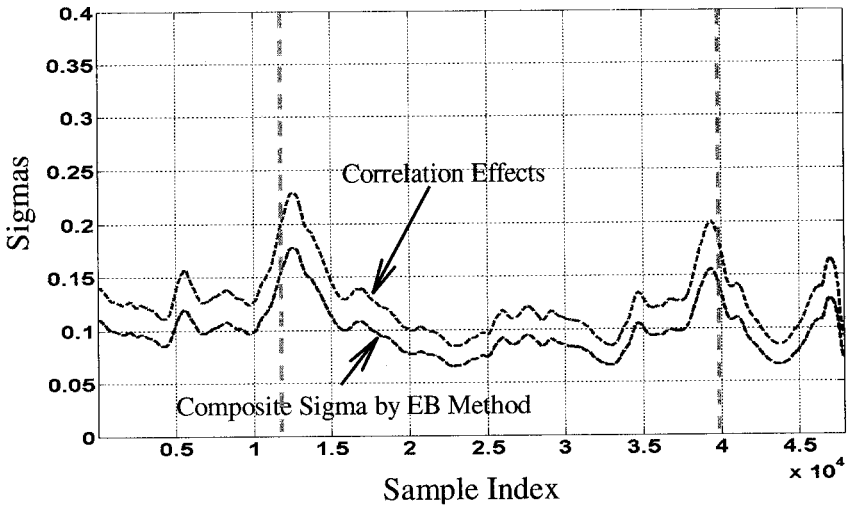

Figure 7.4 EB Sigma Inflated by Correlation Effects

In Figure 7.5, the effect of temporal variation is applied to sigma (after correlation effects have been applied). For the time being, we have available only the temporal variation inflation factor result for RR1. Therefore, we assume that the temporal inflation factors for the other two receivers are the same ($\gamma_1 = \gamma_2 = \gamma_3 = 1.14$). The upper curve is the final sigma trace obtained from data-based estimation.

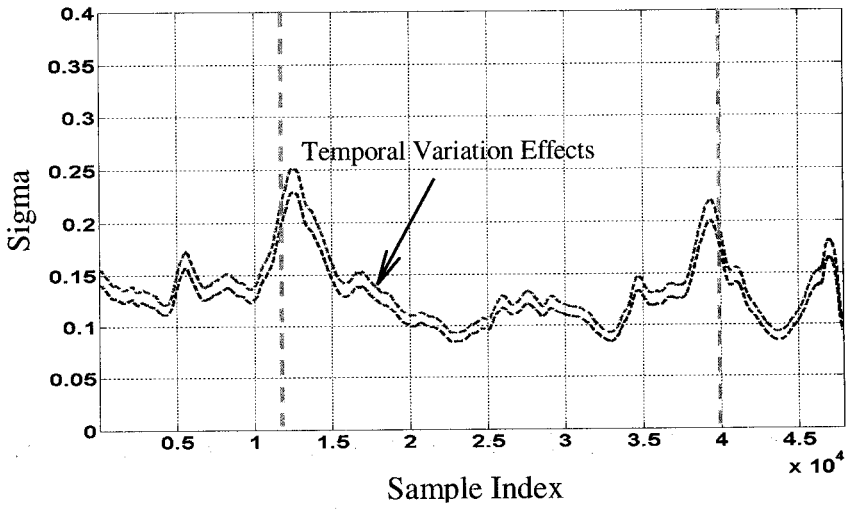

Figure 7.5 EB Sigma Inflated by Correlation and Temporal Variation Effects

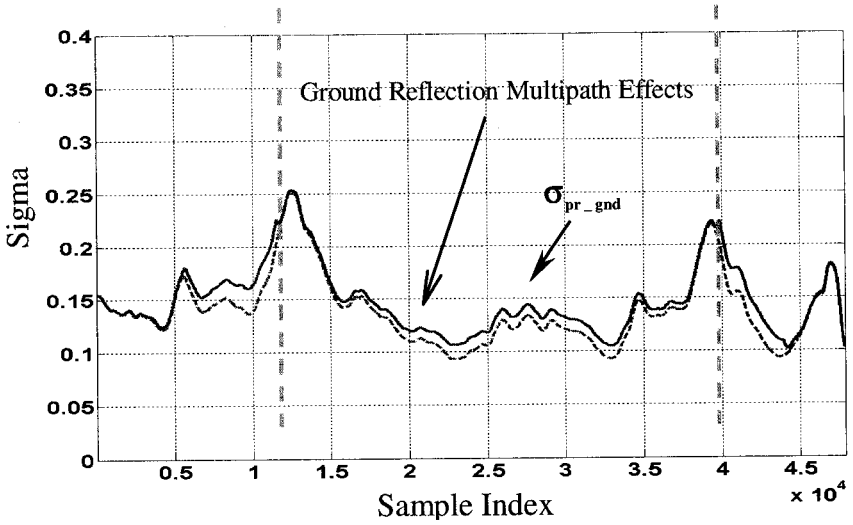

Figure 7.6 Final Sigma (Combined Sigma from both Data and Multipath)

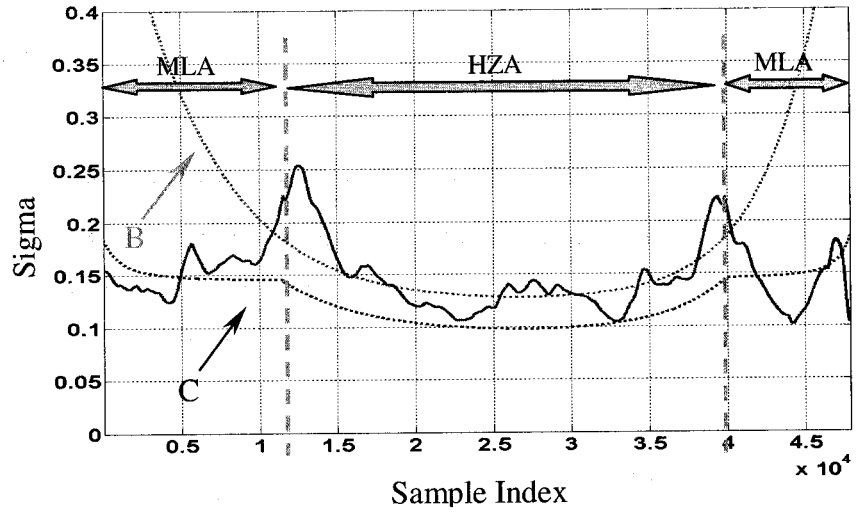

Figure 7.7 Final Sigma Result Versus Specifications (EB)

In Figure 7.6, the theoretical ground reflection multipath sigma is combined with the empirically obtained result of Figure 7.5. The ground reflection multipath sigma is obtained from $\sigma_e = 1.05bc$ using bc values as plotted in Figure 5.10 for antenna height of 2.52 meter. The final composite broadcast sigma result, σ_{pr_gnd}, is plotted in Figure 7.7

and compared with LGF C3 and B3 broadcast sigma specifications [MASPS98]. (See section 2.5.2 for details regarding LAAS B and C Performance types)

In this example, it is clear that the established σ_{pr_gnd} is greater than the C3 and B3 specifications. However, it is possible that σ_{pr_gnd} may be reduced by one or more of the following means:

1) Refined calibration of code-carrier phase center offsets for the LGF data used in this work.

2) Cut-off angle (transition angle between HZA and Dipole) can be varied to reduce sigma peaks.

3) The sigma performance of one or two receivers may be acceptable without the aid of the remaining receivers, which may have higher sigmas. (For this example, RR3 has significantly lower error than the other two receivers near the peaks at 35 deg.) Therefore, RR masking at certain elevations where sigma is large may prevent unacceptable composite sigma results.

4) It may be possible to use smaller inflation factors based on the entire data set, given that data normalized by EB sigmas is overbounded by the standard normal CDF.

Modified EB (MEB): An example of the application of item 4 is discussed in more detail below. The approach is motivated by the observed result that error data

normalized by EB-sigmas which are not inflated for statistical uncertainty are nevertheless still overbounded by a standard normal distribution.

In Figure 7.8, the prior final sigma results are modified by scaling uninflated EB-sigmas by the (statistical uncertainty) inflation factor derived from the number of independent samples within the entire set (satellite pass) of data. Sigma for this case is defined as

$$\sigma^{s}_{m,E} = \alpha_{m,all}(n_{m,all}) \max_{j}\{\hat{\sigma}_{m,E,j}\} \tag{7.7}$$

where $\alpha_m(n_{s,all})$ is the inflation factor given that independent sample size $n_{m,all}$ is available for a bin width corresponding to the entire data set. Obviously, the entire data set has more independent samples than any subset bins, so the effect of inflation due to statistical uncertainty will be much smaller in this case. Therefore, the final sigma results will be reduced even if the other effects (correlation and temporal variation) remain unchanged. It is clear that the new results are significantly improved such that the C3 specification is nearly satisfied, with exceptions at the sigma peaks near the cut-off angle regions. However, because the impetus for this modified approach to inflation is derived primarily from empirical observations, rather than from theoretical arguments, additional work is required to validate the applicability of these results.

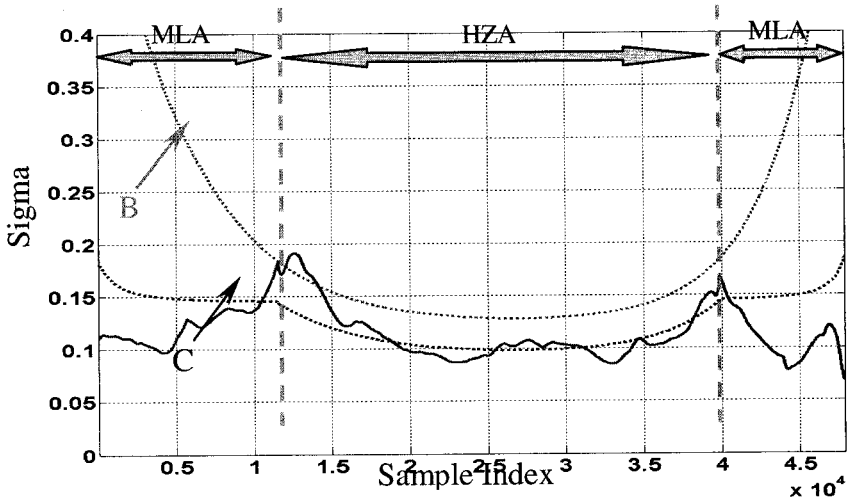

Figure 7.8 Final Sigma Result vs. Specifications (MEB)

7.4 Conclusion

In this chapter, the contributions from various independent error sources are synthesized and a final broadcast sigma is formed. The process applied to actual data from the LTP, and results are compared against nominal LAAS specifications. Suggested approaches to reduce σ_{pr_gnd} are also discussed.

CHAPTER VIII

CONCLUSIONS

8.1 Conclusions

The Local Area Augmentation System is differential GPS architecture that is to be the next generation aircraft precision approach and landing navigation system. The most severe design requirement is associated with navigation integrity. Accordingly, the focus of this research has been on navigation integrity, specifically the establishment of the broadcast correction standard deviation (σ_{pr_gnd}). It is recognized that the broadcast correction standard deviation is a key element for quantifying the integrity risk at the aircraft. *The proper quantification of integrity at the aircraft can only be possible with the proper establishment of* σ_{pr_gnd}.

This research introduced a complete and detailed candidate methodology for establishment of σ_{pr_gnd} to achieve the required navigation integrity. The method involved theoretical bounds, sensitivity analyses, new estimation methods, and the use of empirical data. It is shown that the data commissioning can be limited to a single day.

The following specific conclusions and accomplishments can be drawn from this research:

1. With a comprehensive analysis and simulation of the GPS constellation, the sensitivity of integrity risk was quantified with respect to statistical uncertainties

in the knowledge of σ_{pr_gnd} and correlation between reference receivers. The required inflation factors to ensure a specified level of integrity risk were defined. The results are applicable for gaussian error sources such as diffuse multipath or reference thermal noise.

2. A significant effort was devoted to the bounding of possible mean values of broadcast correction at the LGF or aircraft or both. A reliable model was developed to accommodate the non-zero mean values. The method is simple, effective and does not require any specific prior knowledge of aircraft error statistics. It is potentially useful to account for systematic receiver/antenna biases.

3. Ground reflection multipath, a non-gaussian error source, was investigated and an appropriate methodology for bounding was developed. The methodology consisted the definition of mathematical model for ground reflection multipath error, selection of two limit-case error distributions (bias-type and symmetric bi-modal distribution), and derivation of gaussian overbounds.

4. A new adaptive bin selection approach, known as the Expanding Bin (EB) Method, was developed and successfully applied to a nonstationary and autocorrelated ranging error data for establishment of the LGF broadcast sigma. The results showed that:

- Using the EB method, the upper-bound sigma trace (as a function of time/elevation during the satellite pass) was directly extracted from the available data.
- The EB-method implicitly accounted for nonstationarity and inflation for statistical uncertainty simultaneously.
- Error data normalized by EB-sigmas were conservatively overbounded by a standard normal CDF.
- Abrupt variations in sigma across bin boundaries, which exist in the fixed-bin approaches, were naturally eliminated using the EB approach.

5. An analysis of long-term (seasonal) error variation was performed. The maximum ratio of relative normalized temporal variation, estimated by using seasonally sampled archived LTP data, was selected as a sigma scale factor to account for temporal variation effects. The methodology is recommended for use of newly commissioned LGF sites until sufficient site-specific data is collected.

6. A complete methodology was presented to incorporate all independent error sources in the final establishment of broadcast sigma. The methodology consists of synthesized results from theoretical model/bounds and empirical estimation of sigma.

8.2 Recommendations and Future Work

Finally, in order to continue the effort for sigma establishment and have proper sigma monitoring, the following items are recommended for future research:

1) *Real-time Sigma/Mean Monitoring:* A new EB-based method for real-time monitoring of sigma may be applied to determine whether or not the true sigma exceeds the broadcast sigma. Conventional methods may not be effective because the serial correlation and nonstationary properties of ranging error limit the effectiveness.

2) *Discrete Object Reflection Multipath Modeling and Masking:* Multipath error may be caused by discrete object surfaces that possess exactly the same properties as ground reflection multipath error (see Chapter 5) except for the length of delay and duration of reflections. In general (not always) these types of error have longer multipath delay and shorter duration of reflection. Therefore, carrier aided smoothing filter can successfully attenuate most of these errors. In some airports, however, this may not be the case because of airport surroundings causing discrete object multipath error with shorter multipath delay but longer duration of reflection. Carrier aided smoothing filter may not attenuate these error types. Therefore, they may be hidden in the ranging error broadcast correction. In reality, it is difficult to know exact delays and reflection surface geometry (orientation) with respect to the antenna. Therefore, directly applying a ground reflection multipath model to those discrete object reflections may not be easy. As future work, it is recommended that the effects of discrete object reflection multipath, like ground reflection multipath, be modeled as random variables with non-gaussian error distributions. Empirical site-specific data can also be effective to define sky-masks for strong multipath reflections events.

3) *Extension of Temporal Variation Analysis and Regionalization for Multiple Sites:* It is impossible to collect and quantify a large amount of data for every LGF installation

(for reasonably short LGF system initialization times) in order to define the temporal variation of ranging error. However, for a selected regional LGF site (one representing all others in the region): 1) a large amount of data can be collected, 2) results in this thesis can be extended for more samples and multiple receivers, and 3) the applicability can be investigated for other near by sites. In this research, a sample result is obtained specifically for a given LTP site (the William. J. Hughes FAA Technical Center), but a more generalized analysis should be performed as future work.

APPENDIX A

ALTERNATIVE CANDIDATE MODELS

FOR GROUND REFLECTION MULTIPATH

The models for ground reflection multipath used in Chapter 5 are based on two limiting cases. The detailed validation of physical ground reflection multipath error distribution model is avoided with these conservative models. In this appendix, however, two additional models are introduced for which future empirical validation may be possible.

Model A.1: Uniformly Distributed α and θ.

In this case, the NMP error is the product of RV $z = \cos\theta$ and the uniformly distributed RV α. The resulting PDF of NMP error can be shown as

$$f_{\hat{e}}(x) = \begin{cases} \dfrac{1}{\pi b} \ln\left[\dfrac{b + \sqrt{b^2 - x^2}}{|x|}\right] & -b \le x \le b \\ 0 & \text{otherwise} \end{cases} \qquad \text{(A.1)}$$

This function is plotted in Figure A.1 for an example value of $b = 1$.

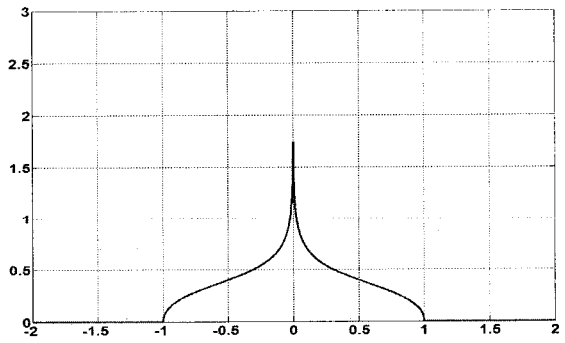

Figure A.1 Normalized Ground Multipath Error Distribution due to Model A.1

It is clear that the PDF is symmetric, unimodal, and truncated. The associated CDF of NMP error is:

$$F_{\hat{e}}(x)=\begin{cases} 0 & -1>x \\ \dfrac{1}{\pi}\left(\pi+\dfrac{\ln\left(|b/x|+\sqrt{(b/x)^2-1}\right)}{(b/x)}-\sec^{-1}(b/x)\right) & -1\le x\le 1 \\ 1 & 1<x \end{cases} \tag{A.2}$$

This function is plotted in Figure A.2 with a gaussian overbound as follows.

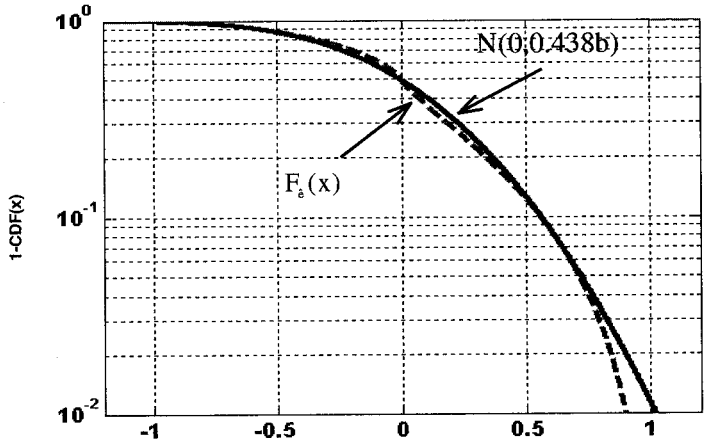

Figure A.2 Gaussian Overbounding of Model A.1

Because the PDF is truncated, it is possible to overbound the CDF of NMP error with a gaussian CDF for all values of x. In Figure A2 it is shown that a gaussian CDF with $\sigma \geq 0.438b$ is sufficient in this regard. The significance of this result is made evident by

the use of a theorem derived in [DeCleene00], which states that if an RV has the following properties:

- CDF is overbounded by gaussian for all x,
- PDF is symmetric, and
- PDF is strictly unimodal.

Then the CDF resulting from an arbitrary linear combination of such random variables is also overbounded by the CDF of the linear combination of the corresponding gaussian RVs for all x. Because Model A.1 satisfies these three conditions, range-domain overbounding implies position-domain overbounding.

Model A.2: Rayleigh Distributed α and Uniformly Distributed θ.

In this case, the NMP error is the product of RV z and the Rayleigh distributed RV α. The resulting PDF of NMP error can be shown to be [Proakis83].

$$f_{\hat{e}}(x) = \frac{1}{b\sqrt{2\pi}} \exp\left[\frac{x^2}{2b^2}\right] \equiv N_{\hat{e}}(0,b) \tag{A.3}$$

Since the result is gaussian, the issue of overbounding need not be considered. However, an appropriate value of the parameter b must be selected. In this regard, we consider two properties of the Rayleigh Distribution:

- Case A: Maximum Likelihood Value (MLV) of $\hat{e} = b$

- Case B: Expected Value (EV) of $\hat{e} = b\sqrt{\pi/2}$

Therefore, if we select $b = -30\,dB$ to be the MLV of α, any gaussian with $\sigma \geq b$ may be used. Alternately, if we choose $\alpha \equiv b/\sqrt{\pi/2}$ ($b = -30\,dB$ is the EV of α), we may use any gaussian such that $\sigma \geq 0.798b$. Note that while some flexibility clearly exists in the precise implementation of the Rayleigh model, the fact that the magnitude of α will always be unbounded suggests that the results derived from the model may be conservative. Conversely, the relative advantage of the Rayleigh model is that it can accommodate uncertainty (should there be any) in the knowledge of the value of the maximum reflection strength.

Summary of Error Models Results

Table A.1 Summary of Alternative Non Gaussian Error Model

	Ground Reflection Multipath
Model A.1 *Uniform Phase* *Uniform Reflection Strength*	$\sigma_e \geq 0.438bc$
Model A.2 *Uniform Phase* *Rayleigh Reflection Strength*	$\sigma_e \geq bc$ (Case-A)
	$\sigma_e \geq 0.798bc$ (Case-B)

APPENDIX B

VALIDATION OF EB METHOD

Validation of EB-method

In Chapter 6, an adaptive estimation method known as EB-method is proposed for proper processing of nonstationary and time-correlated data to estimate broadcast sigma empirically. In this section, a controlled experiment (i.e., input data with known characteristics) is executed to determine whether or not the proposed scheme effective in estimating sigma under a large spectrum of data scenarios (stationary and time-correlated). In this regard, a sample function of white noise is first generated and then nonstationarity is purposely injected into this sample function via two deterministic functions (applied separately). Next, all three sample functions (white sequences) are passed through filters to generate colored products. For the filter, a first order Gauss Markov Process is used. Finally, all sample functions are conceptually located in the Figure B.1 in terms of nonstationarity versus time-correlation to illustrate the coverage of cases in data.

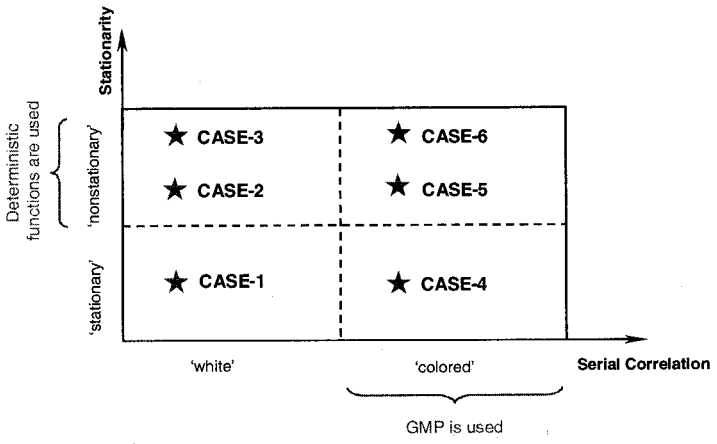

Figure B.1 Serial Correlation versus Nonstationarity

The filtering processes of sample functions are summarized in the Table B.1. In Table B.1 the following notation was used: τ_c is correlation time, τ_s is time between recorded samples, σ is process standard deviation, and e is the random error.

Table B.1 Data Generation for EB and MEB

CASE-#	Whiteness	Process Standard Deviation (σ_{nom})	Data
1	$\tau_c = 1$	$\sigma_v = 0.2$	$e_{c1} \equiv v \sim N(0, \sigma_v = 0.2)$
2	$\tau_c = 1$	$\sigma_{c2,k} = \kappa_{1,k}\sigma_v$	$e_{c2} \equiv \kappa_{1,k} v_k \sim N(0, \xi_{1,k}\sigma_v)$
3	$\tau_c = 1$	$\sigma_{c3,k} = \kappa_{2,k}\sigma_v$	$e_{c3} \equiv \kappa_{2,k} v_k \sim N(0, \xi_{2,k}\sigma_v)$
4	$\tau_c = 20$	$\sigma_{c4} = \sigma_v$	$e_{c4,k} = \frac{e_{c4,k-1} + v_{k-1}}{\sqrt{1-a_k^2}}$ & $a_k = \exp(-\frac{\tau_s}{\tau_c})$
5	$\tau_c = 20$	$\sigma_{c4,k}, = \kappa_{1,k}\sigma_v$	$e_{c4,k} = \kappa_{1,k} e_{c4,k}$
6	$\tau_c = \begin{cases} 20 & 1 \le k \le 3000 \\ 100 & 3000 < k \le 6000 \end{cases}$	$\sigma_{c6,k} = \kappa_{2,k}\sigma_v$	$e_{c6,k} = \frac{e_{c6,k-1} + v_{k-1}}{\sqrt{1-a_k^2}}$ & $e_{c6,k} = \kappa_{2,k} e_{c6,k}$

Two deterministic functions are selected to transform stationary white noise data to nonstationary. Both functions are plotted in Figure B.2 and Figure B.3. The function κ_1 is used to generate nonstationarity data in CASE-2 and CASE-4 that represent a slow variation in sigma. Similarly κ_2 is used to generate nonstationarity in CASE-4 and CASE-6 which is a relatively faster variation type in sigma.

Summary

Although the experiment is performed for the EB-method, a modified method of EB (MEB-method as described in Chapter 6) is also considered here. The results are

generated and then compared for both approaches. As shown in Table B.2, both estimation methods effectively manage both time-correlation and nonstationarity in data through CASE-1 to CASE 6. EB provides the most conservative sigma results (i.e., the largest sigmas which are consistent with data) while MEB provides the less conservative sigma.

Table B.2 Summary of Results of EB and MEB

CASE #	EB-method		MEB-method		EB vs. MEB
	$\sigma \geq \sigma_{nom}$	CDF Overbound	$\sigma_{all} \geq \sigma_{nom}$	CDF Overbound	$\sigma \geq \sigma_{all}$
1	✓	✓	✓	✓	✓
2	✓	✓	✓	✓	✓
3	✓	✓	✓	✓	✓
4	✓	✓	✓	✓	✓
5	✓	✓	✓	✓	✓
6	✓	✓	✓	✓	✓

Specific details of the results are given in the following sets of plots (case by case). In each set of plots, there are three figures. The first figure shows the empirical data. The second figure shows sigma results for both EB ($\sigma_{EB} = \max_j \{\alpha\hat{\sigma}\}$) and MEB ($\sigma_{MEB} = \alpha_{all} \max_j \{\hat{\sigma}\}$) including nominal (i.e., true) sigma (σ_{nom}). The third figure shows details (selected bin width, α, and $\hat{\sigma}$) of the EB sigma maximization process. Finally, in the last two figures (Figure B.22 and B.23), the details of CDF overbound (CASE-1 through CASE-6) are given for EB and MEB-method respectively.

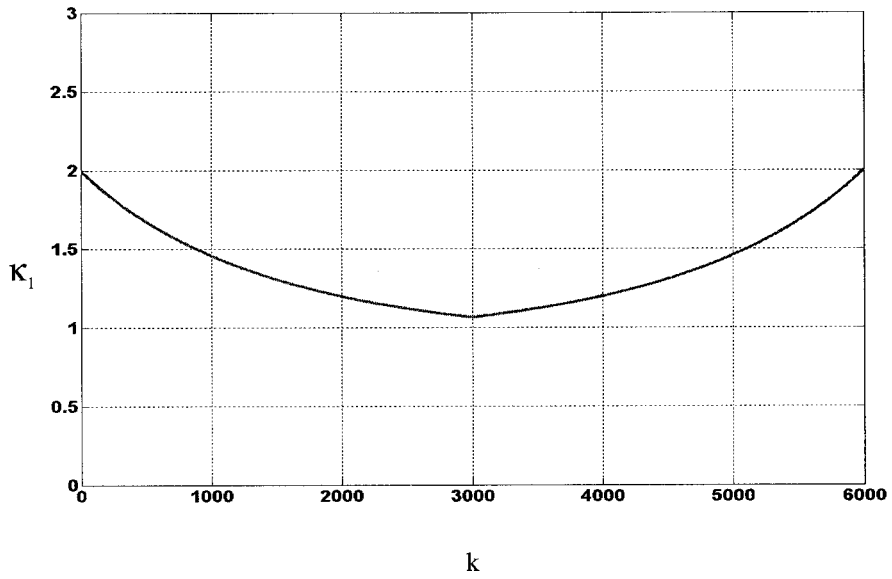

Figure B.2 Deterministic Function (κ_1) for Nonstationarity

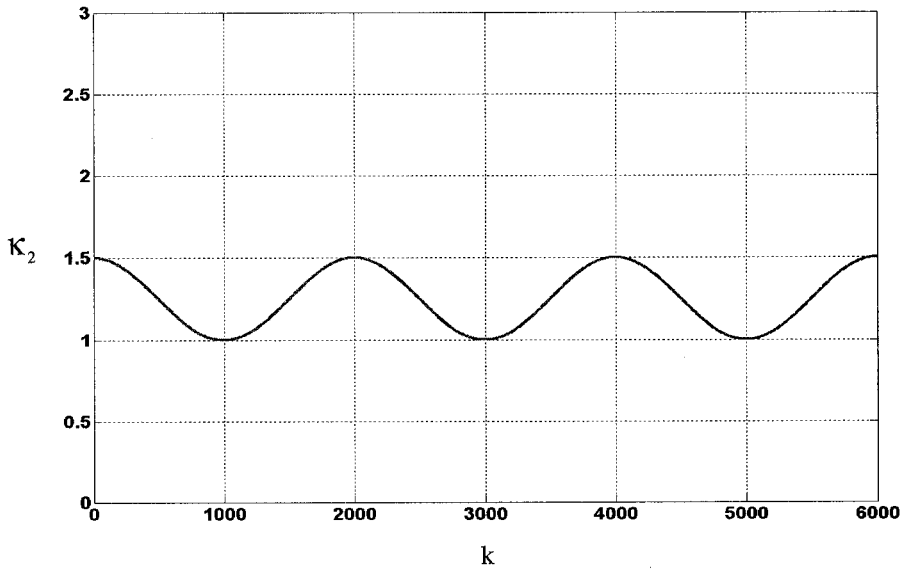

Figure B.3 Deterministic Function (κ_2) for Nonstationarity

CASE-1 White noise, stationary and white

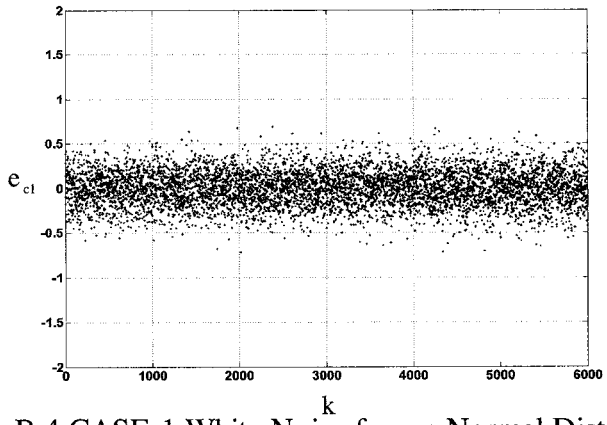

Figure B.4 CASE-1 White Noise from a Normal Distribution

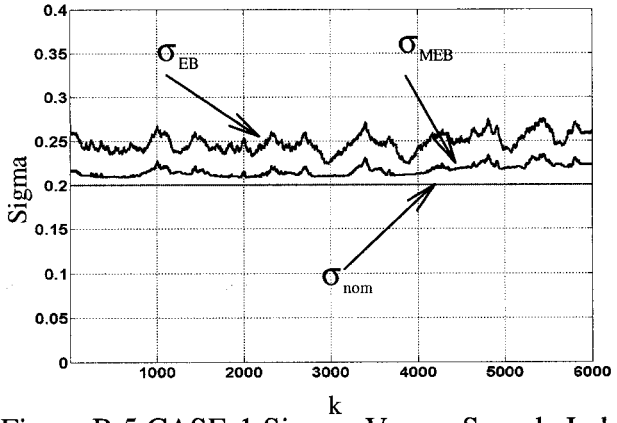

Figure B.5 CASE-1 Sigmas Versus Sample Index

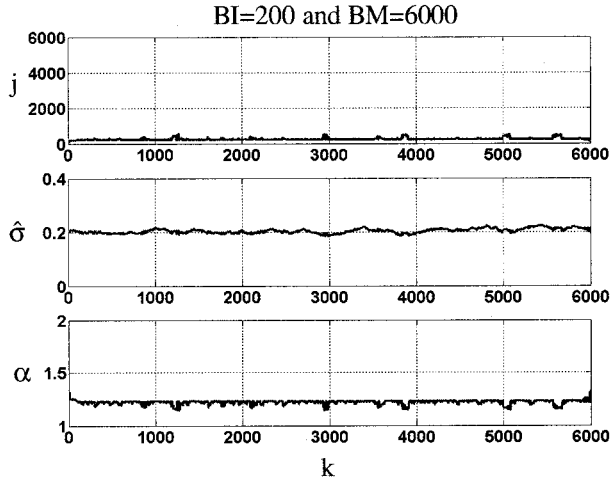

Figure B.6 CASE-1 EB Values Versus Sample Index

CASE-2 White and nonstationary noise (slow variation of nonstationarity)

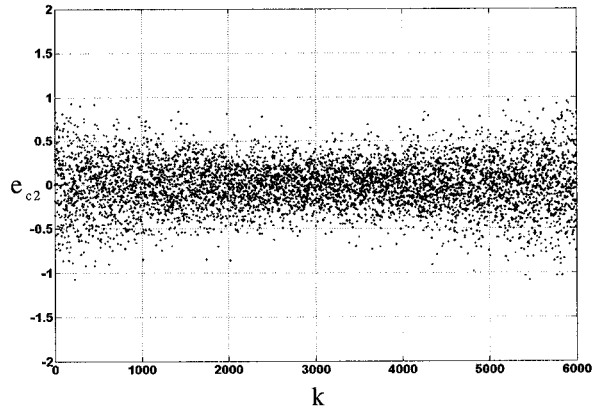

Figure B.7 CASE-2 White Noise from a Normal Distribution

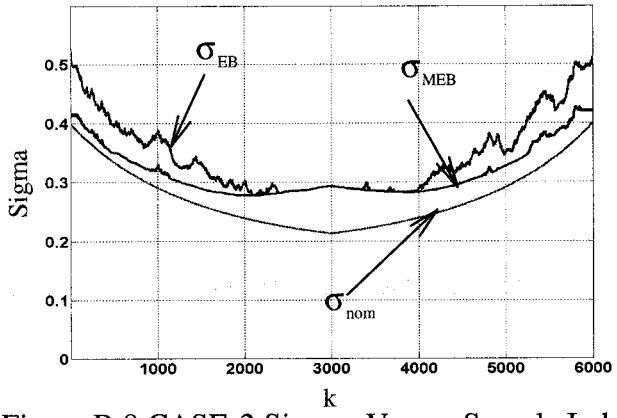

Figure B.8 CASE-2 Sigmas Versus Sample Index

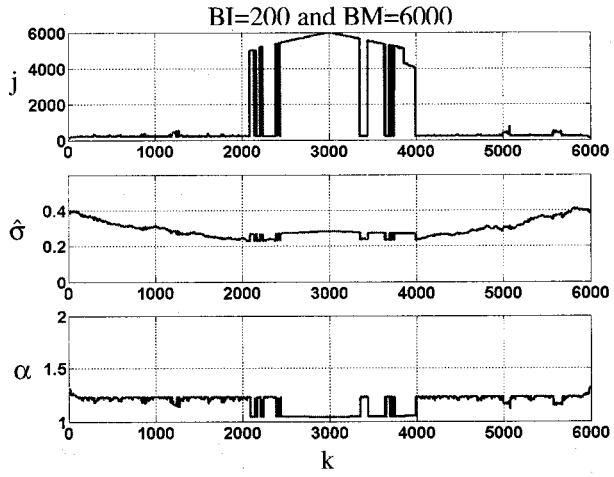

Figure B.9 CASE-2 EB Values Versus Sample Index

CASE-3 White and nonstationary noise (fast variation of nonstationarity)

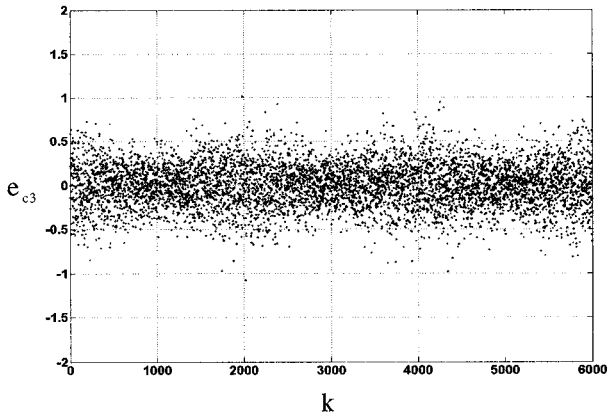

Figure B.10 CASE-3 White Noise from a Normal Distribution

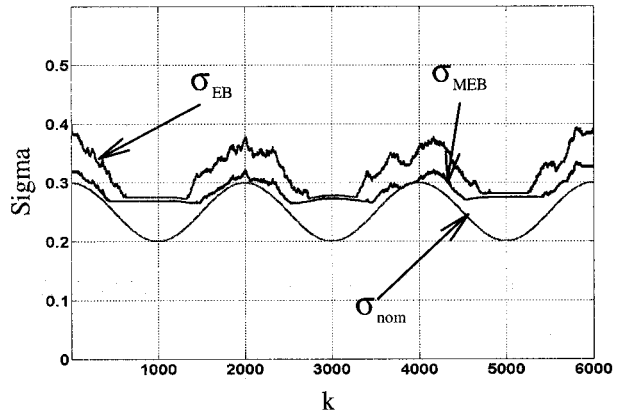

Figure B.11 CASE-3 Sigmas Versus Sample Index

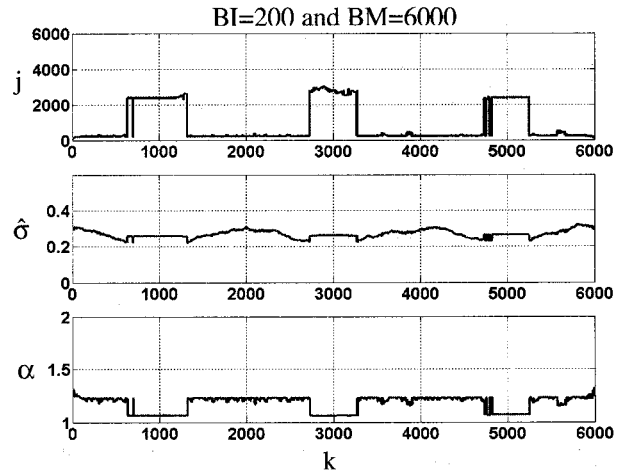

Figure B.12 CASE-3 EB Values Versus Sample Index

CASE-4 Colored and stationary noise

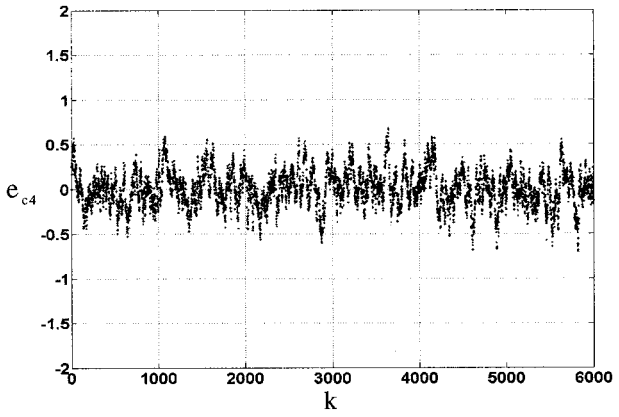

Figure B.13 CASE-4 Colored Noise with Filter

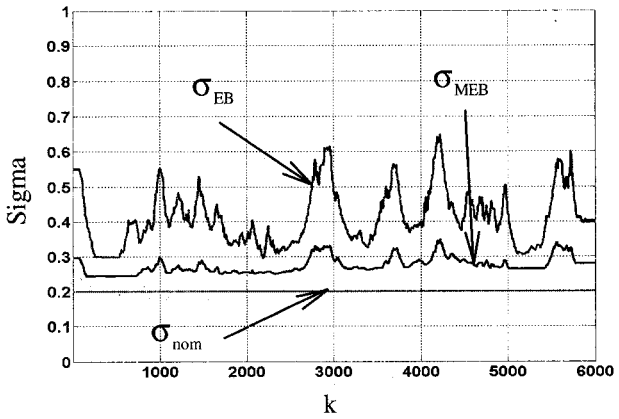

Figure B.14 CASE-4 Sigmas Versus Sample Index

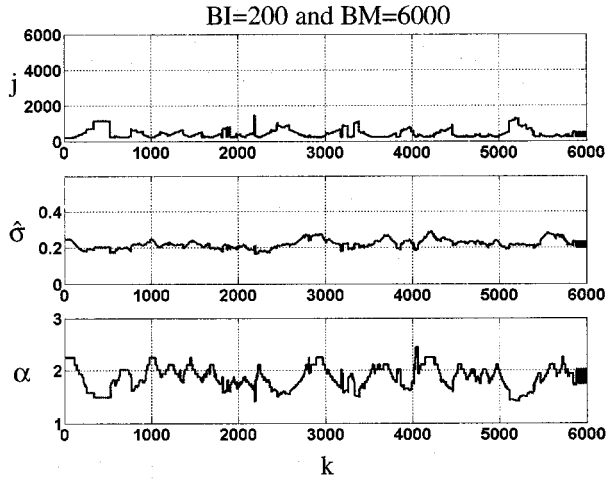

Figure B.15 CASE-4 EB Values Versus Sample Index

CASE-5 Colored and nonstationary noise (slow variation of nonstationarity)

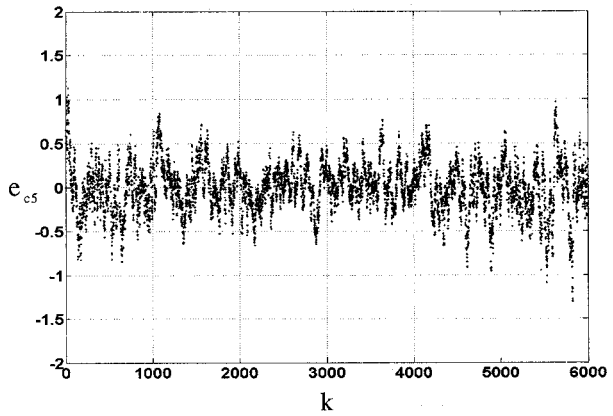

Figure B.16 CASE-5 Colored Noise with Filter

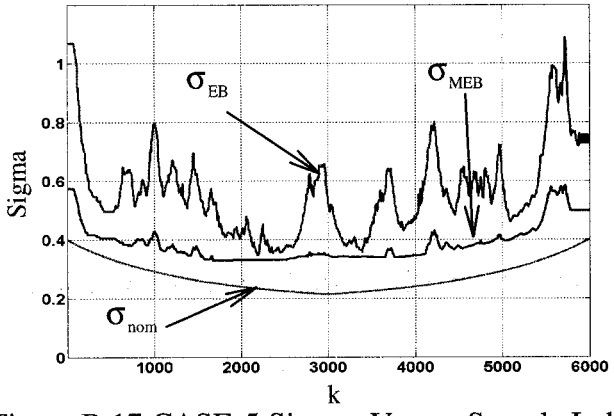

Figure B.17 CASE-5 Sigmas Versus Sample Index

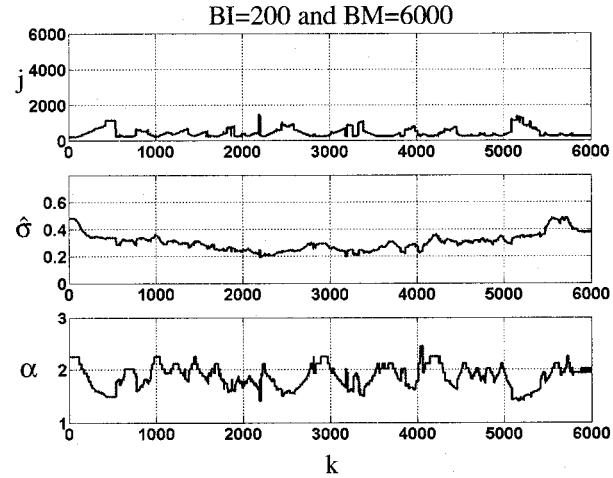

Figure B.18 CASE-5 EB Values Versus Sample Index

CASE-6 Colored and nonstationary noise (fast variation of nonstationarity)

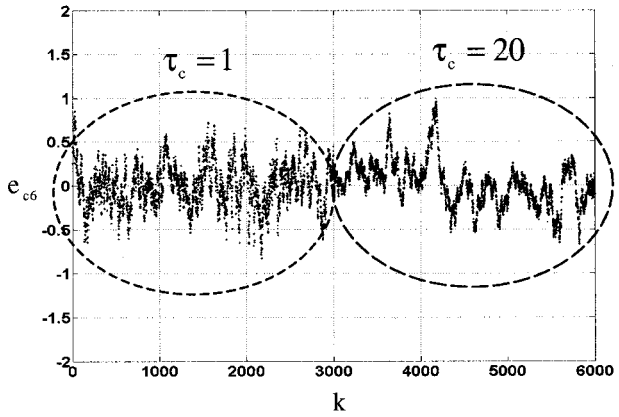

Figure B.19 CASE-6 Colored Noise with Filter (Two Different Time Constant)

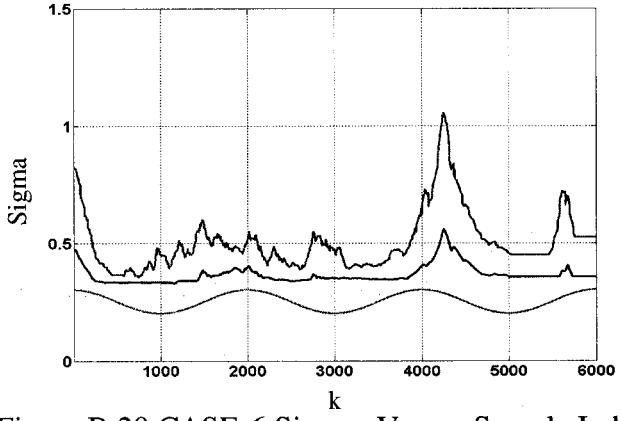

Figure B.20 CASE-6 Sigmas Versus Sample Index

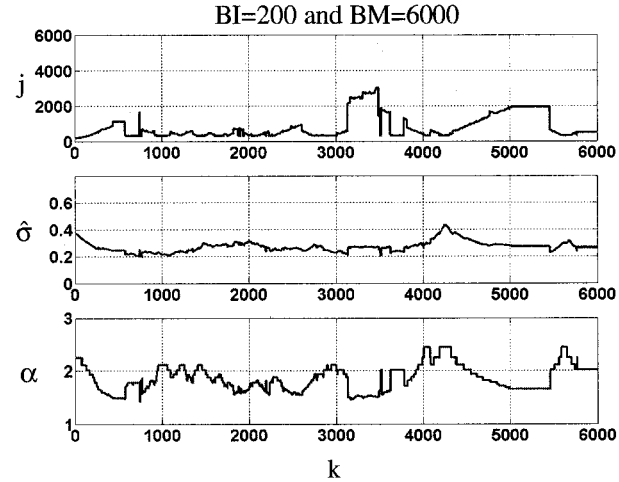

Figure B.21 CASE-6 EB Values Versus Sample Index

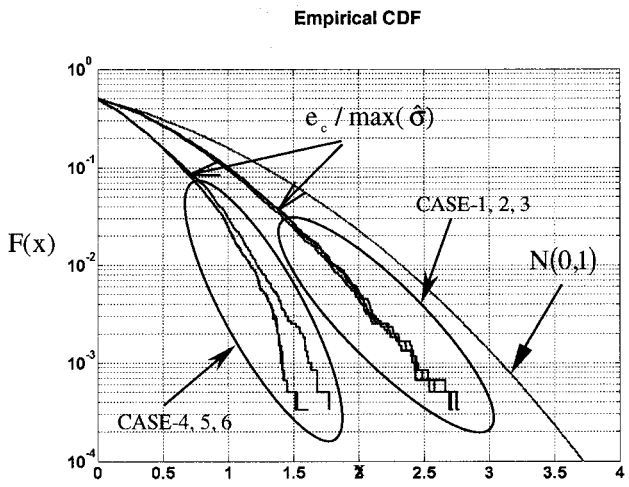

Figure B.22 CDF Overbound of EB with Standard Normal

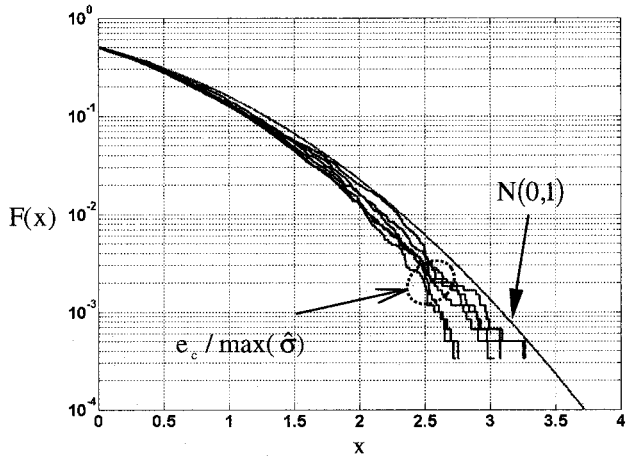

Figure B.23 CDF Overbound of MEB with Standard Normal

BIBLIOGRAPHY

[Bendat86] Bendat, J. S., and Piersol, A.G., "Random Data, Analysis and Measurement Procedure," 2nd Edition, John Wiley & Sons, 1986

[Beser82] Beser, J., and Parkinson, W. B., "The Application of NAVSTAR Differential GPS in the Civilian Community," Journal of the Institute of Navigation, Vol. 29, No.2, summer 1982

[Braasch96] Braasch, M., "Multipath Effects," Global Positioning System: Theory and Applications, Volume 1, AIAA Progress in Aeronautics and Astronautics, Vol. 163, 1996

[Braff98] Braff, R., "Description of the FAA's Local Area Augmentation System of (LAAS) Navigation," Journal of The Institute of Navigation, Vol. 44, No. 4, Winter, 1997-1998

[Brenner98] Brenner, Mats, Reuter, Randy, and Schipper, Brian, "GPS Landing System Multipath Evaluation Techniques and Results" Proceeding of the 11th International Technical Meeting of the Satellite Division of the Institute of Navigation (ION GPS-98), September 15-18, 1998, Nashville, TN

[Brownlee60] Brownlee, K.A., "Statistical Theory and Methodology in Science and Engineering," John Willey & Sons, 1960

[Counsel99] Counselman, C. C., "Multipath-Rejecting GPS Antennas," Proceedings of the IEEE, Vol. 87, No.1, January 1999

[Shively00] Shively, Curtis, and Braff, Ronald, "A concept for Overbounding and Verifying Pseudorange Error From the LAAS Ground Facility," Annual Meeting of the Institute of Navigation, San Diego, CA, June 2000

[DeCleene00] DeCleene, B., "Defining Pseudorange Integrity - Overbounding," Proceedings of the 13th International Meeting of the Satellite Division of the Institute of Navigation (ION GPS-2000), 19-22 September 2000, Salt Lake City, UT

[Enge99] Enge, P., "Local Area Augmentation of GPS for the Precision Approach of Aircraft," Proceedings of the IEEE, Spatial Issue on GPS, Vol. 87, No.1, January 1999

[Gelb99] Gelb, A., "Applied Optimal Estimation," The M.I.T. Press, 1999

[Golub93] Golub, H., Gene, and Loan, Charles, F. V., "Matrix Computations," 2nd Edition, The John Hopkins University Press, Maryland, 1993

[LGF02] Federal Aviation Administration, "Local Area Augmentation System Ground Facility Specification," FAA-E-2937, Washington, D.C., September 21, 1999

[Liu97] Liu, F., Murphy, T., and Skidmore, T., "LAAS Signal-in-Space Integrity Monitoring Description and Verification Plan," Proceedings of ION GPS-97, Kansas City, MO, September 1997

[MASPS98] RTCA (SC-159/WG-4), "Minimum Aviation System Performance Standards for the Local Area Augmentation System (LAAS)," RTCA DO-245, RTCA Inc., Washington, D.C., 28 September 1998

[MOPS00] RTCA (SC-159/WG-4), "Minimum Operational Performance Standards for GPS Local Area Augmentation System Airborne Equipment," RTCA DO-253, RTCA Inc., Washington, D.C., 11 January 2000

[McGraw00] McGraw, G. A., Brenner, M., Pullen, S. and Van Dierendonck, A. J., Development of the LAAS Accuracy Models," Proceedings of ION GPS 2000, September 2000, Salt Lake City, UT

[Misra01] Misra, P. and. Enge, P., "Global Positioning System, Signals, Measurements, and Performance," Gang-Jamuna Press, 2001

[Parkinson96] Parkinson, B. W., Spilker, J. J., Axelrad, P., and Enge, P., " Global Positioning System: Theory and Applications," Volume 1, American Institute of Aeronautics and Astronautics Inc., Washington, D.C., 1996

[Pervan00] Pervan, B., Pullen S., and Sayim, I., "Sigma Estimation, Inflation and Monitoring in the LAAS Ground System," Proceedings of the 13th International Meeting of the Satellite Division of the Institute of Navigation (ION GPS-2000), Salt Lake City, UT, September 2000

[Pervan01] Pervan, B., and Sayim, I., "Sigma Inflation for the Local Area Augmentation of GPS," IEEE Transactions on Aerospace and Electronic Systems, Volume 37, Number 4, October 2001

[Pervan96] Pervan, B., "Navigation Integrity for Aircraft Precision Landing Using The Global Positioning System," PhD Dissertation, Stanford University, SUDAAR 677, 1996

[Proakis83] Proakis, J., "Digital Communications," McGraw-Hill, 1983

[Pullen00] Pullen, S., Luo, M., Walter, T., Enge, P., and Pervan, B., "The Use of CUSUMs to Validate Protection Level Overbounds for Ground Based and Space Based Augmentations Systems," Proceedings of ISPA 2000 Munich, Germany, 18-20 July 2000

[Sayim02] Sayim, I., Pervan, B., Pullen, S., and Enge, P., "Experimental and Theoretical Results on the Sigma Overbound," Proceedings of the 15th International Meeting of the Satellite Division of the Institute of Navigation (ION GPS-2002), Portland, OR, September 2002

[Shanmug88] Shanmugan, K. S., and Breipohl, A.M., "Random Signals: Detection, Estimation and Data Analysis," John Wiley & Sons, 1988

[Teasley80] Teasley, S. P., Hoover, W. M., and Johnson, C. R., "Differential GPS Navigation," Position, Navigation, and Location Symposium (PLANS 80), Atlantic City, New Jersey, December 1980

[Swider98] Swider, R., Kaser, K., and Braff, R., "Recent Developments in the LAAS Program," Position Location and Navigation Symposium, IEEE 1998, 20-23 April 1998